
# Master Dissertation

# Riverine Flooding using GIS and Remote Sensing

Author: Natalia Dambe, Supervisor: Ass. Prof Julian Smit

*A thesis submitted in fulfilment of the requirement for the degree of Masters in Geomatics*

Faculty of Engineering and Built Environment

School of Architecture, Planning and Geomatics

January 2020

# Declaration of Authorship

I, Natalia Dambe, hereby declare that “I know the meaning of plagiarism and declare that all the work in the document, save for that which is properly acknowledged, is my own. This thesis/dissertation has been submitted to the Turnitin module (or equivalent similarity and originality checking software) and I confirm that my supervisor has seen my report and any concerns revealed by such have been resolved with my supervisor."

Signature: Signed by candidate Date: 10 February 2019

# Acknowledgements

My dissertation has been a success because of selfless and kindhearted people whom I would like to appreciate and acknowledge:

- UCT MasterCard Scholarship and Team for sponsoring my studies and giving me all the support during my studies.
- My supervisor, Associate Professor Julian Smit, for continual supervision during the 2 years of my studies.
- My colleagues and friends: Kehinde Babalola, Adadeyo Adeleke, Lucia Mokubedi, Konosoang Lephoto, Chimwemwe Kamkodo, Chikondi Mphamba, Jeffy Palamattam, Nasonkhwe Hamphwaye, Andrew Goodhead, Yamikani Phiri, Gareth Keick, Charlotte Musinga, Danilo Acquisto, Fanny Thindwa, Betty-Ann Frempong, for all your encouragement and positive words, prayers and moral support.
- John Okedi, peer mentor, for giving me direction and words of purpose.
- Akindegele Aroge, Tony Dambe, and Tawanda Madzangaidzo, for editing my work.
- Ms. Mignon Wells, for all the technical support.
- RCMRD (Rose Waswa, Pauline Ogola, Degelo Sendabo), for guidance and opportunity to learn more about flooding and Remote Sensing.
- My beloved family, for always being there for me and trusting in my capabilities.
- Simunye family, for giving me space of joy, love and meaning.
- Kolbe-Nyanga Tutoring Community, for a fulfilling environment to give back and a sense of purpose
- UCT Kolbe Chaplaincy, St Michaels for spiritual and community support.
- God, for always being my strength, wisdom, life, and for giving me everything that was necessary for me to complete my studies.

# Abstract

*Floods are caused by extreme meteorological and hydrological changes that are influenced directly or indirectly by human activities within the environment. The flood trends show that floods will reoccur and shall continue to affect the livelihoods, property, agriculture and the surrounding environment. This research has analyzed the riverine flood by integrating remote sensing, Geographical Information Systems (GIS), and hydraulic and/or hydrological modeling, to develop informed flood mapping for flood risk management. The application of Hydrological Engineering Center River Analysis System (HEC RAS) and HEC HMS models, developed by the USA Hydrologic Engineering Center of the Army Corps of Engineers in a data-poor environment of a developing country were successful, as a flood modeling tools in early warning systems and land use planning. The methodology involved data collection, preparation, and model simulation using 30m Shuttle Radar Topographic Mission (SRTM) Digital Elevation Model (DEM) as a critical data input of HEC RAS model. The findings showed that modeling using HEC-RAS and HEC HMS models in a data-poor environment requires intensive data enhancements and adjustments; multiple utilization of open sources data; carrying out multiple model computation iterations and calibration; multiple field observation, which may be constrained with time and resources to get reasonable output.*

**Key words:** Hydrological modeling, hydraulic modeling, flood mapping, Geographical Information Systems, Remote Sensing.

# Ethics Declaration Form

Application for Approval of Ethics in Research (EIR) Projects
Faculty of Engineering and the Built Environment, University of Cape Town

## APPLICATION FORM

**Please Note:**
Any person planning to undertake research in the Faculty of Engineering and the Built Environment (EBE) at the University of Cape Town is required to complete this form **before** collecting or analysing data. The objective of submitting this application *prior* to embarking on research is to ensure that the highest ethical standards in research, conducted under the auspices of the EBE Faculty, are met. Please ensure that you have read, and understood the **EBE Ethics in Research Handbook** (available from the UCT EBE, Research Ethics website) prior to completing this application form: http://www.ebe.uct.ac.za/ebe/research/ethics1

| APPLICANT'S DETAILS | | |
|---|---|---|
| Name of principal researcher, student or external applicant | | Natalia Dambe |
| Department | | Geomatics |
| Preferred email address of applicant: | | Dmbnat003@myuct.ac.za |
| If Student | Your Degree: e.g., MSc, PhD, etc. | MSc |
| | Credit Value of Research: e.g., 60/120/180/360 etc. | 180 |
| | Name of Supervisor (if supervised): | A/Professor Julian Smit |
| If this is a researchcontract, indicate the source of funding/sponsorship | | N/A |
| Project Title | | Flood Modelling Using GIS and Remote Sensing Technology |

**I hereby undertake to carry out my research in such a way that:**

- there is no apparent legal objection to the nature or the method of research; and
- the research will not compromise staff or students or the other responsibilities of the University;
- the stated objective will be achieved, and the findings will have a high degree of validity;
- limitations and alternative interpretations will be considered;
- the findings could be subject to peer review and publicly available; and
- I will comply with the conventions of copyright and avoid any practice that would constitute plagiarism.

| SIGNED BY | Full name | Signature | Date |
|---|---|---|---|
| **Principal Researcher/ Student/External applicant** | Natalia Dambe | Signature Removed | 05 Feb 2018 |

| APPLICATION APPROVED BY | Full name | Signature | Date |
|---|---|---|---|
| **Supervisor** (where applicable) | Julian Smit | Signature Removed | **06 Feb 2018** |
| **HOD (or delegated nominee)** Final authority for all applicants who have answered NO to all questions in Section1; and for all Undergraduateresearch (Including Honours). | PROF T. BERTRAND Click here to enter text. | Signature Removed | 1/04/18 Click here to enter a date. |
| **Chair : Faculty EIR Committee** For applicants other than undergraduate students who have answered YES to any of the above questions. | | | |

Page 1 of 1

# Table of Contents

# Table of Figures

**List of Tables**

# List of Abbreviation

| | |
|---|---|
| 1D HEC-RAS | 1D Hydrologic Engineering Centers-River Analysis System |
| 1D MIKEII | One- Dimensional Système Hydrologique Européen |
| 2D | Two-Dimensional |
| AMSL | Above Mean Sea Level |
| ASCII | American Standard Code for Information Interchange |
| ASTER | Advanced Space borne Thermal Emission and Reflection Radiometer |
| AWS | Automatic Weather Station |
| CAPS | Convergence Ahead of Pressure Surges |
| CCHE2D | A two-dimensional Sediment Transport Sediment Model |
| CHIRPS | Climate Hazards Group InfraRed Precipitation with Station Data. |
| CMORPH | Climate Prediction Center Morphing Technique |
| CN | Curve Number |
| DEM | Digital Elevation Model |
| DTM | Digital Terrain Model |
| EC | European Community |
| ECMWF | European Center for Medium-Range Weather Forecasts. |
| EFAS | European Flood Awareness Systems |
| E-HYPE | Environmental Hydrological Prediction for the Environment |
| EPA | United States Environmental Protection Agency |
| Esri | Environmental Systems Research Institute |
| ESA | European Space Agency |
| EU | European Commission |
| FAO | Food and Agricultural Organization |
| Fdr | Flow Direction Grid |
| FFWS | Australian Flood Forecasting and Warning Services |

| | |
|---|---|
| Flow Acc | Flow Accumulation Grid |
| GeoSFM | Geospatial Stream Flow Model |
| GFT | GIS Flood Tool |
| GIS | Geographical Information System |
| GLAS | Geoscience Laser Altimeter System |
| GLOFAS | Global Food Monitoring System |
| GLOFFIS | Global Flood Forecasting and Information System |
| GRDC | Global River Discharge Database |
| HBV | Hydrologiska Byrans Vattenavdelning |
| HEC-GeoHMS | Geospatial Hydrologic Modeling Extension. |
| HEC-HMS | Hydrologic Engineering Center- Hydrologic Modeling System |
| HEFS | Hydrologic Ensemble Forecasting Service |
| HFAM | Hydrology Modeling System Health Facility Association of Maryland |
| HRU | Hydrologic Response Unit |
| HYDROTEL | Hydrology Modeling System |
| | IHACRES Identification of Unit Hydrographs and Component Flows from Rainfall, Evaporation, and Streamflow |
| InSAR DEM | Interferometry Synthetic Aperture Radar Digital Elevation System |
| InSAR | Interferometry Synthetic Aperture Radar |
| ISDR | International Strategy for Disaster Reduction. |
| IW | Interferometric Wide |
| LUVALUE | Land Use Value |
| MAP | Mean Areal Precipitation |
| MASDAP | Malawi Spatial Data Platform |
| MDWI | Modified Difference Water Index |
| ME | Model Efficiency |

| | |
|---|---|
| MLC | Maximum Likelihood Classifier |
| MoAIWD | Malawi Ministry of Agriculture, Irrigation and Water Development |
| MSS | Multi Spectral Scanner |
| NASA | National Aeronautics and Space Administration |
| NDWI | Normalized Difference Water Index |
| NIR | Near Infrared |
| NPTEL | National Program for Technology Enhanced Learning |
| NRLgeo | Naval Research Laboratory Geographic |
| NSE | Nash Sutcliffe Model Efficiency Coefficient |
| NWS | Unite States National Weather Services |
| PEPF | Percent Error in Peak Flow |
| PMIR | Passive Microwave-Calibrated Infrared Algorithm |
| RAS | River Analysis System |
| RSR | Standard Deviation Ratio |
| RVE | Relative Volume Error |
| SAR | Synthetic Aperture Radar |
| SBRE | Satellite-Based Rainfall Estimates |
| SCS CN | Soil Conservative Service Curve Number |
| SCS TR55 | Soil Conservative Service Technical Report 55 |
| SCS UH | Soil Conservative Service Unit Hydrograph |
| SLC | Single Look Complex |
| SLR | Sea Level Rise |
| SMA | Soil Moisture Accounting |
| SMHI | Swedish Meteorological and Hydrological Institute |
| SRTM | Shuttle Radar Topography Mission |
| SSURGO | Global Soil Survey Geographic Database |

| | |
|---|---|
| STATSGO | State Soil Geographic Database |
| SWAT | Soil and Water Assessment Tools Model |
| SWIR | Short Wave Infrared |
| SWMM | Storm Water Management Model |
| TM | Thematic Mapper |
| TMPA | TRMM Multi-Satellite Precipitation Analysis |
| TRMM | Tropical Rainfall Measuring Mission |
| UH | Unit Hydrograph |
| USGS | United States Geological Survey |
| VIC | Variable Infiltration Capacity |
| WATFLOOD | Hydrology Modeling System |
| WR | Water Resource |
| WRA | Water Resources Areas |
| WRU | Water Resource Unit |

# 1 Introduction

## 1.1 Background

Over the years people all over the world have been experiencing natural hazards. Natural hazards are natural phenomena that have high potential of harm to people, for instance, drought, volcano eruptions, wildfires, and floods, among others (Sørensen, et al., 2006; Wright, 2007). Floods are classified as natural hazards caused by extreme meteorological and hydrological changes that are influenced directly or indirectly by human activities within the environment (Langhammer, 2008; Els, 2011). Extreme floods have been identified as the most severe natural hazards that impact millions of people worldwide (Emerton, et al., 2016; Niekerk & Nemakonde, 2017; Langhammer, 2008;) due to their increase in magnitude and frequency (Langhammer, 2008). The severity of floods is proven in Figure 1-1, whereby among all-natural hazards, floods have the highest number of deaths (6.9 million) and homeless or displaced (123 million) people. Then followed by earthquakes (1.8 million).

The reoccurring floods have contributed to the greatest concentration of flood-risk hotspots in Sub-Saharan Africa (Niekerk & Nemakonde, 2017). Malawi is one of the developing countries in Sub-Saharan Africa whose economy and livelihoods has been greatly affected by flood occurrences. The country has experienced eight floods between 1967 and 2003 (Government of Malawi, 2015). Severe floods occurred in January 2012, January 2013 and January 2015. The 2015 flood was caused by the highest amount of rainfall ever recorded in Malawi making 1 in 500 year's events.

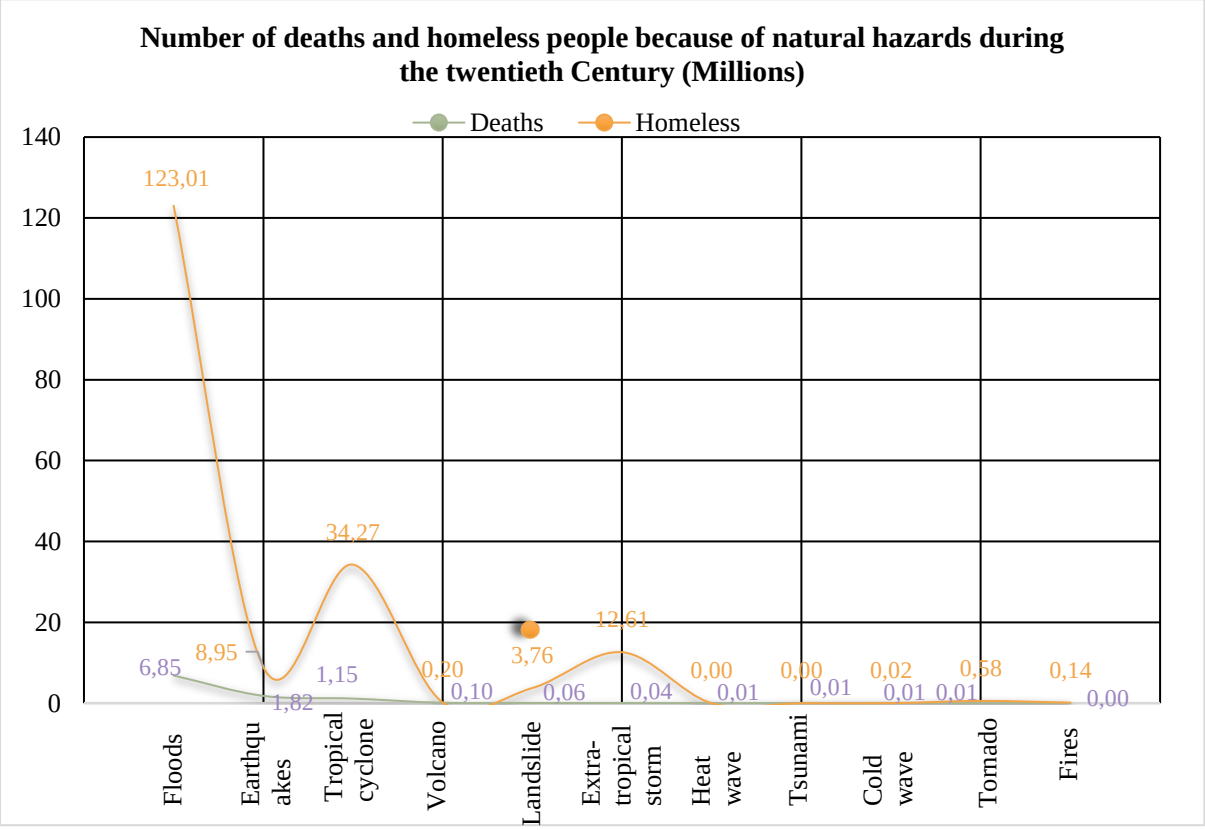


Figure 1-1: Graph showing the number of deaths and homeless people because of natural hazards during the twentieth Century (based on WHO, 2002) (Source: Bryant, 2005:9)

According to Post Disaster Needs Assessment (PDNA) report, in 2015 Malawi experienced floods that affected approximately 1.1 million people, displaced 230 thousand people and killed 106 people (Government of Malawi, 2015). The three major sectors affected by the flood included agriculture covering 47% of the total damage and loss, transport 35%, and 18% for sanitation and water (Government of Malawi, 2015). Some of the damage and loss figure estimates indicated in the 2015 PDNA report included 523, 347 houses, 1220.53 km roads, 183 Bridges, 15 hydrological stations and 4 Dams (Government of Malawi, 2015). The government of Malawi has thus declared 15 of 28 districts of the country's flood prone areas. The major impact of the flood is in the Southern region of the country (Government of Malawi, 2015).

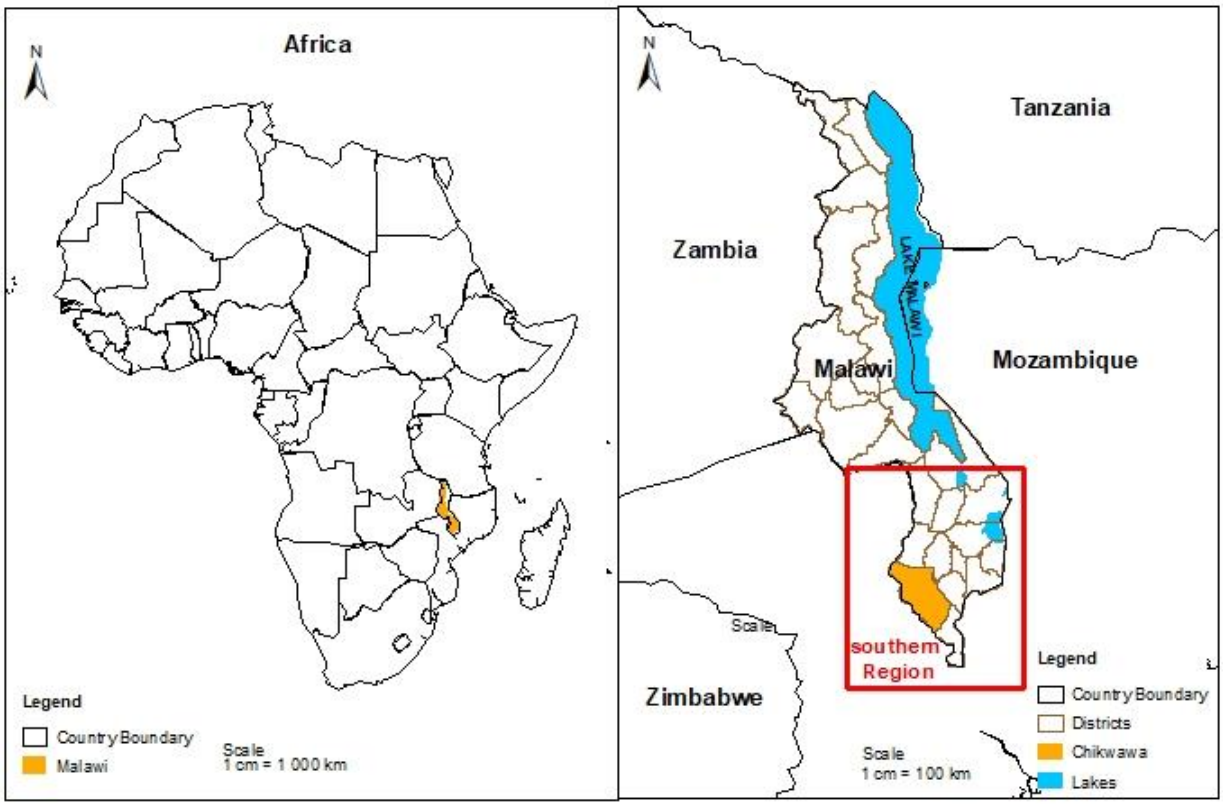


Figure 1-2: Map showing the Southern Region of Malawi

The Southern region (as shown in Figure 1-2) is the key agricultural region in the Malawi (Government of Malawi, 2015). The lake shore plains and lower shire valley are the most vulnerable area in the region. During the 2015 floods, Blantyre, Nsanje and Chikwawa districts in the lower shire valley had the highest damage (in terms of infrastructure, agriculture, and property) with percentage losses of 16.4, 16.4 and 14.3 respectively, and floods erode agricultural land causing smallholder farmers to produce low yields (Government of Malawi, 2015). Among the three districts, Chikwawa (4892 $km^2$ of Shire Basin) is rated the most vulnerable district because of the high exposure to climate variability and soil degradation that influences the occurrence of riverine floods (Adeloye, et al., 2015). The flood situating in Chikwawa district as of January 10 and 13, 2015 is shown in Figure 1-3 where the water extent in shown in blue color.

Therefore, this research applies remote sensing and GIS to model riverine floods of the Shire River in Chikwawa District to contribute to the development of flood risk management system to reduce the risk of floods in Chikwawa. The flood model is developed using meteorological records, hydrological data, land use data, and terrain data (DEM) to understand and analyze the trends of floods during the flood

period. Modeling flood is critical in ensuring well informed and sustainable flood risk management strategies to address the recurrent flooding problem (Wicks, 2016).

According to Wicks (2016). The model is visualized as flood maps to provide timely flood information and depict areas that are flooded or likely to flood, and the consequences of damage or the spatial distribution of the risk in relation to the time of occurrence. Thus, the maps assist in interpreting and understanding flood dynamics. Furthermore, provide reliable observations for well-informed flood response, preventive measures or support to the affected communities.

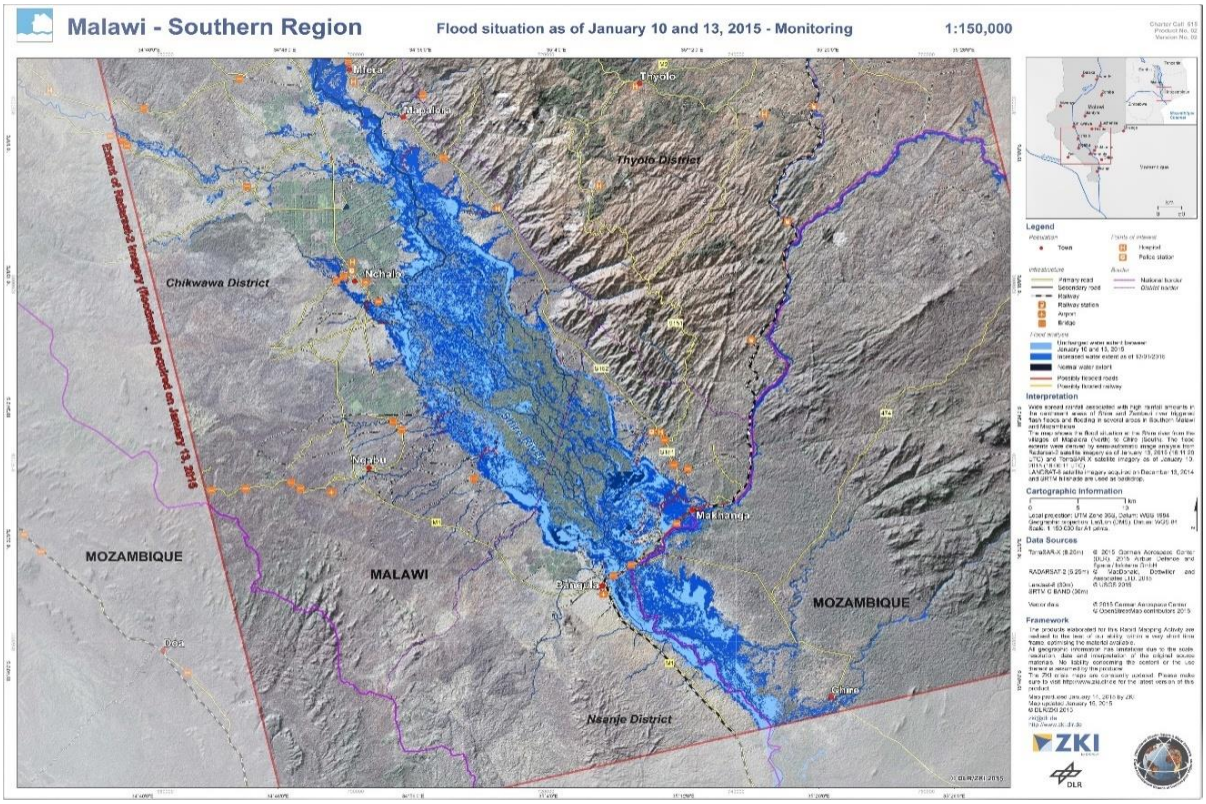


Figure 1-3: Flood situation as of January 10 and 13, 2015 (Source: TerraSAR-X / Landsat-8; Acquired: TerraSAR-X: 10/01/2015; Landsat-8: 13/12/2014 Copyright: TerraSAR-X © German Aerospace Center (DLR), 2015 Airbus Defense and Space / Infoterra GmbH Landsat-8 data and products© USGS (2015) - All rights reserved
Map produced by DLR/ZKI)

## 1.2 Problem statement

The communities in the Shire river basin, particularly in Chikwawa (Malawi) district are faced with the occurrence of floods. The most recent severe floods in the Shire river basin occurred in 2015. The flood frequency analysis of the Shire River in Chikwawa District Figure 1-4 shows that the year 2015

experienced the highest floods. The Global Disaster Alert and Coordination System (GFDS) site number 123 indicates that the highest river discharge measured in cubic meters per second ($m^3/s$) on 10, 11, 12, and 13 January 2015, with readings 13706 $m^3/s$, 14590 $m^3/s$, 13137 $m^3/s$ and 13027 $m^3/s$, respectively.

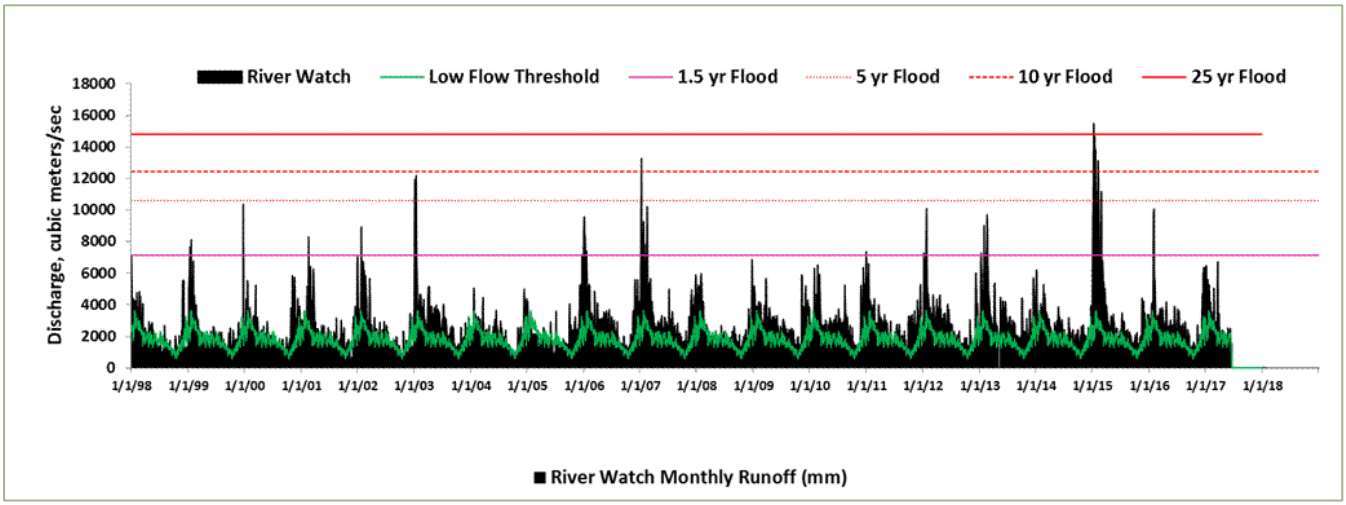


Figure 1-4: The flood frequency analysis, 1998 to 2015 (Source: http://floodobservatory.colorado.edu/SiteDisplays/1283.htm)

The floods caused damages to property, public infrastructure, agriculture and lives. Due to the damages, the affected people are more vulnerable, less resilient, and lack capacity to respond and adapt to floods (Department of Disaster Management Affairs, 2015). In order to minimize the damages caused by floods in Chikwawa, there is a need to develop flood risk management systems that reduce the impacts and the likelihood of flood occurrence. The flood risk management systems ensure sustainable ways of understanding and managing floods. This study analyses the riverine flood that took place in Chikwawa District through modeling and simulating the flood event for the month of January 2015 by: analyzing the hydrology of the catchment; estimating the extent and depth of the floods based on the developed model and simulations; visualization of the flood extent and risk using inundation maps and hydrographs; and to determine what comparison of hydrographs and inundation maps may reveal for proper establishment of flood risk management strategies.

## 1.3 Objectives

The overall objective of the study is to analyze the riverine flood by integrating remote sensing, GIS, and hydraulic and/or hydrological modeling to develop informed flood mapping for flood risk management, case study of Chikwawa District in Malawi.

The following specific objectives are employed to achieve the overall objectives:

1. To develop the hydrological model that integrates with GIS based on the physiographic properties of the watershed and terrain model:
    a. To calculate water loss and runoff due to the rainfall events during the simulation period
    b. To calibrate and verify the hydrological model parameters
2. Developing the hydraulic model that integrates with GIS to calculate the depth, extent, velocity of flooded water
3. Analyzing the risk of flood on different land uses.

## 1.4 Research questions

1. To what extent can application of low to medium resolution data (DEM, soil, land use) in a poor data environment like developing countries affect the accuracy of riverine flood modeling?
2. To what extent is the ability to model floods useful in data poor environment?
3. To what extents are the models fit to simulate acceptable flood flows and volumes?

## 1.5 Research assumptions

1. Floods in Chikwawa will reoccur and shall continue to affect the livelihoods, property, agriculture and the surrounding environment in Chikwawa.
2. There is a need for effective flood risk management systems for Chikwawa District to reduce the impact of reoccurring floods.
3. Remote sensing and GIS techniques are effective techniques to develop flood models, to determine and map the extent and depth of floods.
4. There are freely available datasets that meet data requirements for flood modeling.

## 1.6 Scope and limitations

This research develops flood models for informed flood mapping for flood risk management in Chikwawa District. Flood modeling consist of three main processes: the hydrological modeling to determine the basin characteristics and the extent of floods; hydraulic modeling to compute the depth of floods; and flood mapping visualized in GIS (Alaghmand, et al., 2010). Each of the fore-mentioned processes are dependent on data requirements and accuracy of the methods. The data used included freely available data, such as optical imagery and radar imagery, Digital Elevation Model (DEM) created from interferometry, Shuttle Radar Topography Mission (SRTM) DEM, stream data, soil type data, and rainfall data. Production of reliable flood maps facilitates accurate flood assessments and predictions (Danumah, et al., 2016). However, that is limited by the quality of data used (Matori & Lawal, 2014). According to Emerton, et al., (2016), high quality resolution data for flood plains in most parts of developing countries, including the Chikwawa district in Malawi are captured using high-resolution sensors. Contrariwise, high quality resolution satellite data are expensive. Rainfall and gauge station data are incomplete because some gauge stations are not fully functional. Nevertheless, free satellite data provide the alternative solutions. The free datasets include sentinel-1 and sentinel-2 radar, the Shuttle Radar Topography Mission (SRTM), Climate Hazards Group InfraRed Precipitation with Station Data (CHIRPS), Landsat data, Dartmouth Flood Observatory data. The use of freely available data shall require the combining of datasets from different sensors to improve the accuracy, and to narrow the sensing revisit time to improve temporal resolution for change detection analysis.

## 1.7 Research design

This research analyses the riverine flood that took place in Chikwawa District through modeling and simulating the flood event from the period of 1st January to 31 January 2015.

**Chapter 1:**

Chapter one introduces the background of floods from the global to local level. The local level is this context in Malawi. The introduction further describes the problem statement based on the frequency and magnitude of floods which have severe impact on the people and their environment in Malawi and the requirement of the flood management systems to reduce the impacts. The purpose of the research, the scope, limitations and the research design are also provided as part of the introduction.

**Chapter 2:**

Chapter two discusses related literature to help to develop the methods to achieve the objective of the research. The first part of the chapter discussed floods as a natural hazard, the characteristics of floods, how it is caused, its impacts, particularly the riverine floods, and flood management approaches that are applicable in various flood conditions. The other part of this chapter presented literature on the integration of flood modeling (hydrological and hydraulic modeling) with GIS and remote sensing.

**Chapter 3:**

Chapter three discusses data by analyzing data requirements and sources to conduct flood modeling. The analysis of data requirements focused on: the criteria to accept data for flood modeling, data needs to meet the flood modeling methods described in literature review, data sources (both international and national), the description of basic data set in some detail, and lastly, the data challenges faced due to the case study site location.

**Chapter 4**

Chapter four provides the description of the case study area where the selected methods and theory are tested. The case study area is Chikwawa District in Malawi. The description of the case study consists of the reason why the area was chosen, its characteristics in respect to data and flood parameters.

**Chapter 5:**

Chapter five includes system design, technical and analytical methods of flood modeling considering: the availability and accessibility of data, the purpose of the research, time of flood occurrence, and the usability and availability of the models chosen.

**Chapter 6**

The chapter discusses the results obtained from running the flood models. The expected results are the estimated extent, depth and velocity of floods. Then the results are evaluated and discussed about the research purpose and literature from researchers who conducted similar research.

**Chapter 7**

The chapter explains the conclusions drawn from the whole research with reference to other factors such as research methods, data used, areas of study, and analytical results. Recommendations have also been provided to give directions for future research.

# 2 Literature Review

## 2.1 Introduction

The literature review is composed of two main parts. The first part presents flood as a natural hazard that is defined as a natural phenomenon or event that poses danger to people or the environment. The danger caused by natural hazards is referred to as natural disasters. Natural hazards are categorized in three classes: biological, geological and hydro-meteorological. Examples of each category are outlined with statistics backing up their impacts. One of the examples is flood. Flood is categorized under hydrological and meteorological natural hazard. Flood is reviewed as the top most natural hazard causing death worldwide. The statistics shows that Malawi is among the list of top 10 countries in the world affected by floods. The literature review chapter has discussed floods further based on the probability of occurrence, its characteristic, causes and impact, and flood management approaches.

The second part of this chapter reviews flood in connection with flood modeling. Modeling is a process of representing the abstract or reality of flood. The two models of floods discussed are hydrological and hydraulic models. Literature reviews that hydraulic and /or hydrological modeling can be integrated with GIS and remote sensing through: (1) embedding GIS in the hydrological/hydraulic model, (2) embedding hydrological/hydraulic model in GIS, (3) loose coupling, and (4) tight coupling. The literature review chapter is concluded by looking into flood visualization and discussions on mapping the extent, depth, velocity and risk of floods to meet various requirements of different users such as decision makers and community members.

## 2.2 Natural hazards

Natural hazard is "when unpredictable natural events become extreme in their occurrence and constitute a danger to humans and to the other members of the environment" (Schramm & Dries, 1986: 43). Similarly, the International Strategy for Disaster Reduction-ISDR (2002) defines a natural hazard as natural processes or phenomena occurring in the biosphere that may constitute a damaging event. The damage caused by natural hazard is called "Natural disasters" (ISDR, 2002: 4). According to literature, natural hazards are categorized based on their causes, magnitude and duration (Bryant, 2005; Els, 2011; Sørensen, et al., 2006; Schramm & Dries, 1986). Bryant (2005) categorized natural hazards as chronic and periodic hazards. The chronic hazards are a result of human activities or global warming, and may include soil degradation, melting of permafrost, and desertication. The periodic hazards on the other

hand, are large size events that occur over a small period with massive impact. Good examples of periodic hazards include floods, earthquakes, Tsunami, and Volcanic eruptions.

The main categories or types of Natural hazards are geological, biological, hydro-meteorological hazards (Els, 2011; Bryant, 2005; Sørensen, et al., 2006; Vos, et al., 2010; Guha-Sapir, et al., 2016).

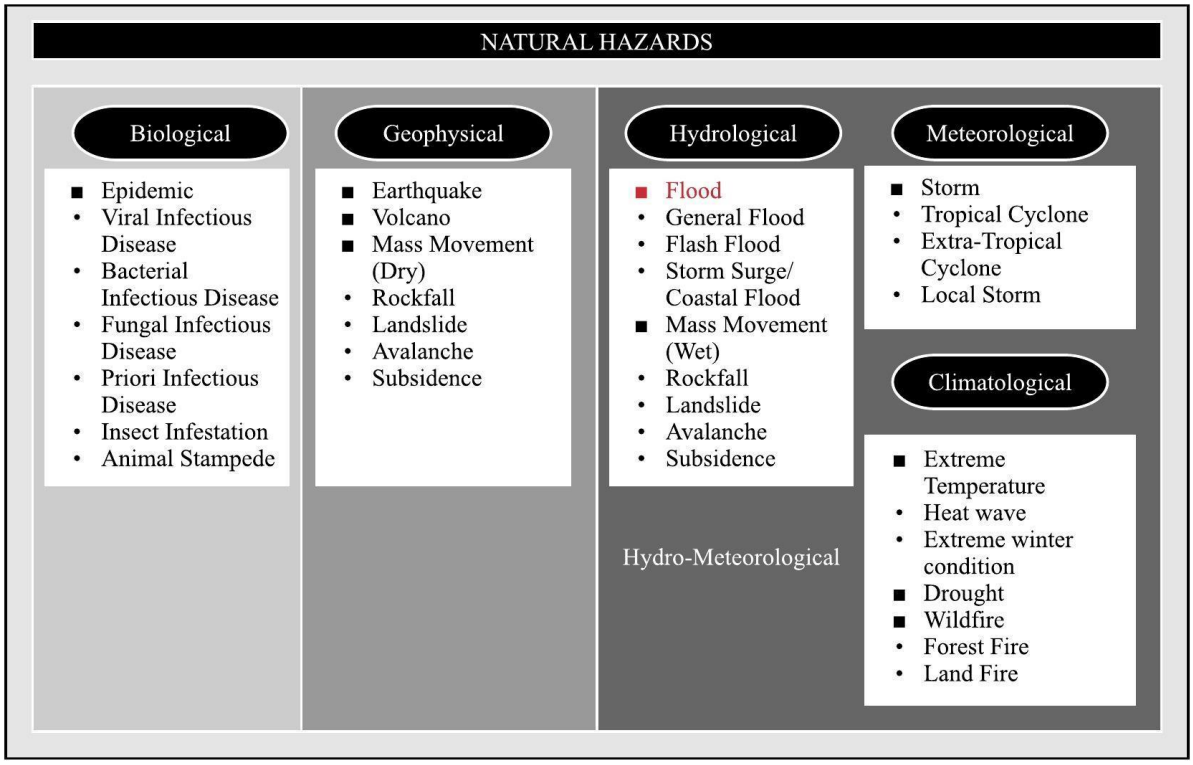


Figure 2-1: Categories of Natural Hazards (Source: Vos et al., 2010: 7)

The categories of natural hazards are discussed below (Sørensen, et al., 2006) and indicated in Figure 2-1:

1. The biological hazards involve biological or organic processes including biological vectors, exposure to pathogenic micro-organisms, toxins and bioactive substances;
2. The geological or geophysical hazards include natural earth processes such as earth mass movement;
3. The hydro-meteorological hazards include atmospheric, hydrological or oceanographic processes that may cause disasters.

Vos et al. (2010) subdivides hydro-meteorological category into three classes: meteorological, hydrological and climatological hazards. These classifications and their example are shown in Figure 2-1

### 2.2.1 Disasters and their impacts

Literature reviews that natural hazards can be beneficial to people. For instance, Bryant (2005) argues that volcanoes provide rich soils to grow three kinds of crops in one year in the tropics, and floodplains provide fertile soil and easy access to water supply for agriculture.

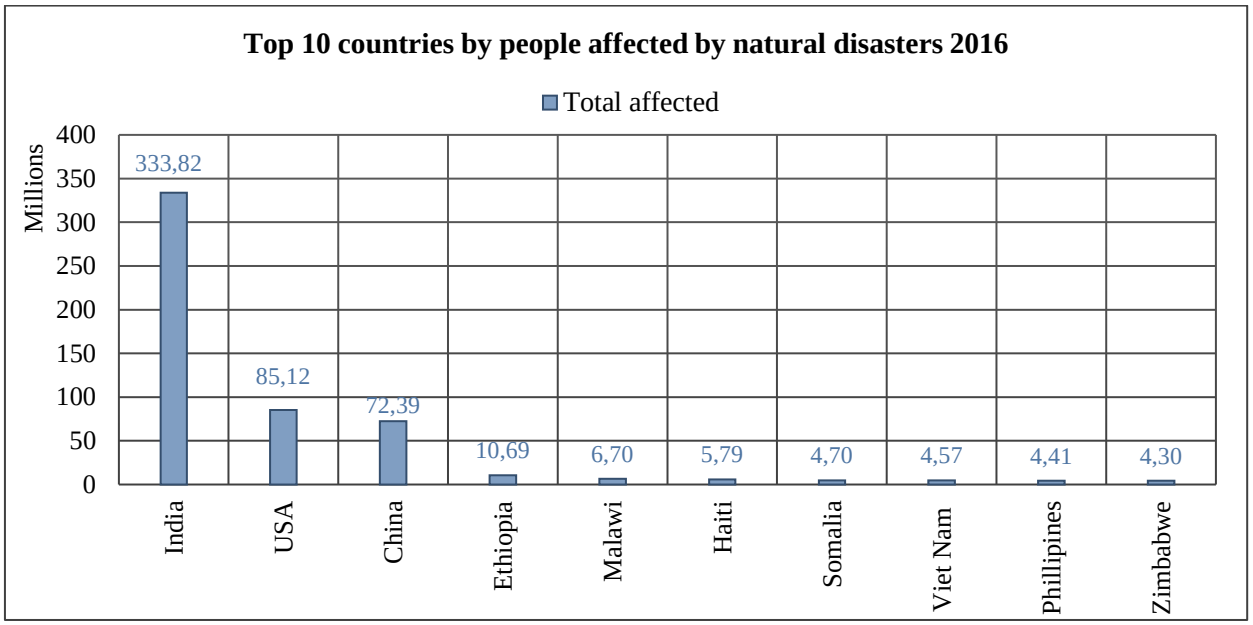


Figure 2-2: Top 10 countries of people affected by natural disasters 2016 (Source: Guha-Sapir et al., 2016: 24)

Despite the proven benefits of natural hazards, the catastrophic impacts of natural hazard cannot be overemphasized as many people in different parts of the world have been greatly affected by natural hazards. The world top 10 countries affected by natural hazards are presented in Figure 2-2. Figure 2-2 shows that India has the highest number of approximately 333 million affected people, followed by United States of America (USA) with approximately 85 million. Malawi has approximately 6.7 million and ranks fifth on the top 10 list of number of people affected in 2016 worldwide.

The number of people affected by disasters as a percentage of their total population is presented in Figure 2-3. According to the Radar Chart represented in Figure 2-3, Micronesia has the top most percentage of people affected by disasters with 95.24%, second by Haiti with 53.42%. Malawi ranks number seven with 37.05 %.

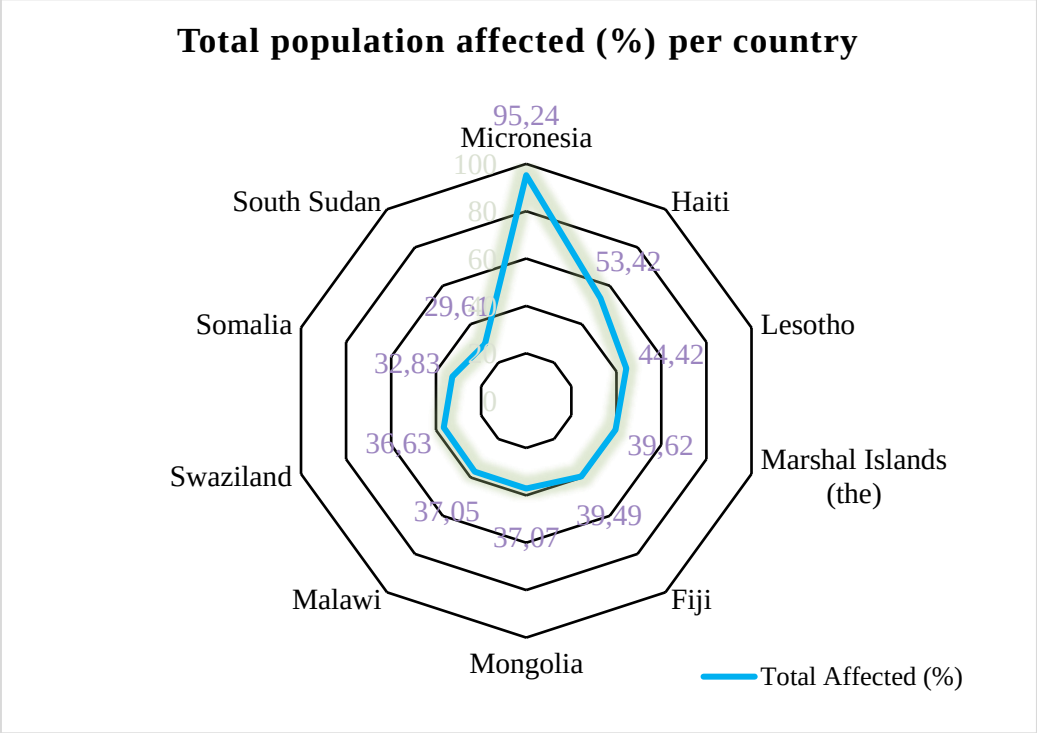


Figure 2-3: Radar chart showing top 10 list countries with the number of people affected by disasters as percentage (%) of their total population (Source: Guha-Sapir et al., 2016: 24)

The most known hazards to cause severe disasters in Africa from 1994 to 2003 are epidemics (329), floods (269), and drought (116), as shown in Figure 2-4.

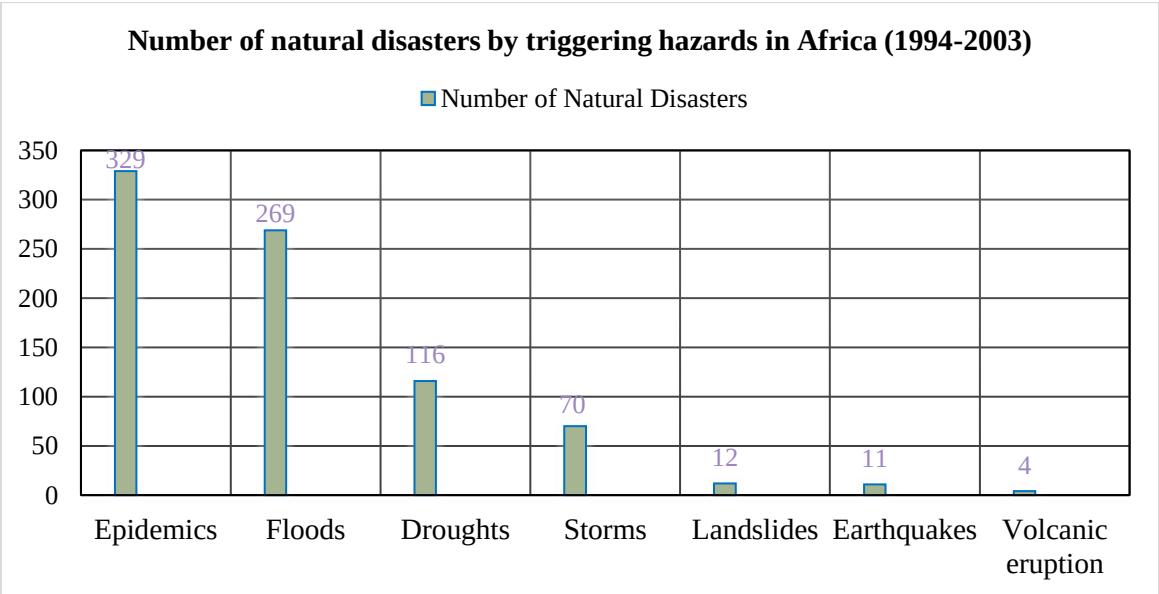


Figure 2-4: A graph showing number of natural disasters by triggering hazards in Africa (1994-2003) (Source: Sørensen et al., 2006: 19)

The most affected countries in Africa include Nigeria, Burkirna Faso, Niger, Tanzania, Sudan, Malawi, Kenya, Ethiopia, Zimbabwe, and Mozambique (Sørensen, et al., 2006) . In the period between January to December 2016, Ethiopia, Malawi, Somalia, South Sudan and Zimbabwe are among the top 10 list of countries in the world with most people affected by natural disaster (Guha-Sapir, et al., 2016). Among the five, Ethiopia has the highest number of 10.2 million, followed by Malawi 6.7 million, Somalia 4.7 and Zimbabwe 4.3 million, and South Sudan 3.6 million (Guha-Sapir, et al., 2016). These five countries are also classified as low-income countries (Guha-Sapir, et al., 2016).

The hazard statistics of the number of deaths and homeless worldwide as per Figure 2-3, and the numbers of people affected as per Figure 2-2 and Figure 2-3 call for attention to flood management systems in order to minimize their severity to people and the environment.

## 2.3 Floods

There are many definitions of floods including:

a) " Water overflowing onto land that is usually dry" (Doswell III, 2003: 769; Doocy, et al., 2013: 2)
b) "The presence of water in the areas that are usually dry" (Jonkman & Kelman, 2005: 75)
c) "A significant rise of water level in a stream, lake, reservoir or coastal region" (Chan, 2017: 97)

This research accepts all of the above definitions. See images in Figure 2-5 depicting floods.


Figure 2-5: Overflowing of water in areas that are dry in Chikwawa District at a Trading Centre (left), and Shire River (right)

### 2.3.1 Probability of flood

The probability of flood occurrence is computed from frequency analysis of a given flood event (Els, 2011). The frequency analysis is a statistical technique through determination of the recurrence interval. The recurrence interval is expressed as the number of years, T. The probability of occurrence is the inverse of T and it is represented 1/T (Els, 2011). The rainfall recurrence interval relies on the size and the length of a rainfall event while the streamflow relies on the measure of the annual peak flow (USGS, 2018). Examples of recurrence intervals are provided in Table 2-1.

The flood that occurred in Chikwawa in January 2015 is regarded as 1 in 500 years (Department of Disaster Management Affairs, 2015). 1 in 500 years means that there is one probability of occurrence of flood event to happen 500 years, and the percentage chance of occurrence is 0.2 % (Els, 2011).

Table 2-1: Recurrence intervals and probabilities of occurrence (Source: USGS, 2018; Els, 2011)

| **Recurrence Interval, in Years (T)** | **Probability of Occurrence in any given year (1 in T)** | **Percent chance of occurrence in any given year (1/T * 100)** |
|---|---|---|
| 500 | 1 in 500 | 0.2 |
| 100 | 1 in 100 | 1 |
| 50 | 1 in 50 | 2 |
| 25 | 1 in 25 | 4 |
| 10 | 1 in 10 | 10 |
| 5 | 1 in 5 | 20 |
| 2 | 1 in 2 | 50 |

### 2.3.2 Flood prone areas

Areas that are vulnerable or most likely to floods are flood prone areas and include the floodplains and the floodways (Els, 2011). The floodplains are all areas covered with water surrounding the river during floods. There is no absolute boundary for floodplain since it varies in size depending on the level of water that floods (Els, 2011). During floods, those areas with high flow velocity, deep water levels and debris flow can be associated with floodway (Els, 2011). The floodplain and floodway are demarcated by a flood line that indicates areas that are most likely to be affected by flood. The flood lines are given the water level and annual exceedance probability of a flood occurrence (Alexander, 2000).

### 2.3.3 Causes of floods

Floods are caused by various factors. These factors can be categorized as natural causes and man-made causes. Niekerk & Nemakonde (2017) explained that the major causes of natural hazards in the Sub Saharan region are changes in weather patterns. In 2015 to 2016, the countries in Sub Saharan region,

including Malawi experienced extreme El Nino, which caused droughts and flood disasters in the region (Niekerk & Nemakonde, 2017). However, there are also many other factors contributing to floods in Sub Sahara Africa and all parts of the world. A summary of causes and their factors contributing to flooding are outlined below.

### 2.3.4 Man-made factors:

a) Heavy rainfall as a result of reduction in vegetation cover and high rate of urbanization that leads to high runoff.
b) Retardation of flow and back water effects because of lack of drainage capacity and urbanization in low lying areas.
c) Poor natural drainage as a result of the high rate of human activities that puts pressure on the drainage systems.
d) Common floods in the main and tributary rivers due to breaking of bunds constructed on the tributary rivers for irrigation purpose.
e) Flow obstruction in river banks caused by construction activities along the river banks.
f) River bank erosion caused by little or no vegetation cover because of careless cutting down of trees.
g) Inadequate capacity within the banks because of high discharge of the rivers due to silting.

### 2.3.5 Natural factors of floods

There are many natural factors that influence the riverine floods. Among the factors include (Disaster Management, 2015):

a) High precipitation that causes heavy rainfall and cyclones thus leading to floods as a result of increased overland flow and reduced lag times. While gentle rains over a long time easily infiltrate into the ground.
b) Topography and obstruction of natural drainage that retards the flow and back water effects. While steep slopes increase the flow and runoff, thereby increasing overland flow.
c) The type of soils also matters in terms of flow of water. Shallow soils do not absorb much water because of small storage capacity and that increases overland flow and vice versa. The same applies to impermeable rocks that prevent groundwater flow and encourage through flow and overland flow.

d) Other natural causes include landslides causing changes in the river course, earthquakes loosening the soil to cause siltation, and falling of the trees thus obstructing flow, among others.

*Causes of 2015 floods in Malawi*

High precipitation is one of the natural factors outlined in section 2.3.5 that directly causes heavy or extreme rainfall. Bryant (2005) described heavy rainfall that occurs in few days as a collision of very unstable air with high humidity air (also called orographic uplift). The collision usually occurs near warm oceans, or around steep high mountains in the direction of moist winds, or in areas prone to understorms (Bryant, 2005). Bryant classifies heavy rainfall that last several days as a product of tropical cyclone, while those that last many weeks to months as a product of seasonal monsoon rainfall or persistence of orographic uplifts. The tropical cyclones are "intense cyclonic storms that originate over warm tropical seas", and it causes three main hazards, namely surge, wind and rain (Bryant, 2005).

The 2015 floods in Malawi were caused by extreme rainfall associated with heavy rainfall (Government of Malawi, 2015). The extreme rainfall occurred between the month of January to March 2015 and it mostly affected the southern region of the country particular along Shire River Basin (Government of Malawi, 2015). The high magnitudes regional floods that occurred in 2015 in Malawi is regarded as "disaster of national or international importance" (Bryant, 2005). According to the UNDAC report on 6$^{th}$ February 2015, the flood affected approximately 1.1 million people, displaced 230 thousand people and killed 106 people, and 172 people were reported missing. The effects of floods on livelihood indicates implications and cost of floods on livelihood. Thus, the need to put in place measures to reduce the effects of floods.

### 2.3.6 Factors influencing severity of riverine floods

The severity of riverine floods is influenced by (a) the characteristics of the basin, (b) drainage network and (c) river channels, as discussed below (Els, 2011).

*a) The basin characteristics*

The basin characteristics are slope, area, altitude, and shape. These characteristics can influence flood. For instance, basins with small area have less runoff that makes water accumulate easily and cause floods, the elongated basins on the other hand have more runoff that influence water to accumulate after a long time. Basins with circular shape are prone to flooding because of surface runoff arriving at the same point

at the same time. This also applies to basins with steep slopes which increases the likelihood of flooding because of less infiltration.

*b) Network characteristics*

The network characteristics include pattern, bifurcation ratio, under drainage and channel length. Some of the factors of network characteristics that can influence flooding are patterns that are complex and slow water absorption into the ground, thus increasing the chances of flooding because of increase of water stored on the surface. If the soil or rock is less permeable, it allows less water drainage, hence contributing to flooding. Again, the decrease in the bifurcation ratio (the ratio between numbers of streams in two sequential hierarchies of basin) causes a high concentration of water flow in one river thereby making the river most susceptible to floods.

*c) Channel*

The channel consists of three characteristics, namely: slope, flood control, and river regulation work. All these characteristics affect the speed and direction of water, which impacts the flow velocity and energy. Similarly, the roughness characteristics of a channel influences the flow resistance of the river and consider adjustment of Manning values. The roughness characteristics include cross-section irregularities, channel variation, obstruction, and channel vegetation.

The natural channels have two categories, namely lower and higher gradient natural channels. The higher gradient is more complex than the lower gradient, thus it requires more parameters. Basic data for higher gradient are river discharge (Q), area of rivers, river velocity ($S_F$), Froude number, water slope ($S_W$), hydraulic radius (R), hydraulic depth, Manning n-value, predicted n- value, bed material size ($d_{S4}$).

The flow resistance of natural overbank is determined from considering:

i. The amount, type, density, and type of vegetation using land classification data acquired from satellite imagery.
ii. Surface roughness and bed material on-site survey
iii. Flow depth on-site survey
iv. Flow velocity computations
v. Obstruction (Roads, fences, etc.) aerial photograph, field verification
vi. Surface irregularities (sediment ridges, old meander scars, potholes).

The agriculture overbank considers the same parameters as natural overbank plus the typical growing or stages of growing seasons acquired from literature and/or aerial photographs.

### 2.3.7 The characteristics of floods

Floods are composed of characteristics or criteria to determine the danger of impact of floods. The higher the energy of water movement during floods, the higher the speed of water, thus the higher the potential for the flood water to cause damage (Doswell III, 2003). The degree of impact is affected by the duration, frequency, scale, and magnitude of floods (Llantwit School, 2010).

The University of Wisconsin established four characteristics of floods which are (Disaster Management, 2015):

a) Velocity: When flow velocity is high the eroding power of water increases and can sweep away vegetation or destroy land or structures.
b) Water depth: High depth of water immerses land which can have effects on vegetation survival and danger to property.
c) Rate of rise: Rate of rise is linked to the rate at which water depth increases. The higher the rate of rise the higher the water depth.
d) Seasonal: Floods normally occur during the crop growing season as a result of heavy rains and can easily affect agriculture.

### 2.3.8 Impacts of flooding

For the longest time in history floods have affected people globally. Doocy, et al. (2013) estimated that on a global scale there were 539 811 fatalities, 361 974 injuries, and 2 821 895 000 people displaced as a result of flood between 1980 to 2009. Based on global exposure analysis of floods, an amount of 24 billion dollars was spent annually strictly on floods from 2001 to 2011 (Winsemius, et al., 2018.).

The impact of floods can be both positive and negative (Els, 2011; Doswell III, 2003). Example of the positive impact that encourage people not to relocate to safer areas are: fertile soil in flood plains along the rivers, usage of water for domestic purposes, flat plains conducive for settlement, and water transport (Els, 2011; Doswell III, 2003).

The negative impacts of floods include the damages that floods cause on people and the environment as a result of uncontrollable movement of water that immerse or/and wash away trees, agricultural land,

community property, and infrastructure, among others. Figure 2-6 below captured effect of flooded water on vegetation in Chikwawa District.

Figure 2-6: Flooded water immersing crops (left), and causing trees to dry because of water saturation (right)

In general, more about the negative impacts of floods on people and the environment are as follows (Els, 2011; Disaster Management, 2015):

a) Human loss
b) Loss of property
c) Economic and social disruption
d) Increase in air and water pollution
e) Disruption of public infrastructure like roads, schools
f) Health problems due to spreading of waterborne communicable diseases like Cholera, Diarrhea
g) Damage to ecosystems
h) Damage to agricultural land, crops and livestock.

The impacts mentioned above can be reduced or prevented if effective flood management approaches are put in place.

### 2.3.9 Flood management approaches

Despite the tremendous impact of floods, floods cannot be absolutely controlled, rather can be managed to minimize losses caused by floods (Disaster Management, 2015). The ideal flood management strategies include (Disaster Management, 2015):

a) Modifying the floods using physical measures such as development of embankments, detection reservoirs, and channel and drainage system improvements.
b) Modify the susceptibility to flood damage through the implementation of activities that minimize the vulnerability of property to floods particularly in flood prone areas. For instance, flood mapping, coastal zone management, land use planning (Llantwit School, 2010).
c) Modify the loss of burden through action that compensates the loss to the entire community. The action may include immediate rescue and relief efforts such as provision of food, shelter, sanitation, and long-term reconstruction (Llantwit School, 2010).
d) Bearing the loss which involves accepting the floods and living with it.

## 2.4 Integration of GIS, remote sensing and hydrological modeling

Over the years, various researches have indicated that integrating hydrological models, hydraulic models and Geographical Information Systems that includes computer models, digital data, satellite images and good network observation, constitute a reliable flood management system (Els, 2011; Feldman, 2000; Abushandi & Merkel, 2013; Abdou et al., 2018; Cabral et al., 2015;Tong et al., 2017). According to ShahiriParsa, et al. (2016) computer modeling is the most efficient tool with the least possible cost to study and provides capabilities to simulate the behavior of the complex rivers during floods. Advancements in remote sensing and GIS techniques utilizes computer modeling and are important in data acquisition, management and analysis to improve flood modeling approaches. The current flood models integrate GIS to improving the analysis and visualization of complex flood scenarios (Emerton, et al., 2016).

### 2.4.1 Remote sensing

(National Academy of Sciences-U.S. (1973) and also cited by Campell (2002) described remote sensing as "*the joints of employing modern sensors, data processing equipment, information theory and processing methodology, communications theory and devices, space and airborne vehicles, and large – systems theory and practice for the purpose of carrying out air or space surveys of the earth."* The air or space survey has evolved from mounting a camera or sensor on balloons (1859) to kites (1880) to pigeon (1903) to airplanes (1908) and to satellite sensors (1970s to current date). The satellite remote sensing brought about global earth observation systems in 1990s. For instance, medium resolution LANDSAT launched in 1972, high resolution WorldView 2 launched in 2009 with 46cm panchromatic resolution and 184cm multispectral resolution, and 100cm resolution IKONOS, among others.

The acquisition of remotely sensed data has provided researchers, organizations and different users reliable information about the earth surface that is applicable in management, mapping, monitoring, modelling in different sectors such as land use management, geology, mining, and hydrology, among others.

## Uses of remote sensing in hydraulic and/ or hydrological modeling

Remote sensing has great potential in hydrological remote sensing, particularly satellite remote sensing because its application is cost effective as compared to field surveys (Thakur, et al., 2017). Two integral parts of satellite remote sensing described by Thakur (2017) include optical, hyperspectral, and microwave remote sensing. Optical remote sensing allows observing and measuring information in remote areas. However, the optical remote sensing has limited penetration capabilities of energy radiation into the earth's surface because is made of the visible and thermal domain. Examples of optical remote sensing include Sentinel 2, Landsat: multi spectral scanner (MSS); Thematic Mapper (TM). The hyperspectral remote sensing is advanced in detecting and recording targeted areas or object because the sensors use more than 100 spectral bands across visible and medium infrared domains. The level of detail in hyperspectral data makes it applicable to detect changes in vegetation, water, and soil (Thakur, et al., 2017).

Microwave remote sensing provides radar images that are created from the backscatter signal of emitted pulses. Radar systems are advantageous because the radar pulse can penetrate cloud cover, thus ideal for flood detection. In addition, remote sensing system has the capabilities of weather radar measurements like rainfall; and can measure small changes in elevation using interferometry synthetic aperture radar (InSAR).

## Errors in remote sensing

Remote sensing as any other technique is subjected to errors and uncertainties (Ameta, 2015). Ameta (2015) classified remote sensing errors as positional and classification errors. Lunetta et al. ( 1991) identified the potential sources of errors in the data process flow during the integration of remote sensing data into GIS. The results by Lunetta et al. (1991) and discussions by Thakur et al. (2017) give more details on remote sensing errors and their sources.

Errors and their sources by Lunetta et al and Thakur et al. are as follows:

a) Data acquisition errors: the errors can be caused by atmospheric conditions, natural variability of landscape, geometrical aspects, sensor systems, sensor platform instabilities, limited ground control points for accuracy assessment, and image and relief displacement due to lack of scene consideration.
b) Data processing errors due to data conversion and geometric rectification.
c) Data analysis errors caused by: assumptions of independence measure of parameters and error variance in quantitative analysis, classification system as a result of mixed classes, transition zones poorly defined or ambiguous class definition, human subjectivity, lack of compatibility between different classification systems, and data generalization.
d) Final product presentation errors that are introduced as geometric errors from base maps with different scales, different national horizontal datum in the source materials, and different minimum mapping units.
e) Data conversion errors, for example raster to vector and vector to raster conversion.

### 2.4.2 GIS

Escobar et al. (2008) argues that GIS is difficult to define because it represents the integration of many fields. Escobar et al. and; (Mekni, 2010) adopt the widely recognized definition of GIS formed by the National Centre of Geographic Information and Analysis:

*"GIS is a system of hardware, software, and procedures to facilitate the management, manipulation, analysis, modelling, representation and display of georeferenced data to solve complex problems regarding planning and management of resources."*

The era of GIS starts from the 1854 (GISGeography, 2018). The pioneering era of GIS was from 1960s to about 1975 (GISGeography, 2018). This era is called the pioneer period. It is during this period that GIS was the broadly accepted and for the first time fully functional at Canada Geographic Information System (Tomlinson, 2012; Khosrow-Pour, 2018). Since 1963, GIS was used for analysis of Canada Land Inventory data and production of statistics to develop land management plans (GISGeography, 2018; Tomlinson, 2012). It was in the mid-1960s when GIS functionalities were extended to combine spatially-referenced data, spatial models and visualization (Khosrow-Pour, 2018).

Ian McHarg who lived from 1920 is 1981 is one of the pioneers to be the "Father of GIS" and the "Father of map overlays" (Waters, 2010). The map overlays transformed the face of GIS. McHarg's map overly allowed to create master overlay for comparison of land cover, aquifer recharge, flood plains,

streams, slope, and impervious soils (McHarg & American Museum of Natural History, 1971). The master overlay highlighted intrinsic natural features such as flood zones and wetlands. Example of map overlay is shown in Figure 2-7 where land and water features are overlaid. The map overlay method allowed limitless combination of mapable attributes for simple representation of the earth's surface and its features (McHarg & American Museum of Natural History, 1971). McHarg's map layering concept (see Figure 2-7) is composed of four "Ms" namely Measurement, Mapping, Monitoring, and Modeling.

The second era is the mid-1970s to the early 1980s and it is referred to as the government-funded experimental research period. During this period the concepts and software developments were carried out within academia, government agencies, and industry.

The commercial period followed, between early 1980s to late 1980s. It was during the commercial period that GIS software was more utilized in both government and commercial organizations, and widely applied in transport and facility planning and management, cadastral systems, agriculture and the environment, the forestry and civil engineering sectors. The first commercial GIS software called ARC/INFO was released during this period in 1982 by Esri.

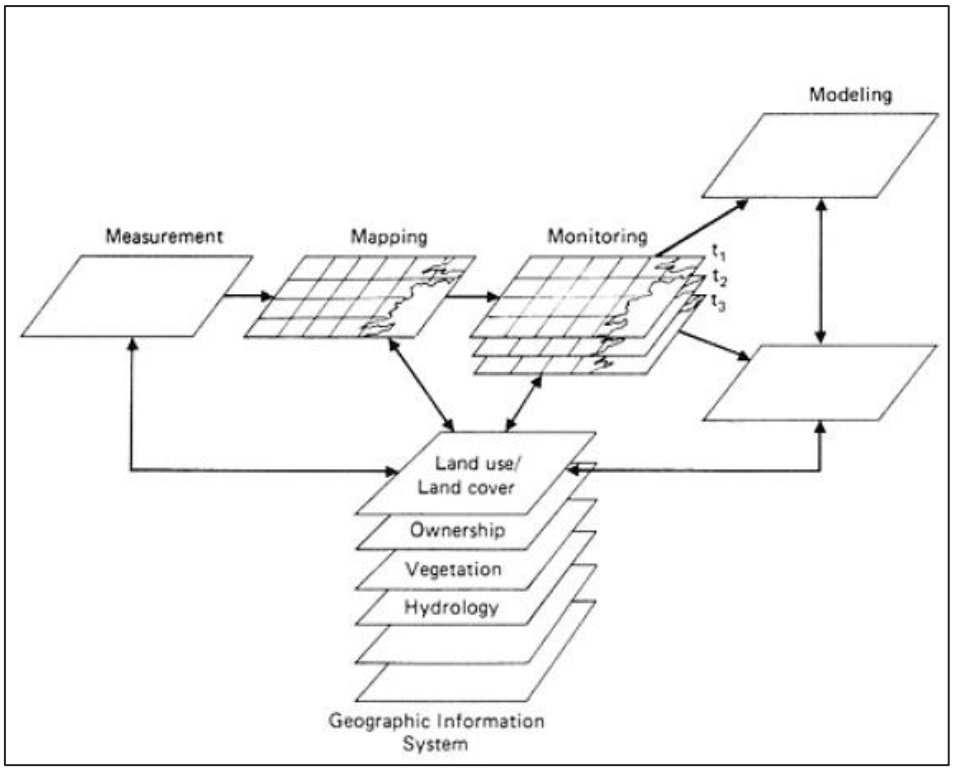


Figure 2-7: McHarg's map layering concept (Adapted from McHarg & American Museum of Natural History, 1971)

The end the 1980s to the mid-1990s forms the period of user dominance and interaction. GIS was most employing analysis. There was significant progress of GIS vendors and improvements from a command line interface to graphical user interface (GUIs), and continual developments in computer hardware and commercial operating systems. The user had capabilities to sort, select, extract, reclassify, re-project and display data based on complex geographical, topological and statistical criteria (Brovelli, n.d.). More advancements in GIS proceeded from 2005 to current date, where crowdsourcing and social networks have influenced the capabilities of computing technology. Now it is a universal world of volunteer GIS, of the Spatial data Infrastructure inspiring information flow (Brovelli, n.d.), web-based mapping and mobile GIS, cloud computing and big data. People have access to freely available GIS software such as Google Earth, OpenStreetMap, QGIS, saga GIS, among others.

## The role of GIS within hydrological and hydraulic modeling

GIS has many functionalities that encourage the integration of GIS with hydrological and hydraulic modeling (Thakur, et al., 2017). Some of the general roles provided by Djokic (2015) include speeding up the model running process. The GIS functionalities are:

a) Pre-processing of spatial depth before importing it into the hydraulic model (Djokic, 2015)
b) Creation of digital terrain models (Djokic, 2015)
c) Calculation of watershed characteristics (Djokic, 2015)
d) Image overlaying (McHarg & American Museum of Natural History, 1971)
e) Network analysis (Esri, 2012)
f) Database management (Thakur, et al., 2017)
g) Visualization of results (Esri, 2012; Djokic, 2015)

## Integration of GIS into hydraulic and/or hydrological modeling

Originally, in 1960s and 1970s GIS and hydrological modeling were developed and employed in isolation and with minimal interaction with each other (Sui & Maggio, 1991). Sui & Maggio (1991) review that the integration of GIS with hydrological modeling is a recent innovation that took better shape in the 1980s to improve the analytical capabilities of GIS. During that time, GIS powerful capabilities to process Digital Elevation Model (DEM) for hydrological modeling provided a new technique for data management and visualization. The integration of GIS with hydrological modeling allowed hydrologists to obtain accurate digital representation (Sui & Maggio, 1991), fast production of results, and reduced model simulation time (Thakur, et al., 2017).

The GIS integration methods keep developing over time (Thakur, et al., 2017). Kopp (1996) states that there are three general approaches to GIS model integration, which are: GIS based modeling, data bridge and embedded. While Els (2011), Sui & Maggio (1991), and Thakur et al. (2017) present four integration approaches, namely: (1) embedding GIS in hydrological modelling, (2) embedding hydrological modeling in GIS, (3) loose coupling and (4) tight coupling. The approaches by Kopp have the same general concepts as the approaches discussed by Sui & Maggio, Thakur, and Els. For instance, data bridge is similar to loose coupling, embedded code agrees with embedding GIS in hydrological modeling, and GIS-based modeling with tight coupling. The approaches are described below, including their advantages and disadvantages.

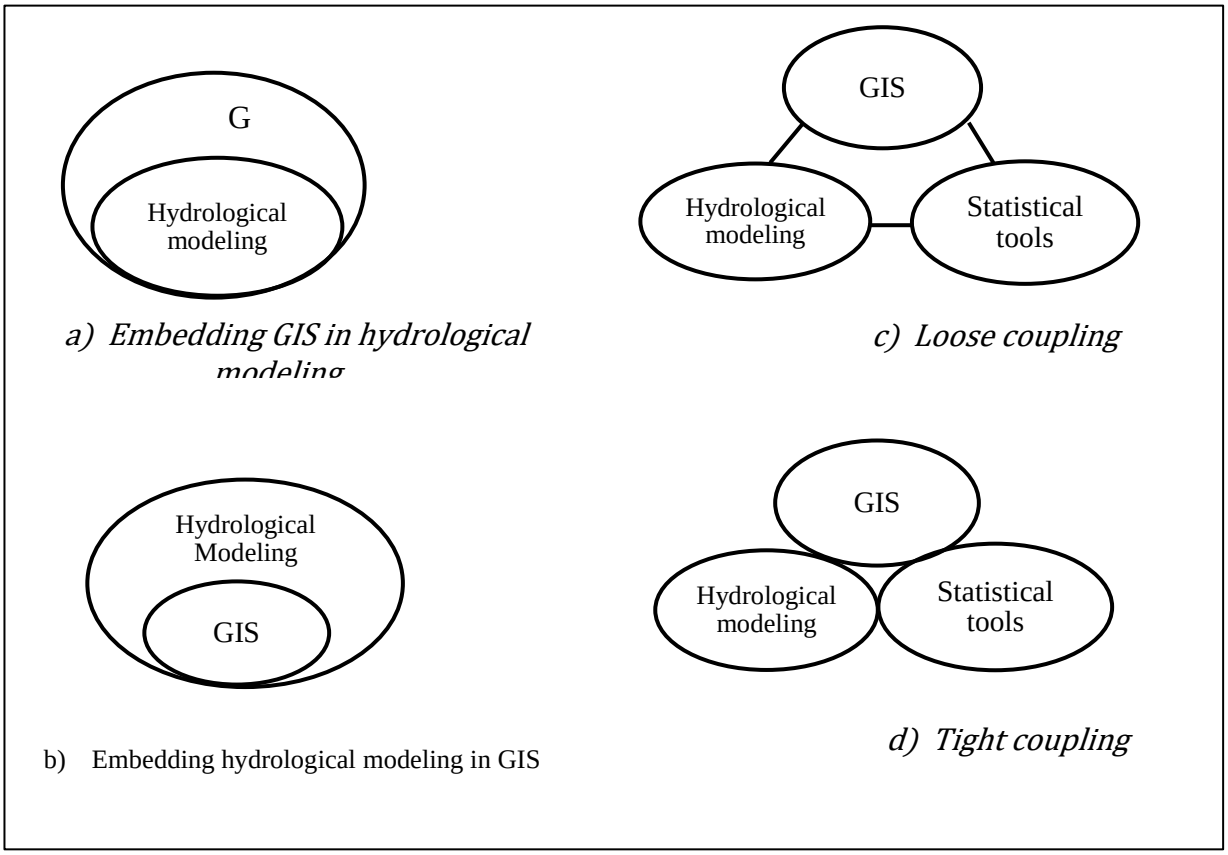


Figure 2-8: Four approaches to integrate GIS with hydrological model: current practices (Source: Sui & Maggio, 1991: 35)

### *d) Embedding GIS in hydrological modeling*

The approach (see Figure 2-8a) integrates GIS functionalities into a hydrological modeling package. Examples of the latest versions of this approach are RIVERCAD, HEC-RAS 20.0, RIVERTools, and MODFLOW. The hydrological modelers using this approach restrict GIS functionalities to mapping only

and regard GIS as conceptually irrelevant to the fundamentals of hydrological modeling. The two disadvantages of this approach are: the limited data management and visualization capabilities of the hydrological modeling software packages as compared to the commercial GIS software packages; and intensive programming requirements that are sometimes redundant.

*e) Embedding hydrological modeling in GIS*

The approach (see Figure 2-8b) uses stand-alone GIS modules with functions of hydrological modeling to improve the analytical modeling capabilities such as HEC-RAS developed by Army Corps of Engineers. The main advantage of the approach is the full utilization of GIS functionalities. The downside of the approach is that the modules are very simplified and may be validated or not to meet the industry standards.

*f) Loose coupling*

The approach (see Figure 2-8c) integrates a standard GIS package (such as Arc/info), hydrological or hydraulic model (such as HEC-1, HEC-2, STORM), and statistical package via data exchange using either ASCII or binary data format. Unlike embedding GIS in hydrological modeling, loose coupling avoids programming redundancies and minimal programming requirements making loose coupling flexible to use. However, problems may arise when converting data formats between packages. The data format conversion process can be tedious or cause errors.

*g) Tight coupling*

The approach (see Figure 2-8d) embeds hydrological models within a commercial GIS software package (Sui & Maggio, 1991). The approach allows users to run a series of individual commands in a batch mode or develop a customized user interface for specific applications (Sui & Maggio, 1991).

## Problems in integration GIS with hydrological and/or hydraulic modeling

Thakur (2017) categorises the problems of integrating GIS with hydrological modeling into three parts: existing, inherent, and computational problems. The existing problems are technical problems in integrating database. Most of the problems that are documented deal with technical issues, and little is said about the broad conceptual issues concerning integration (Sui & Maggio, 1991). The broad conceptual issues are directly linked to randomness, space and time in deterministic lumped models. The conceptual issues arise because currently the models such as HEC-1, HEC 2, USGS'S DRM3, are accepted and used though the models are not validated in the scientific sense (Sui & Maggio, 1991).

According to Sui & Maggio (1991) the loose coupling of GIS with conceptual models improve the scientific foundation of hydrological modeling.

The computation problems are a result of GIS databases being in vector format because GIS functionalities are meant for map layers and geometric transformation. The vector format makes it challenging to carry out hydrological modeling analysis (Thakur, et al., 2017).

Furthermore, the problems of GIS integration with a hydrological model also arise because of complexity of hydraulic and/or hydrological models. The model complexity limits operation capabilities of users, and mostly requires large scale data which are not always available (Els, 2011). Another challenge is time variability because hydrological and hydraulic modeling are dependent on time and require time series simulations, which are limited in GIS; and a wide range of data formats for various software packages.

Despite all the problems that need to be resolved to integrate GIS with hydrological and hydraulic modeling, the integration of GIS and hydrological modeling is still employed. However, Els (2011) recommends complex modeling to be carried out in its hydrological modeling environment.

### 2.4.3 Modeling

A model is an abstract or representation of reality, and modeling is a process of representing a real phenomenon or process (Hamburg University of Technology, 2010). Dooge (1973) described a Model as a simple illustration that approximates the actual complex system. The mathematical model simulates mathematical data and equations (Hamburg University of Technology, 2010).

#### Flood modeling

Historically, flood modeling used simple methods to measure the magnitude or frequencies of floods (Alexander, 2012). According to Alexander (2012) the measurements for analysis were computed through the application of linear extrapolation using slide rules and graph papers; and annual flood peak maxima were plotted on Log-probability graph papers. Hydro-meteorological records were scarce and limited to 30 years in length (Alexander, 2012). The measurement techniques became complex in the 1950s, when the mainframe computers were invented and were overly adopted in processing hydrological data and calculations to produce clear graphs and tables (Alexander, 2012). Recent developments have led to the use of sophisticated computers with high power and speed; employment of

numerical models in both statistical (measured) and deterministic (predicted) approaches (Alexander, 2012).

There are two mathematical modeling processes for flood management. The modeling processes are: hydrological and hydraulic modeling. Hydrological modeling is important in flood management to answer the question of *"how much water is there?"* Hydraulic model is relevant in answering the question "where will the water go?" (Djokic, 2015). Hence, the hydrological models represent precipitation-runoff modeling to compute the amount of water that translated into runoff for a given rainfall event. On the other hand, the hydraulic models determine the quantity, speed, depth, and coverage (extent) of water, and the shape of the landscape and the stream channel. River flood modelling is made of three main components (1) hydrological modeling, (2) hydraulic modeling and (3) river flood visualization using a geographic information system - GIS (Alaghmand, et al., 2012).

## Hydrological modeling

Hydrological models are used to estimate the flow of water depending on the level of complexity of the water channel, the available data, and the technical complexity of the model itself (Simonov, 2017). Hydrological models have many applications including flood forecasting, geographical and environmental management (Simonov, 2017). Three different types of hydrological modelling include routing, which is based on the description of river channel processes; catchment which relates to the description of watershed processes; and combined routing and catchment modelling where the catchment model simulates the response of catchment to produce runoff at a point, and the routing model directs the runoff in the catchment.

Hydrological models can also be classified as data driven models, conceptual models and physical processes. The data driven models are simple and easy models that use recorded long-time series data if available. The conceptual models are widely used and are easily interpreted by the decision makers. The physical process models are complex and require a spatially distributed rainfall, geomorphological and hydromophological data.

Some of the examples of hydrological models include the Storm Water Management Model (SWMM) by United States Environmental Protection Agency (EPA) (Pretorius, 2011); E- HYPE (Environmental Hydrological Prediction for the Environment) multipurpose model that uses open source data for flood forecasting, water management and research experiments (Emerton, et al., 2016); Variable Infiltration Capacity (VIC) model; TOPMODEL; HBV; MIKESHE; Soil and Water Assessment Tools (SWAT)

model (Devi et. al, 2015); the Hydrologic Engineering Centre- Hydrologic Modelling System (HEC-HMS).

## Hydraulic modeling

There are two main types of hydraulic modeling that are commonly used: the one-dimension (1D) and two-dimension (2D) model. The 1D model employs the 1D equation of flow to calculate single water level, flow rate and velocity of each cross-section. The 2D model solves 2D equation of flow to determine the water depth and average velocity on a grid and mesh (DTM and/or bathymetry) of channels. The 2D model is better at calculating velocity variations on the floodplain, and it is a more accurate model in situations where high details are required. However, the 1D model is simple, fast and better in representation of in-channel water levels, flows and point features such as weirs, bridges and sluices. Nevertheless, 1D and 2D models can be combined to improve the results of a model. With regards to flood mapping, 1D and 2D models are linked together such that 1D model is used in areas where the risk is low and 2D model is applied in high risk areas to obtain the high details required.

ShahiriParsa, et al., (2016) compared the 1D model (Hydrologic Engineering Centers-River Analysis System) and 2D model (CCHE2D) by simulating the flood zone of the Sungai Maka district in Kelantan state, Malaysia. The comparison results of the two models indicated that there was not much difference in the simulated sections.

Gharbi, et al. (2016), carried out a flood hydrograph simulation of the Medjerda River in Tunisia to estimate flood routing on both steady and unsteady flow rivers using 1D HEC-RAS and 1D MIKEII and 2D TELEMAC hydraulic models. The 1D HEC-RAS provided the rough definition of floodplains, however, the riverbed was generated precisely. On the other hand, the 2D TELEMAC model generated a precise topography of the river's floodplain. Thus, Gharbi, et al. used the 2D model to improve the 1D model. Like Gharbi, Al-Abed, et al. (2005), Snead (2000) carried out comparative analysis between the unsteady flow and steady flow of 1D HEC RAS and MIKE II. The results showed that the surface elevation of the steady flow hydraulic model was less than the unsteady flow because the movement of the flood wave drainage basin.

## Existing flood models

The development of flood systems has escalated the flood risk management (Langhammer, 2008). Over the years, the innovations in flood modeling have led to the development of global systems to

provide large-scale flood early warning systems. Recently, there have been two operational Global Flood Forecasting Systems in the world (Emerton, et al., 2016). Firstly, the Global Awareness System of the European Centre for Medium-Range Weather Forecasts (ECMWF) and European Community (EC). Secondly, the Global Flood Forecasting and Information System (GLOFFIS) operated by Deltares. The other large-scale system, however, not operational, is an experimental Global Flood Monitoring System (GLOFAS) developed by the National Aeronautics and Space Administration (NASA) and the University of Maryland. GLOFAS functioned based on the real-time global maps and flood events.

The other larger scale hydro-meteorological Flood Forecasting Systems include the four continental Flood Forecasting Systems (Emerton, et al., 2016). The four systems are the European Flood Awareness Systems (EFAS) owned by European Commission (EU), the European Hydrological Predictions for the Environment (E-HYPE) owned by Swedish Meteorological and Hydrological Institute (SMHI), the Australian Flood Forecasting and Warning Services (FFWS) that is operated by the Bureau of Meteorology, and lastly the Hydrologic Ensemble Forecasting Service (HEFS), a United States system that is run by the United States National Weather Services (NWS).

Additional examples of the hydrological model utilized by researchers, governments and organisations include: Stormwater Management Model (SWMM) by United States Environmental Protection Agency -EPA (Pretorius, 2011), European Hydrological Prediction for the Environment by Swedish Meteorological and Hydrological Institute- SMHI (Emerton, et al., 2016); the Hydrologic Engineering Centre- Hydrologic Modeling System (HEC-HMS); MIK E SHE; Hydrologiska Byrans Vattenavdelning (HBV) model; Variable Infiltration Capacity (VIC) model by University of Washington (Devia & Dwarakish, 2015) TOPMODEL; Soil and Water Assessment Tools (SWAT) model; and Identification of Unit Hydrographs and Component Flows from Rainfall, Evaporation, and Streamflow (IHACRES) Model.

*a) TOPMODEL*

Durand, et al., (1992) used TOPMODEL to simulate two small granitic catchments where the calibration and validation of the model proved to be satisfactory with good fits from 0.80 to 0.94. TOPMODEL is a semi-distributed conceptual model (Devia & Dwarakish, 2015, Tarboton, 2003). Devia & Dwarakish (2015) suggested TOPMODEL to be used in shallow soil and moderate topography.

*b) HBV model*

HBV model is a semi-distributed model that can produce reasonable river flow results (Jones, 2017; Devia & Dwarakish, 2015). The input data may include precipitation, runoff, soil moisture, upper and lower groundwater zone, lakes, and snowpack (Devia & Dwarakish, 2015).

*c) HEC-HMS*

HEC-HMS system software is a physically-based distributed, continuous and watershed model (Abushandi & Merkel, 2013; Al-Abed, et al., 2005) developed by the Hydrologic Engineering Center of the Army Corps of Engineers in the United States of America with the purpose of determining flows of centenary rain (Cabral, et al., 2015). The software is widely used to simulate and forecast streamflow or rainfall- runoff of watershed systems (Abushandi & Merkel, 2013; Al-Abed, et al., 2005) and is applicable in large river basin water supply, flood hydrology and small urban or agricultural watershed runoff (Al-Abed, et al., 2005). The model can be applied in humid, tropical, subtropical, and arid catchments (Abushandi & Merkel, 2013; Chu & Steinman, 2009). Chu & Steinman (2009) applied HEC-HMS to simulate four rainfall events and continuous runoff of the Mona Lake watershed in West Michigan to estimate the quantity, variability, and sources of water flow. Baumbach, et al. (2015), Bueche, et al. (2015) developed and examined the watershed of Upper White Sub-basin and HEC-GeoHMS and ArcHydro extensions in ArcGIS to estimate the flood area and depth using ArcHydro extension in ArcGIS. The main input data used included DEM (raster), rtreams (vector), catchment area (vector), gauge station data, such as stream flows, gauge station location, time series data (table).

*d) MIKE SHE model*

MIKE SHE Model is a physical based model developed in 1990 to simulate surface and ground flow. As a physical model, MIKE SHE relies on the spatial variations and topography, which makes the model applied in a large area. The model determines the interaction of surface and groundwater, water quality problems, including prediction of sediments and nutrients, and the movement of pesticides in water. MIKE SHE model uses many input parameters such as saturated groundwater flow, unsaturated groundwater flow, river flow, evapotranspiration, and precipitation among others.

*e) VIC model*

VIC model is a semi-distributed model that employs energy and water balance equations to calculate the saturated excess runoff, infiltration excess runoff, groundwater interactions, and groundwater table (Devia & Dwarakish, 2015). The input data of VIC model are precipitation, minimum and maximum daily temperature, soil heterogeneity, infiltration, runoff, base flow and land cover (Devia & Dwarakish, 2015). The soil heterogeneity is divided into three layers: the top layer where water evaporation occurs

from the soil, the middle layer that allows dynamic responses like excess infiltration of runoff and the lower layer, a storage of runoff water that contributes to soil moisture (Devia & Dwarakish, 2015). The layers above allow the structuring of water during a rainfall event into surface runoff and saturation excess runoff. VIC model is applied in the prediction of climate and land cover changes over moist and cold areas, irrigation planning, and water management for agriculture.

*f) SWAT*

The SWAT Hydrological model produces efficient predictions so that only minor calibrations are necessary (Devia & Dwarakish, 2015). The model has many applications including continuous simulation of flow, movement of nutrients and sediment, runoff, and soil erosion (Yang et al, 2000).

*g) IHACRES*

IHACRES is a lumped rainfall-runoff model that can be run on a small and large catchment, and in different climatic zones (Dye & Croke, 2003). The model is known to be simple, fast and uses less input data (Dye & Croke, 2003; Abushandi & Merkel, 2013). Furthermore, the model has the capabilities to evaluate variations in streamflow due to land cover change and determine the dynamic reactions of various characteristics of catchments. Dye & Croke (2003) used IHACRES model to assess streamflow predictions in Lambrechtsbos and Groot-Nylriver catchments in South Africa. The simulations done by Dye & Croke indicated that IHACRES underestimated quick flow events, particularly in drier areas of the catchment.

*h) GIS Flood Tool (GFT)*

The GIS Flooding Tool (GFT) was created by US Geological Survey in collaboration with the US Agency for International Development Offices of US Foreign Disaster Assistance. The tool was developed as a solution for making reconnaissance level flood inundation mapping for communities where data and resources for flood mapping are limited.

## Uncertainties of flood modeling

Flood modeling is subjected to uncertainties. These uncertainties are subjective to change depending on the catchment characteristics, event magnitude, and lead time for forecasting (Emerton, et al., 2016). Emerton, et al. (2016) stated four sources of uncertainty of hydrological models, which are: input data, evaluation data, model structure, and parameters. Uncertainties mostly arise where there is generalized prediction because of modeling a large area at a small scale. The generalization is corrected by comparing

the modeled historic events with the observed events. However, the comparison of historic and observed events cannot eliminate the under predicted or/and the over prediction of rainfall intensity.

Fortunately, the limited access to quality real-time and lengthy data, to some extent has been overcome by availability of new types of remote sensing techniques like satellites, and standardization of inhomogeneous data through international and interdisciplinary data sharing and open source data. Otherwise, most developing countries have limited tools or approaches to measure or compute spatially distributed evaporation and rainfall because of the difficulties in predicting of conventional and orographic enhancement processes. In turn, the complexities of the actual model cannot fully represent the uncertainties due to data limitations.

### 2.4.4 Related works that integrated remote rensing, GIS and flood modeling

Cabral, et al. (2015) and Musa, et al. (2016) integrated remote sensing and a geographic information system (GIS) techniques to model and map floods. Cabral, et al. delineated flooded areas in the medium-sized Acaraú River Basin in Ceará State, Brazil to quantify the areas affected by floods. Overall, the flood model satisfactorily represented the affected areas and showed the locations with the greatest flooding. Musa, et al. carried out flood Modeling of complex deltas in an area with scarce data and analyzed the vulnerability of the area to flooding, erosion and inundation. The final calibrated model had a correlation coefficient of 0.97 with the measured data.

Abushandi & Merkel (2013) compared the performance of HEC-HMS with IHACRES model from a single storm event based on an hourly scale. The input datasets that Abushandi & Merkel used for the HEC - HMS model included runoff, land use, and slope, while the inputs for IHACRES included rainfall and temperature data. Among the input data, it was found out that Curve Number (CN, representing runoff) was the most sensitive parameter in the HEC-HMS model with an average of 2.7 and impervious relative sensitive value of 3.1. All the other parameters in the HEC-HMS model indicated weak effect on the model, implying that changing CN can have an impact on the output for various rainfall events (Abushandi & Merkel, 2013). The most sensitive parameter for IHACRES model was rainfall with an average coefficient of 0.5, and almost all the other parameters strongly affected the output of the model. The results obtained from each model were validated using the observed streamflow data from a discharge station. The comparison results indicated that HEC-HMS fitted well with the streamflow data and yielded the Nash-Sutcliffe coefficient of 0.88, while IHACRES model had Nash-Sutcliffe coefficient of 0.51.

Yang, et al. (2000) compared the characterization and spatial variability of three physical-distributed hydrological model: MIKE SHE, TOPMODEL and Geomorphology-based (GB) models. Yang et al. recommended the use of MIKE SHE model in smaller catchments. Similarly, Devia & Dwarakish (2015) recommended the use of MIKE SHE in smaller catchments because of the demanding data requirement which may be challenging to acquire. Again, Devia & Dwarakish stated that some users find it challenging to manipulate MIKE SHE code to meet their requirements. Devia & Dwarakish experienced that MIKE SHE had the highest processing ability as compared to HBV model, VIC model, IHACRES model, and TOPMODEL.

Jones (2017) applied HBV and TopNet model with climate change as a variable to measure river flow of Shotover Catchment in New Zealand. Jones's findings showed that complexity of the fully distributed model such as TopNet affects the model output more than the input data or modeling uncertainties. Jones's results indicated that semi-distributed HBV models are dependent on the minimal data inputs as compared to fully distributed models such as MIKE SHE and TopNet. For instance, the HBV model used accurate physical parameters that were not well distributed to the catchment thus performed poorly as compared to TopNet model which only used interpolated data that covered the entire catchment area. Thus, semi-distributed models can be used as alternatives in cases where fully distributed models cannot be employed and can be applied in flood forecasting (Jones, 2017: Devia & Dwarakish, 2015).

## 2.5 Flood visualization using GIS

Flood visualization aims at communicating the right flood information to various audiences, hence there is no general style for visualizing floods. The important aspect of visualization is knowing the users, the purpose of visualizing, the type of data to be presented, and the exact information to rely. For instance, to visualize flooding, the event can be presented on a map depicting the spatial extents and depth of flooded water.

Visualization can be presented in many ways, such as maps, charts, graphs, tables, animations and statistics, among others. The most employed means of visualization for floods include maps and hydrographs. Since GIS represents features on the earth by linking geographical information with descriptive information (Esri, 2012), GIS has been utilized in creating flood maps (Brovelli, n.d.; Alaghmand, et al., 2010; Bueche, et al., 2015; Esri, 2012; Kopp, 1996).

The two main types of flood mapping are flood hazard maps and flood risk maps (EXCIMAP, 2007; Díez-Herrero, et al., 2009). Flood risk maps show the resources at risk, vulnerabilities and estimates of the damage caused (Díez-Herrero, et al., 2009).

Flood hazard maps in simple terms show areas that are most likely affected by flooding. Flood hazard maps are described as *"detailed floodplain maps complemented with: type of flood, extent of the flood; water depth or water level, flow velocity or the relevant water direction"* (Prinos, 2008, EXCIMAP, 2007). The various aspects of flood hazard maps and other types of maps are shown Table 2-2 (Díez-Herrero et al., 2009).

Table 2-2: Type of flood hazard maps and examples (Source: Díez-Herrero et al., 2009: 112)

| **Type of flood hazard maps** | **Examples** |
|---|---|
| Spatial-temporal development | Maps of areas flooded during a specific flood, or single event mapping<br>Maps of potentially flooded areas caused by rainfall and in situ accumulation<br>Maps of areas or points flooded during historical flood and palaeofloods for the purpose of stocktaking or local studies<br>Maps of groundwater resident times or seasonality<br>Maps of characteristics times of the hyetograph-flood relationship like times of concentration, travel |
| Natural phenomena severity | Water depth maps during an actual flood or modeled flood.<br>Water velocity maps during an actual or modeled flood<br>Sediment load transport map |
| Probability of the phenomena | Hydrologic-hydraulic maps<br>Geological-geomorphological maps |
| Other accompanying maps to represent the risks associated with floods, particularly fluvial floods | Risk damage maps caused by floods<br>Lithological map reclassified according to excavatability, surface formation and slope stability<br>Landslides, rockfalls, active erosion processes<br>Modification in the channel and/or plain following flood |

Table 2-3 presents a summary of the flood map (for both flood hazard and flood risk maps) in terms of characteristics, purpose, use, scale, accuracy and target group or users (EXCIMAP, 2007). Another parameter that can be added is flood duration in the context of inundation maps to show the time period when an area was or may be inundated (Els, 2011). From the table, it can be derived that flood hazard and flood risk maps have different parameters, purpose and use. However, scale and accuracy requirements are the same.

The users or target groups have different map information because of varying purposes specified by various users (EXCIMAP, 2007). The varying purposes may affect content, scale, accuracy and readability of the maps to match requirements (EXCIMAP, 2007). Obviously local level flood maps will require higher accuracy and larger scale than national or regional level maps.

Based on EXCIMAP (2007), generally, the core uses of flood maps are:

a) Flood risk management strategy (prevention, mitigation),
b) Land-use planning, land management,
c) Emergency planning,
d) Raising public awareness, and
e) Private sector, mostly insurance sector

Table 2-3: Summary of flood hazard maps and flood risk maps in respect of the content, purpose, scale, accuracy and target group or user (EXCIMAP, 2007)

| | **Flood hazard map** | **Flood risk map** |
|---|---|---|
| Content | Flood parameters such as:<br>✓ Flood extent according to probability classes<br>✓ Past events<br>✓ Flow depth<br>✓ Flow velocity<br>✓ Flood propagation<br>✓ Degree of danger | Risk parameters such as:<br>✓ Assert risk<br>✓ Flood vulnerabilty<br>✓ Probable damage<br>✓ Probable loss (per unit time) |
| Purpose / use | ✓ Land use planning and land management<br>✓ Watershed management<br>✓ Water management planning<br>✓ Hazard assessment of local level<br>✓ Emergency planning and management<br>✓ Planning of technical measures<br>✓ Overall awareness building | ✓ Basic for policy dialogue<br>✓ Priority setting measures<br>✓ Flood risk management strategy (prevention, mitigation)<br>✓ Emergency management (e.g. the determination of main users)<br>✓ Overall awareness building |
| Scale | ✓ Local level: 1: 5 000 to 1: 25 000<br>✓ National level, whole river basin: 1: 50 000 to 1: 1 000 000 | ✓ 1: 5 000 to 1:25 000<br>✓ 1:50 000 to 1: 1 000 000 |
| Accuracy | ✓ High: Cadastre level for detailed maps<br>✓ Low: whole river basin, national level | ✓ High: Cadastre level<br>✓ Low: whole river basin, national level |
| Target group/user | ✓ National, regional or local land-use planning<br>✓ Flood managers<br>✓ Emergency services<br>✓ Forest services (watershed management)<br>✓ Public at large | ✓ Insurance<br>✓ National, regional or local emergency services<br>✓ National, regional or local water and land use managers |

The flood risk management (strategy and planning) specifications are given in Table 2-4. The mapping scale at the national or regional level ranges from 1: 100 000 to 1: 1 000 000, while at the local level is 1: 5 000 to 1: 50 000.

Table 2-4: Flood risk management map specifications: scale or level, use of flood maps, complexity and content of flood maps (source: EXCIMAP 2007)

| **Level/ scale** | **Use of flood maps** | **Complexity** | **Content of floods** |
|---|---|---|---|

| | | | Essential parameter | Desirable parameters |
|---|---|---|---|---|
| National/ regional: 1: 100 000 – 1: 1 000 000 | • Broad-scale planning/prioritization of flood risk management measures/ strategies<br>• Flood risk management within the river basin<br>• Delineation of strategic flood storage zones (retention areas, wash lands) | • Decision makers<br>• Technical services<br>• Easy to understand simplified maps | • Flood extent<br>• Flood risk<br>• Site environmental vulnerability<br>• Pollution risks<br>• Assets at risk | • Indicative vulnerability |
| Local: 1: 5 000 – 1: 50 000 | • Planning, design and evaluation of localized/specific flood management measures | • Decision makers<br>• Technical services<br>• Complex maps possible | • Flood extent<br>• Water depth<br>• Other flood parameters (if appropriate) | • Vulnerability<br>• Risk (economic assessment)<br>• Environmental impacts |

## 2.6 Conclusion

The literature review chapter provides detailed review of related literature on natural hazards with emphasis on flood. Flood poses severe impact on people in terms of deaths, displacement and damage to property and environment. The review of GIS, remote sensing and flood modeling indicates the power of integrating (with consideration to errors and uncertainties) these three techniques in analyzing flood for better understanding and management of flood to reduce flood impacts. Based on the review, many researchers have integrated remote sensing and GIS in hydrological and hydraulic systems to compute flood extents (water depth and velocity) and to visualize floods. Various computer models, digital data, satellite images and good network observation have been applied by other researchers. The literature review formed a basis for considering appropriate flood model software packages, data and accuracy requirements to develop a fit flood model.

# 3 Data and Study Area

## 3.1 Study area

The study area and data Chapter provides descriptions of the study area – Chikwawa District in the Southern Region of Malawi, see Figure 1-2. The Chikwawa district is within the Shire River Basin in Malawi. It was selected as a case study for development of flood modeling because the areas experience frequent floods and the vital element of data requirements in the context of developing countries. Malawi is considered one of developing countries and faces problems to access good quality and updated data. Therefore, this research has selected Malawi to explore other viable options of maximizing available data and methods to improve quality of the results in flood modeling.

### 3.1.1 Chikwawa within Shire basin catchment area

Chikwawa District is within the Shire River catchment area, an international drainage basin located in three countries: Tanzania, Malawi, and Mozambique. The Lake Malawi drainage is called Shire catchment. The shire catchment is divided into three sub-catchments: North, Central, and South. The study area selected is within South sub-catchment and is situated below the lower part of Lake Malawi. The mass area of Shire River Basin within the Malawian border is approximated as 22, 317 square km. The basin consists of one administrative city and fourteen districts with estimated total population of five million and thirty-three thousand in 2015. The districts are divided into Traditional Authorities (TA), sub-traditional authorities or Sub-Chiefs (SC), towns, national parks, game reserves and water bodies.

The basin is beneficial to the country because of its natural resources. For instance, the basin provides fresh water for both urban and local communities, serves as a major hydro-electric power generation station in Malawi, provides irrigated agriculture, aquaculture, and transportation. The basin also has marshes that are home for wildlife and flora, major sugar estates, and small-scale subsistence agriculture.

Chikwawa experiences three seasons per year: cool dry season from May to August, hot dry season from August to October, and wet hot season between November and March. Therefore, the dry season is from May to October; and rainy season is from November to March. As part of Shire River Basin the annual estimated mean rainfall is 897mm. The rainfall is influenced by three factors. Firstly, the mountainous terrain in the upper reaches of the Shire Basin, secondly, the Convergence Ahead of Pressure Surges (CAPS), and thirdly, the easterly wave system and the tropical cyclones (Department of Disaster Management Affairs, 2015). The CAPS usually cause locally heavy rains that extends the rainy

season. The easterly wave system mostly triggers rain in March or April when rainy season is ending, causing isolated but locally heavy rains. The tropical cyclones influence heavy rainfall resulting into severe flooding (Department of Disaster Management Affairs, 2015). Flooding happens frequently and causes loss to life, damage to property such as settlements, national infrastructures (schools, hospitals, roads, and railways among others), because of water accumulation in some areas. The records by Department of Disaster Management shows that extreme floods occurred in 1988/89, 197/98 and recently in 2014/15.

### Rivers and streams

The basin has rivers and streams that flow into and out Shire River. The Shire River flow is controlled by Kamuzu Dam to ensure that there is enough water for hydropower generation. The amount of water that flows down Shire River is reduced during dry season and overflows in rainy season and during floods when water is excessive. The Ruo River is the major river situated in the Southern part of Malawi that drains a large amount of water into Shire River and forms a border between Malawi and Mozambique.

### Soil classes

Soil Classes found in Chikwawa are loam, clay loam, loamy sand and sandy clay, sandy clay loam, sandy loam and rock outcrops. The FAO classified soils in the basin as Calcaric Cambisols, Calcic Luvisols, Cambic Arenosols, Chromic Cambisols, Chromic Luvisol, Eutric Cambisols, Eutric Fluvisols, Eutric Gleysols, Eutric Regosols, Eutric Vertisols, Gleyic Cambisols, Haplic Luvisols, Humic Alisols, Leptosols, Mollic Fluvisols. The soils are exposed to erosion due to poor farming practices, and transformation of woodlands and forests to agricultural land. The soil loss is deposited in the dams, reservoirs, wetlands, and rivers, to form silt layers. Fifty percent of the Shire River Basin land is vulnerable to slight soil erosion and twelve percent of the land is subjected to moderated soil erosion. The total volume of soil that is lost from agricultural land annually is estimated to be 5,566, 000$m^3$. The areas with steep terrain and escarpment such as mountains have the highest slope of at least twenty-four percent.

### Land cover and land use

The land use of the basin is mostly agriculture, forests, water, built-up and grasslands. Other land use categories are rock, gravel and marsh, woodland and plantation, and water bodies. The land use change detection from 1991 to 2008 indicated that there was 41% to 38% decrease of forests because of

deforestation. The deforestation causes include clearing trees for farming and over-dependence of people on trees for domestic use. The deforestation has contributed to flooding because of increase in runoff.

**Geology**

Chikwawa geology is mainly made of Alluvium or superficial deposits and sedimentary and volcanic rocks (Chiwambo, 2017).

## 3.2 Data

Determination of flood extent, depth, and velocity through flood modeling requires sourcing necessary information to develop the model (Dimet, et al., 2000). The availability of data are important to decide on the methodology and flood parameters to be modeled (Els, 2011). The basic sources of flood modeling data are field observations and remote sensing (Dimet, et al., 2000). This section analyzes data requirement for this study by considering both international and national data sources. Data requirements involve outlining and reviewing data specifications (Baumbach, et al., 2015).The chapter consists of discussion of criteria for accepting data to model floods, data need to meet the various flood modeling methods, data sources, followed by the data challenges faced due to the case study site location, and finally the description of each data set in detail.

### 3.2.1 Criteria for the admissibility of data for flood modeling

To ensure the integrity of the research, criteria are set forth for data that are acceptable (Leedy & Ormrod, 2011) for flood modeling. The criteria help in checking the quality of data and their sources to ensure reliable output results (Westen, 2015; Els, 2011). The criteria for admissibility of data are as follows:

a) Thematic accuracy: making sure the data used for example maps, have the right information (Westen, 2015).
b) Temporal accuracy: the data must match the time required (Westen, 2015).
c) Appropriate scale: using maps with equivalent scale (Westen, 2015)
d) Coverage: the data must cover the case study area (Els, 2011)
e) Resolution: the data have at least medium resolution (Els, 2011)
f) Availability and cost: if the data can be accessed for free (Pretorius, 2011; Baumbach, et al., 2015)
g) Type and format of data (Baumbach, et al., 2015)

h) The purpose of research and budget (Baumbach, et al., 2015)

i) Data storage capacity (Baumbach, et al., 2015)

j) Duration of the project (Baumbach, et al., 2015)

The research is set up on a local level, the case study area is Shire River in Chikwawa District, Malawi. Hence, the recommended scale range as per Table 2-4 is 1: 5 000 to 1: 50 000. The flood event to be modeled and mapped took place in January 2015. The flood extent, depth, velocity, and duration parameters are mapped for flood risk management (refer to Table 2-4).

### 3.2.2 Basic data requirement for flood modeling

Despite that different methodologies may have different data requirements, the basic data requirements for flood modeling are as follows:

a) **Topographical data** describe the distribution of physical and artificial feature of an area of interest (İcaga, et al., 2016; Els, 2011, Farooq & Rabbani, 2018; Kourgialas & Karatzas, 2011; Abdou, et al., 2018; Abushandi & Merkel, 2013; Al-Abed, et al., 2005; Alaghmand, et al., 2010; Ameta, 2015; Balasubramanian, 2017; Baumbach, et al., 2015, Djokic, 2015; Sinclair & Pegram, 2004; Feldman, 2000, Asante, et al., 2008)
b) **Rainfall and discharge data** describe the amount of rain received in millimeter cubic and discharge, which is the flow of water in a river channel in meter cubic (Baumbach, et al., 2015; Asante, et al., 2008; Djokic, 2015; Demir & Kisi, 2016; Farooq & Rabbani, 2018)
c) **Historical data** to calibrate and validate the model (Djokic, 2015; Els, 2011)

The datasets are discussed in detail below while taking into consideration the case study area (Chikwawa, Malawi) and the criteria for admissibility of the data.

#### a) Topographical data

The topographical data help to determine the water depths, extent, and velocity by incorporating the data in the hydrological and hydraulic models. The main hydrological data include terrain elevation, climate, land cover, soil type or characteristics, and river channels (İcaga, et al., 2016). The sources of these topographical data include contours, DEMs, satellite imagery, aerial photographs, field survey data (Els, 2011).

**Terrain elevation**

Terrain elevation describes the topographical relief of a catchment area and is used to calculate other physiographic characteristics which contribute to runoff and necessary for hydrologic analysis (Raghuwanshi, 2014). These examples of the physiographic characteristic include: area, slope, shape, drainage density, aspect, and relief (Raghuwanshi, 2014). Terrain elevation is represented by DEM. Balasubramanian (2017) defines DEM as a three-dimensional representation of the land surface elevation with respect to a reference datum. DEM provides the physical and topographical aspect of the earth (Makineci & Karabörk, 2016) and it is used for elevation computations. Terrain elevation (DEM) is important in determining SLR (sea level rise) impact; coastal zones flooding risk assessment; and hydrological attributes modeling and extraction (Abdou, et al., 2018).

The DEM is a key input for hydrological model because it is necessary for determining the drainage network and catchment boundary. The three sources of DEM data are ground survey technique, remote sensing such as photogrammetric or stereo methods and RADAR, and existing Topographic Maps (Nelson, et al., 2009). The three structures of DEM as per Wilson & Gallant (2000) include regular grid, Triangulated Irregular Networks (TIN) and contours. The various DEMs are sourced from Remote Sensing such as Shuttle Radar Topography Mission (SRTM), Advanced Spaceborne Thermal Emission and Reflection Radiometer (ASTER) Global Elevation data, Global Multi-resolution Terrain Elevation Data 2010 (GMTED2010), LiDAR, Geoscience Laser Altimeter System-GLAS (Nelson, et al., 2009), and DEM generated from interferometry Synthetic Aperture Radar-SAR (Gao, et al., 2017). DEM can be generated from interferometry SAR (InSAR) using at least two co-registered Sentinel-1A images (Dongchen, et al., 2004; Kamaruddin, et al., 2003; Makineci & Karabörk, 2016). Example of a DEM is shown in Figure 3-1.

Table 3-1: Terrain elevation data type, sources, coverage

| Type | Dataset | Coverage | Resolution | Source |
|---|---|---|---|---|
| DEM | ASTER Global Digital Elevation Model | Global | 30 m and 90 m | **https://earthexplorer.usgs.gov/** |
| | JAXA's Global ALOS 3D World | Global | 30 m | **https://www.eorc.jaxa.jp/ALOS/en/aw3d30/** |
| | Space Shuttle Radar Topography Mission (SRTM) | Global | 30 m and 90 m | **https://earthexplorer.usgs.gov/** **http://srtm.csi.cgiar.org/srtmdata/** **http://www.waterbase.org/download_data.html** |
| | DEM interferometry Synthetic Aperture Radar (InSAR) | Global | 10 m to 15 m | Generated from DEM interferometry of coregistered Sentinel 1 TOP SAR images (Source of Sentinel 1: **https://scihub.copernicus.eu/dhus/#/home**) |
| Contours | Malawi SRTM Contours | Malawi | 50 m | Malawi Department of Surveys, **http://www.masdap.mw/layers/** |

Table 3-1 indicates DEMs and their coverage, resolution and sources. Referring to Table 3-1 InSAR, DEM has the highest resolution of 10m to 15m depending on the accuracy of the generation process. However, InSAR DEM located below waterbodies is poorly interpolated because the smoothness of water causes deflection of backscatter away from a sensor, such that sensors record waterbodies as zero (Chatterjee, et al., 2010). Therefore, InSAR DEM could misrepresent river channels and other waterbodies hydrologically, hence less reliable in water studies (Chatterjee, et al., 2010).

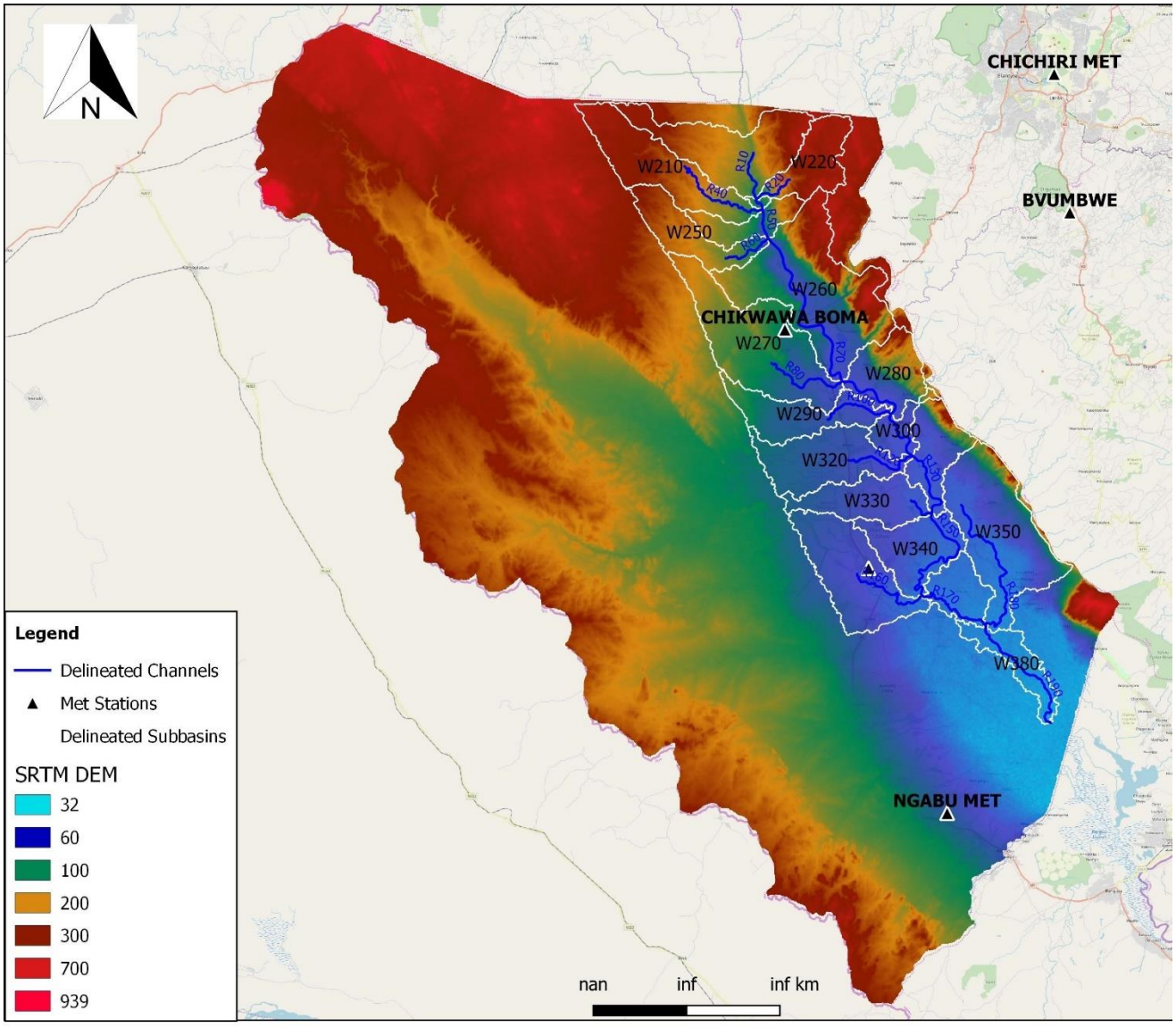


Figure 3-1: DEM as a main flood modeling input

## Land use

Land use data are used to calculate runoff in hydrological modeling and compute Manning's roughness coefficient in hydraulic modeling (Baumbach, et al., 2015). Land use maps were created in Malawi by four different organizations, namely JICA, World Bank, FAO, and RCMRD or USAID. JICA created national land use maps for years 1990, 2000, 2010 using Landsat image and Spot sensor (Haack, et al., 2015). The World Bank conducted national land use mapping for 1973, 1992, 2000 using Landsat Multispectral Scanner (MSS) and 2010 using Terre (SPOT) sensor. RCMRD created land use maps for 1990, 2000, and 2010 using Landsat images (Haack, et al., 2015). Haack et al. (2015) compared the different land use maps created by the organizations and their comparative results showed that the maps were different though they all achieved thematic accuracy within the range of 85% to 89%. For instance, the National percentages of forest and cropland ranged from 18.2% to 28.7%, and 40.5% to 53.7% respectively. The differences implied that the Government of Malawi lacks complete and consistent national-scale land use base data (Haack, et al., 2015).

Other sources of land use are DIVA-GIS (http://www.diva-gis.org/gdata) grid data at a resolution of 30seconds; RCMRD geoportal; the Sentinel- 2 global land cover; and Malawi Spatial Data Portal (MASDAP) by the Malawi Department of Surveys. Malawi has also Atlases: Shire River Basin Atlas and Malawi Hazards and Vulnerability Atlas, which are collections of different information including land use information.

Due to lack of complete and consistent land use data, this research has created land use data from classification of Landsat images captured before the flood into land cover themes (water, bare soil, sparse vegetation, vegetation, roads, sand and built-up). The classification is based on the different spectral reflectance and remittance properties of each pixel of a Landsat image (Al-doski, et al., 2013).

### Soil data

Soil data are useful in a hydrological model for computation of runoff (Asante, et al., 2008; Baumbach, et al., 2015). The main source of soil data in Malawi is the Food and Agriculture Organization of United Nation (FAO) at a scale of 1: 1 000 000 maps (Dijkshoom, et al., 2016). The FAO data can be accessed from a SOTER database through ISRIC World Soil Information that started from 1986 to 2016. MASDAP has also soil data sets that are downloadable. Another source of soil data is the global Soil Survey Geographic Database (SSURGO) that was developed by National Cooperative Soil Survey.

### River channels

The river channel data represent the location and distribution of river channels and they are used to delineate watersheds. The main provider of river channels in Malawi is the Malawi Department of Survey at a scale of 1:50 000. Otherwise, the river channels can also be digitized from DEMs or satellite images.

### Rainfall data

Rainfall data are an important input of a hydrological system (Dooge, 1973). The different sources of rainfall data include ground-based rain gauges, ground-based radar, Satellite-Based Rainfall Estimates (SBRE). Examples of Satellite-Based Rainfall Estimates are TRMM TMPA, CMORPH, NRLgeo, the Passive Microwave-calibrated Infrared algorithm (PMIR), and CHIRPS (Sinclair and Pegram, 2013), as shown in appendix 7.1. The sources of data for this research are rain gauge and satellite-based. Rainfall can be measured using ground observation and/or satellite. The Malawi Meteorological Department provides ground observations using rain gauge instrument to measure average daily rainfall data. Disdrometers and Radar (Sun, et al., 2017) are not yet adopted in Malawi. The primary source of weather and climate information for Malawi is the National Meteorological and Hydrological Agency in the Department of the Climate Change and Meteorological Services within the Ministry of Environment and Climate Change Management (Vincent, et al., 2014). The department provides weather and climate services to all sectors in the country, namely aviation, insurance, marine, environment, agriculture, fishing, water resources, flood disaster, road and railway transport, energy, sports and recreation, building and construction industry, health, retail, disaster preparedness including flood forecasts, legal, banking, and to the general public.

The meteorological data collected by the Malawi Meteorological Services dates to 1890s when Malawi firstly became a British Protectorate (DCCMS, 2006). Back then the data were collected by administrators at the district level, farmers, missionaries, and other interested individuals. The records were measured by various people and once or twice a day at varying hours every day (DCCMS, 2006). The changing of observers, inconsistency in hours of observation and the minimal number of observations per day led into gaps and inconsistency in the records (DCCMS, 2006).

### Historical data

Historical records for floods provide information of past flood events (Prosdocimi, et al., 2016). The historical records are useful for validation and calibration of flood modeling (Els 2011). The sources of historical records may include annals, chronicles, memory books, memoirs, weather diaries, letters, special prints, official economic and administrative records, newspapers and journals, sources of a

religious nature, chronogramme, early scientific papers, compilations and communications, stallikeepers' and market songs, pictorial documentation, and epigraphic sources. In Malawi the most reliable sources of historical records are official economic and administrative records such as natural hazard assessment reports; newspaper articles about floods for previous years; gauge station records; aerial and satellite photos; camera videos and pictures; phone messages; flood marks; and dated flood maps.

**Water level and discharge data**

The water level and discharge can be measured using traditional ground –based (Terrestrial) monitoring or space-borne remote sensing (Fekete & Vörösmarty, 2007). The Surface Water Division under the Department of Water Resources within the Ministry of Agriculture and Irrigation, Water Resources Monitoring (MoAIWD) is responsible for hydrological observations of water level and discharge. According to MoAIWD (2014) in their final report of Project for National Water Resources Master Plan in the Republic of Malawi, there were 300 hydrological stations in the country. These hydrological stations include river gauging stations that use daily chart automatic recorders to record water level and discharge (MoAIWD, 2014). 173 of the stations were developed in 1988 (MoAIWD, 2014). In 2011, it was recorded by MoAIWD that 139 stations were operational, and 169 stations were closed. 164 stations of 169 belong to MoAIWD, and the remaining four stations are owned by a water supply utility organization in Malawi called Water Board (MoAIWD, 2014). The Shire River Basin, where the case study of this research is located has forty eight stations whereby twenty five are operational and twenty three are closed (MoAIWD, 2014) as presented in see Table 3-2.

Table 3-2: Summary of physical conditions of hydrological stations in Shire River Basin (Source: MoAIWD, 2014)

| | **Open** | | | | | **Closed** | **Total open & closed** |
|---|---|---|---|---|---|---|---|
| | **Good** | **Average** | **Poor** | **N.A** | **Total open** | | |
| Number of hydrological stations | 17 | 6 | 1 | 1 | 25 | 23 | 48 |

The Surface Water Division under MoAIWD initially stored water level and discharge data in the hydrometric database of HYDATA software (Ministry of Agriculture, Irrigation and Water Development, 2015). Currently, the data are moved from HYDATA to HYDSTRA to fulfil the SADC-HYCOS initiative (Ministry of Agriculture, Irrigation and Water Development, 2015).

The space-borne remote sensing observations also provide river discharge data. Dartmouth Flood Observation (http://floodobservatory.colorado.edu/DischargeAccess.html) is a satellite platform that provides discharge and runoff data for daily, weekly, and monthly measurements for different parts of

the world. The measurements are verified by local gauge stations. The data can be downloaded in an excel format. Other global platforms that provide river discharge data that cover the case study area is Global River Discharge Database - GRDC (https://www.bafg.de/GRDC/EN/02_srvcs/21_tmsrs/riverdischarge_node.html) which operates under World Meteorological Organization. GRDC contains terrestrially observed data of river discharge for all stations in Africa from 1869 to 2017.

**Satellite images**

*i) Google Earth images and base maps*

Google Earth images were accessed online using Google Earth Pro software which is installed on the computer hard drive. Like Google Earth images are Base Maps that one can input in ArcGIS provided there is internet access. Both the Google Earth images and Base Maps are used as a reference for digitizing the channel and floodplain parameters because of high resolution which makes it easy to identify features that need to be digitized as compared to Landsat or Sentinel images, see Figure 3-2 below.

The Base Maps were well geo-referenced to Geographical Coordinate Systems. However, the spatial geo- referencing of Google Earth may not be good because of the tilting of the image, hence the requirement to validate the data digitized in the study area.

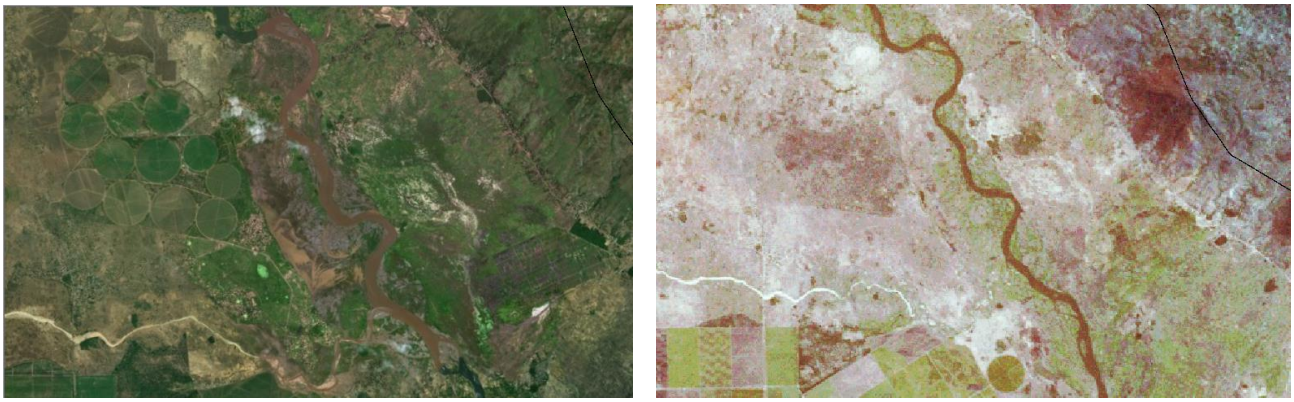

Figure 3-2: Gooogle Earth Image (Left), Landsat Image (right)

*j) 30m resolution Landsat image*

The Landsat 8 images can be downloaded from USGS website for land classification, extraction of water bodies. The Landsat 8 image has eleven bands. This research only requireed band 1 to band 6 (Blue, Green, Red, Near Infrared (NIR), and Shortwave Infrared (SWIR) 1). The bands are prepared by

stacking, which involves combining the bands into a single multispectral image. Since 6 multispectral images are covering the study site, the images are mosaicked (combined) to create one single seamless image. The mosaicking uses histogram matching color correction and set in overlapping areas of the images using "Feather" function, and resamples the image using the bilinear interpolation method. After mosaicking, a subset of the study area is clipped so that areas that are not necessary are removed and also to reduce the size of the image in order to increase the processing speed of the machine learning.

### 3.2.3 Data challenges faced due to case study site location

Based on the review done by the Department of Disaster Management in Malawi, provision of flood warning and monitoring system is based extensively on the basic flood routing procedure of predicting downstream water levels from observation of water levels upstream of the gauging stations. The system does not determine the exact extent of inundation and the expected time when flood surges would reach downstream areas. Unavailability of accurate or reliable monitoring and warning services increases the probability of the vulnerable communities to have lower response capacity.

There are limitations in accessing data of sufficient quality and time period. The limitations are caused by technical challenges in capturing, storing and transfer of data, limited data in real time, difficulties in retrieving, controlling quality, formatting, archiving and redistributing the data collected (Emerton, et al., 2016). Nevertheless, there have been new data possibilities and open data policies that have been utilized in this research to acquire data for modeling, though it may not be ideal (Emerton, et al., 2016). For example, freely available data access for educational and research purposes provided by some government and other organizations; online satellite and earth observation data platforms that provide options of downloading data for free.

The other challenge is that the Department of Meteorology lacks operational weather stations. Since the 1930s and 1940 the department had 102 weather stations, however, approaching mid the 1940 only half of the existing stations were operational. Worse still, those stations that are operational only recorded rainfall data. According to the Inception Report on modernizing hydrological and meteorological monitoring systems in the Shire River Basin (2015), there have been declines in all monitoring networks, equipment, laboratories, and communication networks. These declines in monitoring are illustrated in Table 3-3.

Table 3-3: Current situation of hydrological and meteorological monitoring in Shire River Basin, Malawi Source: Ministry of Agriculture, Irrigation and Water Development (2015: ii)

| | |
|---|---|
| Network, equipment and laboratories | All monitoring networks are in a significant state of decline. The sites are generally in despair because of vandalism, lack of maintenance, flooding, incomplete construction and commissioning, and long-term degradation.<br>Regular monitoring appears largely to have ceased for the water quality and groundwater monitoring. Less than 10% of the meteorological stations in the Shire Basin area are operating as required and there are no more than two gauging stations which data are reliably received.<br>Equipment for many sites missing or not functioning. Many of the gauge boards are missing or damaged. A significant number of the meteorological monitoring stations are not working and some of the loggers and equipment are no longer manufactured or supported by the original suppliers.<br>There are significant shortages of instruments, equipment, consumables and reagents at the water quality monitoring laboratories. A number of groundwater monitoring sites have been vandalized and are missing equipment.<br>New equipment which has been purchased has in many cases not been used due to lack of appropriate training. |
| Communication networks | None of the surface water automatic telemetry stations have been functioning recently, with problems due to damaged, obsolete and failing equipment.<br>The methods for manual communication of gauge readings have also broken down, with very few gauge readers operating in the post. Where readings are being taken, the time for data sheets to reach the headquarters for input to the archive can be several months.<br>37 of the 40 Automatic Weather Stations (AWSs) have loggers which are no longer supported by the original supplier (a new company has taken over support of these systems). The communication systems for these are only semi-automatic, requiring human intervention and only occurs once a day. The other 7 Automatic Weather Stations are working well.<br>There are 31 automatic rainfall loggers, but data are no longer received from them due to lack of funding for the ongoing data collection |

### 3.2.4 Conclusion

"*Data contains pieces of the truth, but rather in unrefined state*" (Leedy & Ormrod, 2011: 90). Data and methodology are dependent of each other. To attain the meaning of data, research methodology needs to be employed. However, the nature, accuracy and amount of data available determines the methodology to be used. The case study area is faced with many data challenges because of malfunctioning systems such as non-operational meteorological stations in the Shire Basin area, poor data storage, only two gauging stations to provide reliable data, and no access to high resolution images by developing countries including Malawi because they are expensive. Despite the data challenges discussed, alternative data sources have been identified by evaluating the data requirements. The analysis of the data requirements has formed a foundation for establishing the appropriate methodology to carry out flood modeling for flood risk management.

# 4 Methodology

## 4.1 Introduction

The methodology chapter outlines the design, technical and analytical methods of flood models that integrates with GIS and remote sensing to achieve the overall objective of this research. The overall objective of this research as discussed in section 1.3 is to analyze the riverine flood by integrating remote sensing, GIS, and hydraulic and/or hydrological modeling to develop informed flood mapping for flood risk management for Chikwawa District in Malawi. Thus, the methodology is structured in three main sections of analytical flood models is carried out in this research to:

1. **Develop and analyze the hydrological model** that integrates based on the DEM using HEC HMS and in ArcGIS to calculate channel flow/discharge due to the rainfall events during the simulation period.
2. **Develop and simulate the hydraulic model** in GIS and HEC RAS to calculate the depth and extent of flooded water
3. **Analyze the risk of flood** on different land uses based on flood inundation maps.

### 4.1.1 System design of a flood modeling and analysis system

This research has designed a flood modeling system to:

a) Provide a framework for flood modeling processes and improve the analysis of flood modeling processes
b) Contribute to decision making for sustainable flood modeling system by ensuring efficient flow of data from one process to the other.

Figure 4-1 consists of data providers and/or departments, input and output data. The data are either external (sourced outside the system) or internal (created within the system) as shown.

The internal data are created by processes within the system and are used as input data for other processes. The context diagram in Figure 4-1 provides the general view of the system showing the terminators (data providers or users) and the data inputs and outputs of the system. The direction of the arrow in Figure 4-1 shows the flow of data into and out of the system. Only the community level management and the public sector (government) are the users that obtain the flood maps and hydrographs output data from the system.

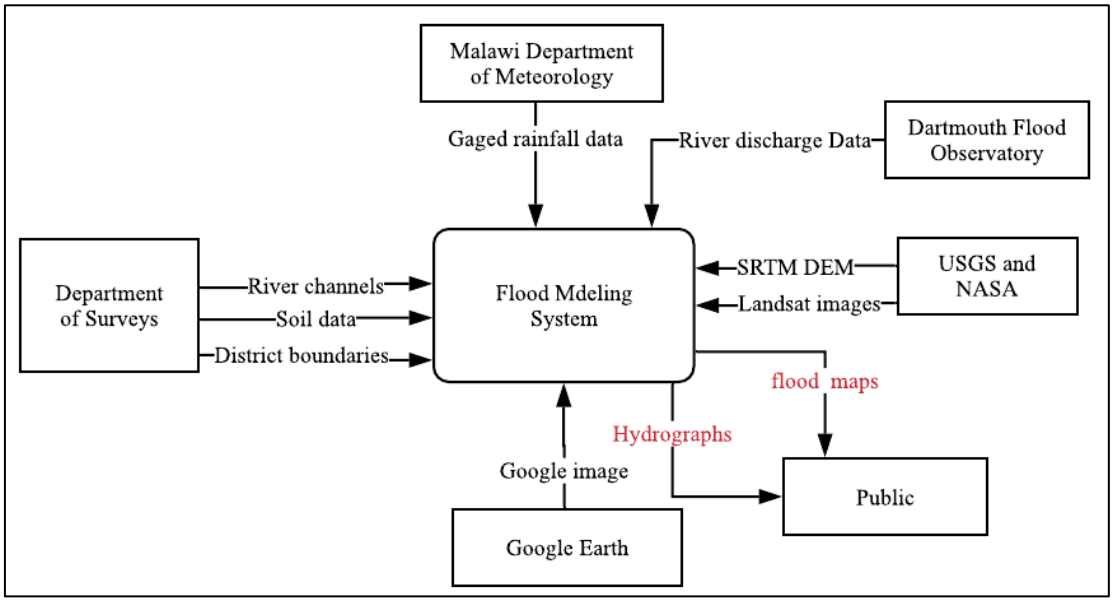


Figure 4-1: The context diagram

The flow of data and the processes within the system are demonstrated in the flow diagram shown in Figure 4-2. Flood risk management and flood protection framework outside the orange circle are conceptual. These conceptual processes are implemented outside the context of this project and ensure that the outputs of the flood models are materialized into well informed decisions.

Figure 4-1 consists of data providers and/or departments, input and output data. The data are either external (sourced outside the system) or internal (created within the system) as shown. The internal data are created by processes within the system and are used as input data for other processes. The context diagram in Figure 4-1 provides the general view of the system showing the terminators (data providers or users) and the data inputs and outputs of the system.

The direction of the arrow in Figure 4-1 shows the flow of data into and out of the system. Only the community level management and the public sector (government) are the users that obtain the flood maps and hydrographs output data from the system.

The flow of data and the processes within the system are demonstrated in the flow diagram shown in Figure 4-2. Flood risk management and flood protection framework outside the orange circle are conceptual. These conceptual processes are implemented outside the context of this project and ensure that the outputs of the flood models are materialized into well informed decisions.

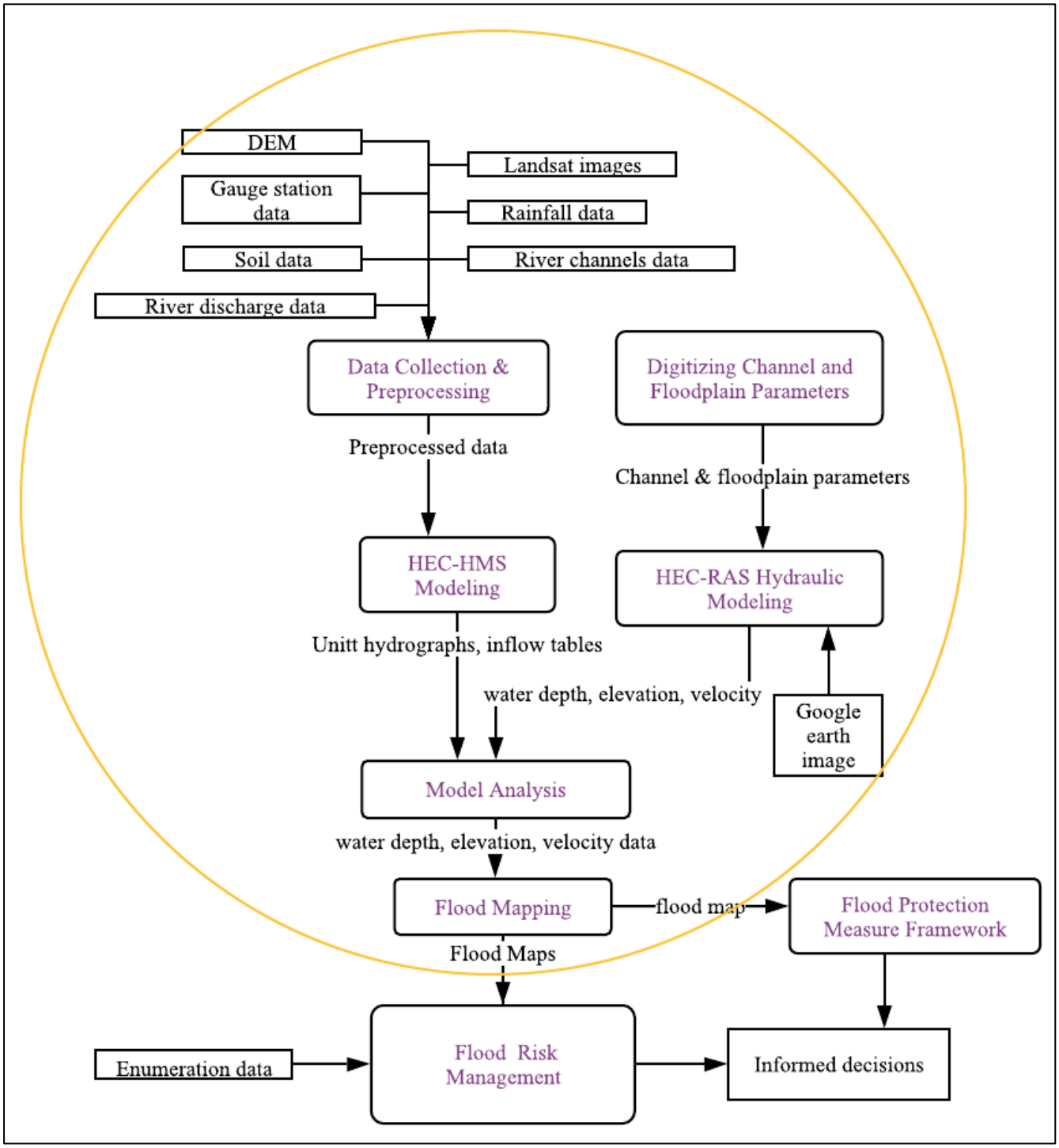


Figure 4-2: Data Flow Diagram

### 4.1.2 Flood models selection criteria

This research has mostly considered project-dependent criteria. Therefore, the three-fundamental project-depended criteria as per Cundelik (2003) are as follows:

a) Necessary outputs of the research. The question that is asked to estimate the criteria is: Does the model predict the parameters required by the research dissertation such as the flood extent, depth and velocity of flooded water?
b) Hydrological processes that are required to be modeled to compute the anticipated outputs appropriately. The question that is posed is: Is the model capable of simulating single-event or continuous processes, routing or catchment or combined routing-catchments?
c) Availability of input data. The question asked is: can all the inputs required by the model be provided within time and cost constraints of this research?
d) Price or investment of the hydrologic modeling. What are the costs of running the model?

This research study aims at modeling riverine floods of Shire River in Chikwawa District, Malawi by integrating GIS and Remote Sensing to develop informed flood mapping for flood risk management. The desired outputs to fulfil the aim of this research are as follows:

a) Simulated flood water extent surrounding the river and flood plain.
b) Simulated depth of the water during the flood
c) Simulated velocity of water during the flood event

The key hydrological processes that need to be measured in the structure of the hydrological model to obtained desired output are:

a) Single-event rainfall-runoff transformation dependent on the spatial and temporal rainfall distribution, and catchment physiographic properties.
b) Land use and soil distribution.
c) The runoff volume, the overland flow, the interflow, and the channel flow.

Due to limited resources, the research was mostly restricted to the use of free software and data. The use of freely available resources means that there is limited technical support to use the selected software, and some input data.

Considering the criteria mentioned above, the selection of the software was conducted by reviewing the existing hydrological model software that other researchers have used or reviewed. Cunderlik (2003) reviewed 40 existing hydrological models according to the aforementioned four fundamental criteria and carried a thorough review of eighteen models which were grouped into lumped, semi-distriuted, and

distributed models. Cunderlik evaluation results showed that among the lumped models IHACRES model scored the highest score of 20 points.

Among the semi-distributed models HEC-HMS and HFAM scored equal highest score point of 25; and for distributed model HYDROTEL and WATFLOOD. When these five top scored models were compared HEC-HMS suited better the requirements.

The lumped model requires set-up and calibration of another model, thus requires more time (Cunderlik, 2003) however due to time constraints to carry out this research they could not be adopted. On the other hand, the distributed models are costly (Cunderlik, 2003) and due to limited funding for the research they could not also be adopted. The semi-distributed models are a good trade off , however most of them do not have enough technical documentation which limits referencing and how to operate the software (Cunderlik, 2003). Therefore, this research has adopted HEC-HMS and HEC RAS models by the US Army Corps to simulate the floods. The software are public domain and have been used by other researchers.

**HEC –HMS**

HEC –HMS was selected for the following reasons, it is:

a) A free software,
b) The input data format is the same as esri data format (shapefiles and raster),
c) Readily available technical documentation, that makes it easy to operate,
d) Simulate both single-event and continuous models,
e) The temporal and spatial scale are flexible,
f) Process interception and infiltration,
g) On the scale of short, medium and long, set up time, ease of use, and expertise requirements are medium,
h) The Operating system includes Windows and Linux, there is enough technical support.

**HEC-RAS**

This study adopted HEC-RAS models to determine the depth and extent of the riverine flood for the following reasons (Abushandi & Merkel, 2013; Chu & Steinman, 2009):

a) Availability of open-source software to run the model

b) The standardized input data format, same as the Environmental Systems Research Systems Inc. (ESRI) data format (shapefiles and raster grid),
c) Readily available technical documentation, that makes it easy to operate,
d) The temporal and spatial scales are flexible,
e) On the scale of short, medium and long, set up time, ease of use, and expertise, the requirements are medium,
f) The Operating System includes Windows and Linux, thus there is enough technical support.
g) Applicable in large river basin, flood hydrology and small urban or agricultural watershed runoff.
h) Applicable in humid, tropical, subtropical, and arid catchments.

## 4.2 Develop and analyze the hydrological model

As demonstrated in section 2.4.3, there are different hydrologic software that integrate GIS and hydrological modeling. Similarly, there are various criteria for choosing the appropriate software (Cunderlik, 2003). The criteria are either user- dependent or project-dependent (Cunderlik, 2003). The user-dependent criteria consider user preference while project dependent considers the project requirements and purpose.

### 4.2.1 Data and software

**Computer requirement**

The following computer software are installed and used:

a) ArcGIS 10.5 for visualization, analysis and interface
b) HEC-GeoHMS extension installed in ArcGIS 10.5 for delineation of basin characteristics to create a model
c) ArcHydro tool installed in ArcGIS 10.5 for delineation of basin characteristics
d) HEC-HMS model software to simulate the model

**Data**

The following datasets are used as inputs for the model:

*a) DEM*

The SRTM DEM in Figure 4-3 covering the catchment of the Shire river catchment in Chikwawa was downloaded in raster format from USGS data portal (U.S. Geological Survey, 2019). The DEM was acquired on 11 February 2000 at a resolution of 1-arc and was published on 23 September 2014. This the latest DEM available online by US Geological Survey. The DEM was used as a main data input to delineate the subbasins and drainage lines, analysis of the area hydrology and compute slope and elevation.

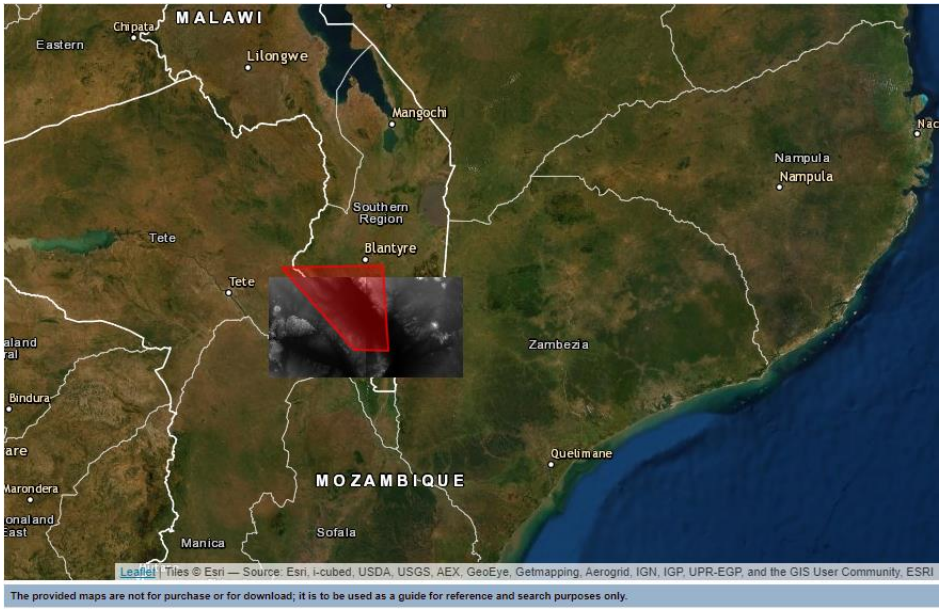


Figure 4-3: SRTM DEM downloaded on US Geological Survey data portal

*b) Soil type data (polygon shapefile)*

The soil data show in Figure 4-9 was sourced from National Spatial Data Center at Malawi Department of Surveys through the online data portal called MASDAP (National Spatial Data Center, 2019). The soil type is grouped as A, B, C, D. Table 4-1 illustrates the soil codes in relation to Chikwawa soil types and their infiltration rates. The infiltration rates were provided as attribute data of the soil data. The soil data was digitized from Topographical Map with scale of 1: 150 000. The soil data was used together with land use data to compute runoff Curve Numbers (CN).

Table 4-1: soil codes in relation to soil types and loss rates (source: (Fleming & Doan, 2013)

| Soil Code or Group | Soil Type | Infiltration rate | Range of loss rate (mm/hr) |
|---|---|---|---|
| A | Sand, Loamy sand, Sandy Loam | Low runoff potential and high infiltration rates | 7.6 – 11.4 |
| B | Silt loam or loam | Moderate infiltration rate when wetted | 3.8 - 7.6 |
| C | Sandy clay loam | Low infiltration rate when thorough wetted | 1.3 - 3.8 |
| D | Clay loam, Silty clay loam, Sandy clay, Silty clay, Clay | Highest runoff potential and low infiltration when wetted thoroughly | 0.0 - 1.3 |

*c) Land use data (polygon shapefile)*

The land use in Figure 4-9 has four classes namely: water, vegetation, built-up, bare land and each land use class is assigned land use value (LUVALUE as indicated in Table 4-6), 1, 2, 3, and 4 respectively. The land use data was created Maximum Likelihood Classifier (MLC) method of classification in Envi Software. Training sites were digitized using the mosaicked Landsat image as reference to specify the distinguished classes. The land cover themes included:

i. The agricultural land: included herbaceous and vegetation planted or cultivated thus presented as tillage, harvest and irrigation
ii. Built-up area: included artificial construction including buildings and roads
iii. Dense vegetation: high, closed, continuous, multi-layered and broad leaves tree and shrubs.
iv. Waterbodies: water covered surfaces like rivers, dams, reservoirs.
v. Bare areas: surfaces not covered by any artificial or natural features, examples are bare rock areas and soil. Barren and sparsely vegetations were categorized in this theme

The classification results of each classifier were assessed for accuracy using confusion matrix by determining overall accuracy and kappa- coefficient.

Overall accuracy in Figure 4-4 was calculated by adding the number of correctly classified values and dividing the total number of values. For instance, the overall accuracy of MLC was calculated as below, the corrected classified values were obtained from Figure 4-4, where the values used are highlighted in Orange:

$$Correctly\ classified\ values = 676 + 685 + 3805 + 50363 + 31071 + 3954$$
$$= 92\,989$$

$$Total\ number\ of\ values = 680 + 733 + 53021 + 31684 + 2437 + 3956$$

$$= 96\,672$$

$$Overall\ accuracy = \frac{92989}{96672} = 0.96$$

$$Overall\ accuracy\ \% = 0.961793 * 100\% = 96.18\%$$

| Class | Prod. Acc. (Percent) | User Acc. (Percent) | Prod. Acc (Pixels) | User Acc. (Pixels) |
|---|---|---|---|---|
| Road | 99.41 | 77.43 | 676/68 | 676/873 |
| Sand | 93.45 | 71.95 | 685/73 | 685/952 |
| Built-up | 91.44 | 92.20 | 3805/416 | 3805/4127 |
| Sparse Vegeta | 94.99 | 98.84 | 50363/5302 | 50363/50952 |
| Bare Soil | 98.07 | 93.53 | 31071/3168 | 31071/33219 |
| Water | 99.92 | 99.31 | 2435/243 | 2435/2452 |
| Vegetation | 99.67 | 99.95 | 3954/396 | 3954/3956 |

Figure 4-4: Snap shot of accuracy assessment report of MLC

Kappa coefficient,$k$ measures the agreement between classification and truth values. A kappa value of 1 represents perfect agreement, 0 represents no agreement.

$$k = \frac{\mathrm{N}\sum_{i=1}^{n} m_{i,i} - \sum_{i=1}^{n}(G_i\, C_i)}{\mathrm{N}^2 - \sum_{i=1}^{n}(G_i\, C_i)} \qquad \text{Eq 1}$$

Where: N is the total number of classified values compared to truth values, $i$ is the class number

$m_{i,i}$ is the number of values belonging to the truth class $i$ that have also been classified as class $i$, $G_i$ is the total number of truth values belonging to class $i$, $C_i$ the total number of predicted values belonging to class $i$

Apart from creation of CN, land use data was used in development of hydraulic model to compute Manning n values, and flood risk assessment.

*d) Channel data*

Like soil data the river network in vector format was obtained from Malawi Department Surveys and was also digitized from 1:50 000 Topographical Map. The channel data was used to delineate basin characteristics as input data for computing hydrologically correct DEM called 'Hydro DEM'.

*e) Gage rainfall data*

The rainfall data observed at met stations within the catchment of interest was acquired in Excel format from Malawi Meteorological Services. The data was measured in millimeters (mm) dated from year 1946 to 2016 recorded as average daily rainfall observation of different met station. The met station

that was used for this study were Chikwawa and Nchalo met stations as it is within the study catchment, see data table in appendix 7.2.

*f) River Discharge data*

The Surface Water Division under the Department of Water Resources within the Ministry of Agriculture and Irrigation, Water Resources Monitoring (MoAIWD) in Malawi is responsible for hydrological observations of water level and discharge. This study could not access MoAIWD data because of lack of data due to inadequate up-to-date observation (MoAIWD, 2018). Alternatively, it used satellite river discharge data as observed flows for validation and calibration of both HEC HMS and HEC RAS models. The satellite obtained using Advanced Microwave Scanning Radiometer- Earth Observing System (AMSR-E) by Dartmouth Flood Observation-DFO and the Global Flood Detection System-GFDS (De Groeve, et al., 2015). Each river discharge is an average of the mean annual flows for 5 consecutive years of the record at a time. The satellite gauging site in the study area were represented as yellow pins in Figure 4-5. The annual maximum discharge for 2015 was 14 590 $m^3$/sec at 253 GFDS site (refer to Figure 4-5 below) and 10 645.58 $m^3$/sec at 56 GFDS site. 56 GFDS site was close to the subbasin outlet.

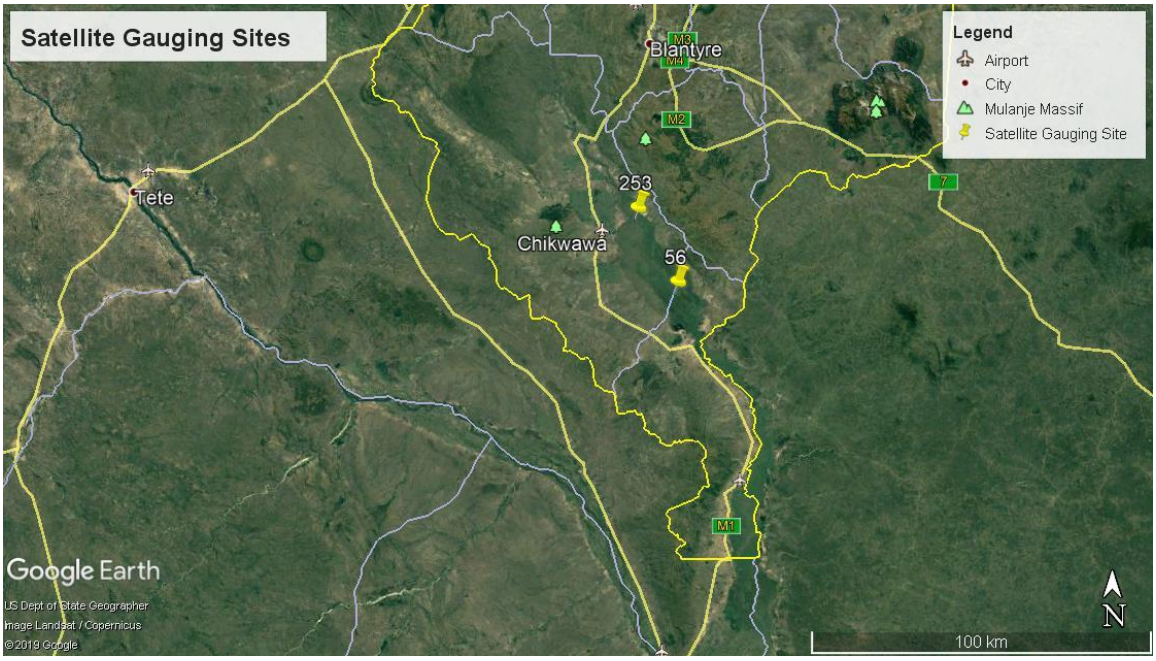


Figure 4-5: Satellite river discharge for Shire Gage Station in Chikwawa

All the data used above were projected to the Universal Transverse Mercator coordinate system based on the datum Arc 1950 and Geographic Coordinate System (GCS) as provided in Table 4-2 below.

Table 4-2: The projection system for all the data

| Projection | Details |
|---|---|
| Projected coordinate system | Arc1950 Universal Transverse Mercator (UTM) Zone 36 South |
| Projection | Transverse Mercator |
| False Easting | 500000 |
| False Northing | 10000000 |
| Central Meridian | 33 |
| Scale Factor | 0.9996 |
| Latitude of Origin | 0 |
| Linear Unit | Meter |
| Geographic Coordinate System | GCS Arc 1950 |
| Datum | Arc 1950 |
| Prime Meridian | Greenwich |
| Angular Unit | Degree |

### 4.2.2 Development of HEC HMS model in ArcGIS

The development of HEC HMS required delineation of basin/watershed characteristics and stream that were inputs of the model simulation. Figure 4-6 summaries the model development process.

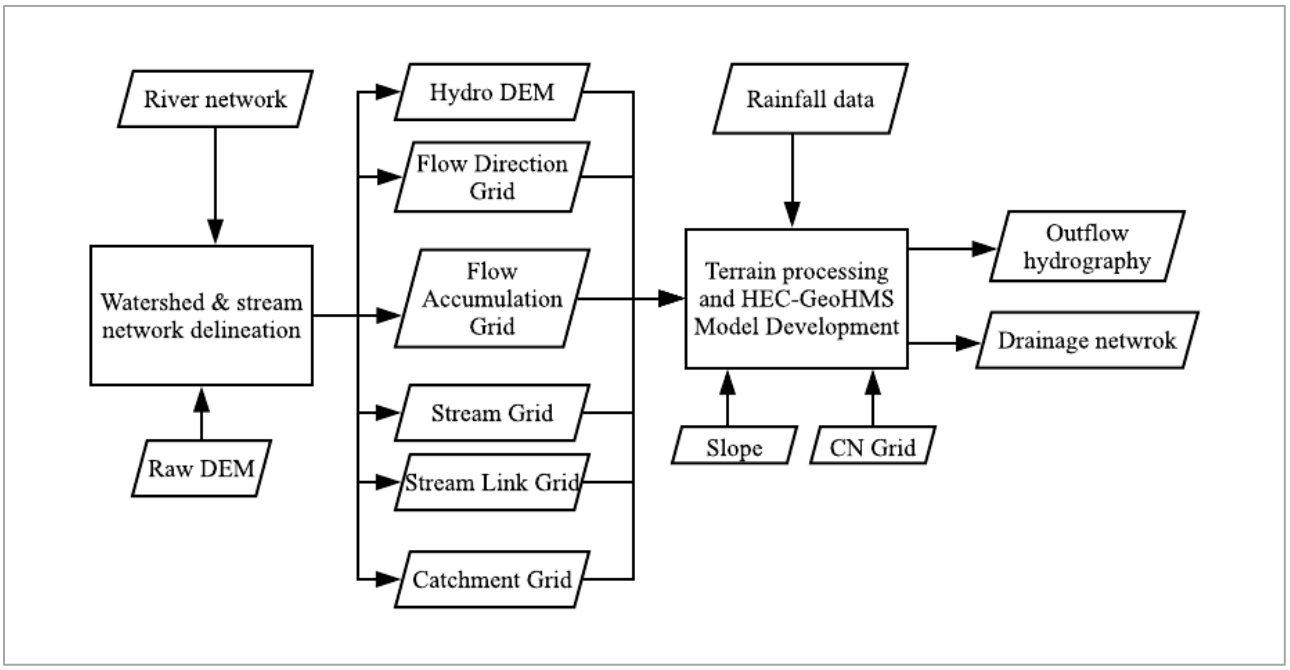


Figure 4-6: Processes and data for computing hydrological model (Source: Sabatini, 2014: 9)

The initial steps to delineate the watershed and stream network involve generation of various raster grids from the raw DEM. The following grids were generated using ArcHydro tool extension in ArcGIS tool their sequence:

a) Hydro DEM (see Figure 4-7a): is a reconditioned DEM created by filling the sinks of the DEMs to modify the elevation of the reconditioned DEM that could limit water flow,
b) Flow direction (see Figure 4-7b): represents DEMs' flow direction based on eight-point pour model
c) Flow accumulation (see Figure 4-7c): to generate the number of upstream cells draining to a given cell.
d) Stream grid (see Figure 4-7d): represents grid cell with stream and no streams. The stream cells have a value of "1" for grid values greater than the threshold.
e) Stream link grid (see Figure 4-7e): the streams are segmented and assigned a unique identification, either as head segment or two segment junctions. All the cells in a segment contained the same grid code that was particular to that segment
f) A catchment grid (see Figure 4-7f): is delineated from grid code value corresponding to the stream segment value to which each cell of the catchment belongs. During this process Drainage Line, Adjoint Catchment, and Drainage Point grids are converted from raster grid format to vector format. The vector layers form part of the basin network.
g) Slope grid: is computed as a hydrologic skeleton to delineate watersheds or sub-watersheds for any given point on delineated stream network.

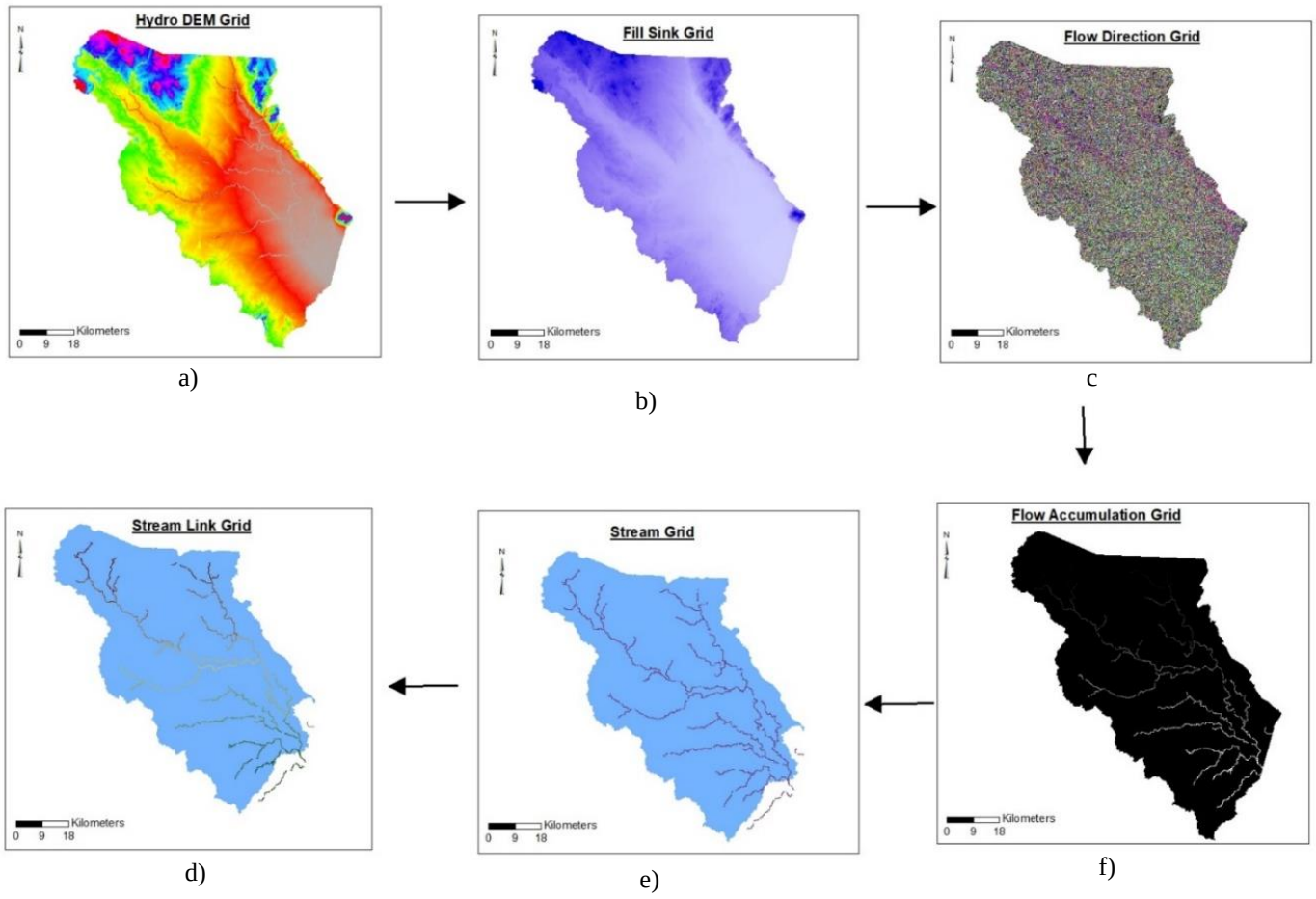


Figure 4-7: Delineated grids (a)-(f)

The simulation of a hydrological model requires the understanding of physical characteristics like the actual system by estimating the hydrologic parameters (Dooge, 1975). Generally, the physical characteristics that were extracted are listed in Table 4-3 below.

Table 4-3: The extracted physical or topographic characteristics of the subbasin and streams (Source: Fleming & Doan, 2013: chapter 9)

| **Data layer** | **Physical Characteristics (in meters)** |
|---|---|
| Channel layer (Table 4-4) | Length; upstream elevation; downstream elevation; slope |
| Subbasin layer (Table 4-5) | Area; subbasin average slope |
| Centroid layer | Centroid location; centroid elevation |
| Longest flowpath layer | Location of the longest flowpath; longest flow length; upstream elevation; downstream elevation; slope between endpoints; length to project outlet; elevation at 10% of longest flowpath (from the outlet); elevation at 85% of longest flowpath (from the outlet); slope along the longest flowpath based on point 10% and 85%. |
| Centroidal flowpath layer | Location of the centroidal flowpath; centroid length |

The computed river characteristics are listed in Table 4-4, and that of the subbasins in Table 4-5**.**

Based on the river extent, the delineated basin consisted of 9 junctions, 19 subbasins, 19 river reaches, 1 source, 1 outlet and 1 sink (Figure 4-8). Out of the 19 river reaches, 9 reaches (R30, R50, R70, R90, R110, R130, R150, R170, R190 as highlighted in Table 4-4) formed part of the Shire river. The other 10 reaches were tributaries connected to the Shire river.

Table 4-4: Channel characteristics

| Name | Elevation upstream (m) | Elevation downstream (m) | River length (m) | Slope (Percentage Rise) |
|---|---|---|---|---|
| R10 | 158 | 92 | 5982.9 | 0.011031 |
| R20 | 230 | 92 | 5207.4 | 0.026501 |
| R30 | 92 | 87 | 1669.4 | 0.002995 |
| R40 | 234 | 87 | 13546.6 | 0.010851 |
| R50 | 87 | 84 | 3498.5 | 0.000858 |
| R60 | 153 | 84 | 6201.4 | 0.011127 |
| R70 | 84 | 74 | 22835.1 | 0.000438 |
| R80 | 108 | 74 | 10969.3 | 0.0031 |
| R90 | 74 | 70 | 9039.7 | 0.000442 |
| R100 | 84 | 70 | 8817.5 | 0.001588 |
| R110 | 70 | 67 | 6597. | 0.000455 |
| R120 | 79 | 67 | 9091.7 | 0.00132 |
| R130 | 67 | 64 | 910.5 | 0.00033 |
| R140 | 64 | 64 | 3402.5 | 0 |
| R150 | 64 | 60 | 16646.6 | 0.00024 |
| R160 | 72 | 60 | 10690.8 | 0.001122 |
| R170 | 60 | 57 | 10052.4 | 0.000298 |
| R180 | 64 | 57 | 20410.4 | 0.000343 |
| R190 | 57 | 57 | 16467.4 | 0 |

The delineated basin in Figure 4-8 has five hydrologic elements (Merwade, 2012) as described below:

a) Junction - combines flows from upstream reaches and subbasin.
b) Sink – represents the outlet of the watershed and has no outflow.
c) Source –introduces flow into the basin model from a stream outside the boundary of the modeled basin. The source has no inflow.
d) Subbasin – converts the rainfall to runoff on a watershed.
e) Reach - transfers streamflow downstream.

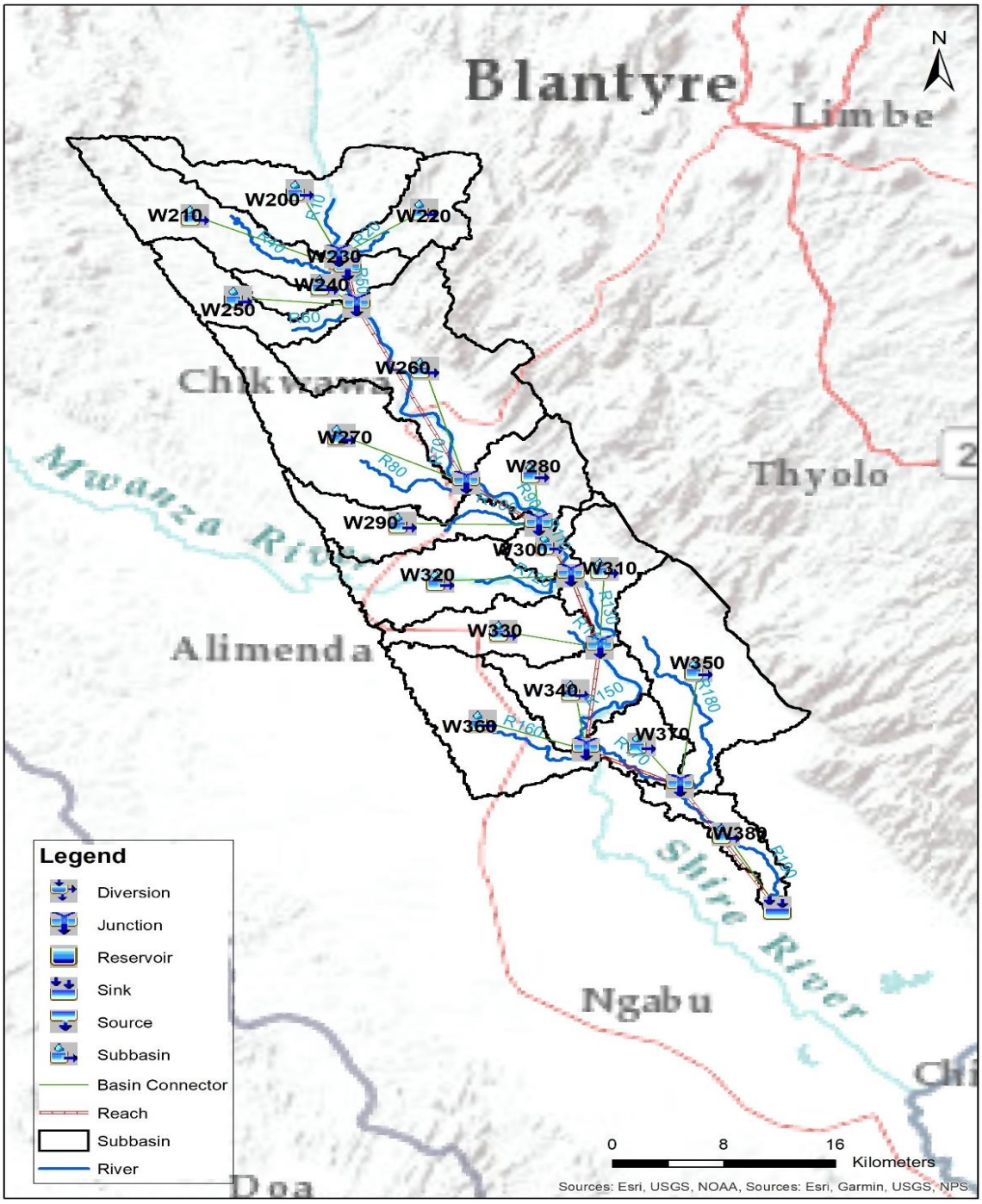


Figure 4-8: Elements of the basin model

### 4.2.3 The simulation of the model

HEC-HMS assumes that the land and water is categorized in two surfaces: direct connected impervious surface where there is no infiltration and all precipitation becomes runoff; pervious surface, where volumes of water infiltrate the soils and become losses. The losses for a specific period are

determined using loss model and are subtracted from the MAP depth. The MAP depth represents runoff volume and is assumed to be evenly distributed over the watershed. The remaining depth is excess precipitation.

Basically, runoff is computed as follows:

$$Runoff\ volume = Precipitation\ volume\ - Losses\ volume \qquad Eq\ 2$$

HEC-HMS model is subdivided a number of seven parameters namely: loss, transform, canopy, surface, routing, loss/gain and baseflow. The parameters are further subdivided into other parameter. This study had simulated four parameters to meet its objectives: loss, transform, routing and baseflow. All the subbasin parameters values used in the model are in Table 4-5 and river channel parameters in Table 4-8. The computations of the applied parameters and their subdivided parameters; the meteological model; model time specification; and model flows and volumes, are explained further below.

*a) Loss*

Various infiltration models are employed for different transformation. The loss models applicable in HEC-HMS are initial and constant-rate, SCS Curve Number (CN), initial and constant, Gridded SCS CN, Green and Ampt, Deficit and constant rate, Soil moisture accounting (SMA), and Gridded SMA. This research has applied initial and constant, because it is a simple, predictable using range of constant loss rates (mm/hr) based on subbasin's soil groups (Fleming & Doan, 2013). The constant loss rates (in Table 4-5 for each subbasin were estimated based the subbasin's the soil groups and range provided in Table 4-1. The other parameter assigned to the subbasin are impervious percent (%) and initial loss (mm), as shown in Table 4-5.

Table 4-5: Subbasin characteristics and parameters

| | Subbasin characteristics | | | | Loss: Initial and constant | | | | | Transform SCS UH | | Baseflow: Recession | | |
|---|---|---|---|---|---|---|---|---|---|---|---|---|---|---|
| **Basin name** | **Basin area (km)** | **Basin Average Slope (%)** | **Basin CN** | **Soil Group** | **Maximum retention, S (mm)** | **Initial constant ratio** | **Initial loss (mm)** | **Impervious (%)** | **Constant rate (mm/hr)** | **Hydraulic length (m)** | **Lag time** | **Initial Discharge (m3/s)** | **Recession Constant** | **Ratio to Peak** |
| W200 | 973.05 | 8.03 | 32.85 | D | 519.22 | 0.05 | 25.96 | 2.5 | 1.3 | 120725.86 | 110.73 | 113 | 0.9 | 0.35 |
| W210 | 865.98 | 7.32 | 3.26 | A | 7546.22 | 0.05 | 377.311 | 2.5 | 11.4 | 125198.84 | 753.87 | 113 | 0.9 | 0.35 |
| W220 | 47.23 | 16.15 | 43.52 | A | 329.68 | 0.05 | 16.48 | 2.5 | 11.4 | 113784.24 | 55.20 | 147 | 0.9 | 0.35 |
| W230 | 23.47 | 8.09 | 64.69 | A | 138.64 | 0.05 | 6.93 | 2.5 | 11.4 | 95797.57 | 39.58 | 147 | 0.9 | 0.35 |
| W240 | 311.39 | 8.1 | 39.66 | A | 386.45 | 0.05 | 19.32 | 2.5 | 11.4 | 103259.43 | 80.04 | 147 | 0.9 | 0.35 |
| W250 | 508.13 | 6.12 | 34.02 | A | 492.69 | 0.05 | 24.63 | 2.5 | 11.4 | 114341.43 | 117.29 | 147 | 0.9 | 0.35 |
| W260 | 1670.98 | 12.43 | 55.22 | A | 205.94 | 0.05 | 10.29 | 2.5 | 11.4 | 98799.26 | 41.64 | 147 | 0.9 | 0.35 |
| W270 | 1275.12 | 3.44 | 55.87 | A | 200.60 | 0.05 | 10.03 | 2.5 | 11.4 | 99537.62 | 78.33 | 147 | 0.9 | 0.35 |
| W280 | 530.15 | 10.17 | 54.42 | D | 212.76 | 0.05 | 10.63 | 2.5 | 1.3 | 76453.93 | 38.26 | 147 | 0.9 | 0.35 |
| W290 | 569.50 | 2.85 | 65.26 | D | 135.19 | 0.05 | 6.75 | 2.5 | 1.3 | 85621.75 | 60.08 | 147 | 0.9 | 0.35 |
| W300 | 216.23 | 4.08 | 79.82 | D | 64.21 | 0.05 | 3.2107 | 2.5 | 1.3 | 63314.98 | 26.19 | 147 | 0.9 | 0.35 |
| W310 | 485.77 | 7.52 | 72. | D | 98.77 | 0.05 | 4.938 | 2.5 | 1.3 | 62385.01 | 23.98 | 147 | 0.9 | 0.35 |
| W320 | 777.61 | 2.71 | 72.83 | A | 94.77 | 0.05 | 4.73 | 2.5 | 11.4 | 75671.49 | 45.53 | 147 | 0.9 | 0.35 |
| W330 | 556.61 | 2.97 | 65.7 | A | 132.59 | 0.05 | 6.62 | 2.5 | 11.4 | 67674.84 | 48.23 | 147 | 0.9 | 0.35 |
| W340 | 602.38 | 2.99 | 64.28 | D | 141.12 | 0.05 | 7.05 | 2.5 | 1.3 | 47613.99 | 37.61 | 147 | 0.9 | 0.35 |
| W350 | 1321.95 | 4.97 | 79.3 | D | 66.29 | 0.05 | 3.31 | 2.5 | 1.3 | 47185.07 | 19.07 | 147 | 0.9 | 0.35 |
| W360 | 943.30 | 3.06 | 74.91 | C | 85.08 | 0.05 | 4.25 | 2.5 | 3.8 | 51295.62 | 29.6 | 147 | 0.9 | 0.35 |
| W370 | 352.36 | 3.01 | 99. | C | 2.56 | 0.05 | 0.12 | 2.5 | 3.8 | 21332.30 | 5.65 | 147 | 0.9 | 0.35 |
| W380 | 352.53 | 3.22 | 99. | C | 2.56 | 0.05 | 0.12 | 2.5 | 3.8 | 20638.82 | 5.32 | 147 | 0.9 | 0.35 |

Initial loss is expressed as:

$$I_a = \lambda \times S \qquad Eq\ 3$$

Where: $\lambda$ is initial abstraction ratio which ranges from 0.002 to 0.005. Valle Junior (2019) in recommended the use of 0.005 instead on 0.002; $S$ is the maximum retention (mm) and is solved using the equation below:

$$S = \frac{25400}{CN} - 254 \qquad Eq\ 4$$

The computed S is found in Table 4-5. The CN values for each subbasin in Table 4-5 were derived from CN Grid. In this research, the CN Grid is created in ArcGIS by employing these steps:

i. Merging soil and land use data and creation of CN Lookup table

Land use, soil map layers, and CNLookUP in Figure 4-9 were merged, followed by creation of the CN Look-up table in ArcMap. The table was formed by populating manually the CN number of waters, settlements, forest and agriculture with respect to the assigned SoilCode, as shown in the CNLookUP Table 4-6. Columns A/B/C/D have curve numbers for corresponding soil groups for each Land Use class (LUValue). These numbers are obtained from SCS TR55 (1986).

Table 4-6: CNLookUP table

| **Object ID** | **Description** | **A** | **B** | **C** | **D** | **LUVALUE** |
|---|---|---|---|---|---|---|
| 1 | Water | 100 | 100 | 100 | 100 | 1 |
| 2 | Built-up | 57 | 72 | 81 | 86 | 2 |
| 3 | Vegetation | 30 | 58 | 71 | 78 | 3 |
| 4 | Bare land or Agriculture | 67 | 77 | 83 | 87 | 4 |

ii. Creation of CN grid

Lastly, the CN grid was created using the raw DEM, merged soil and land use layer, and CNLook-up table as presented in Table 4-6. Within HEC-GeoHMS, the merged soil and land use feature classes, and the lookup table (CNLookUp) combined to form the curve number grid in Figure 4-9.

CN for each subbasin with diverse soil types and land use is referred to as composite CN, and was computed using the formula below:

$$CN_{composite} = \frac{\sum A_i CN_i}{\sum A_i} \qquad Eq\ 5$$

Where: $CN_{composite}$ is the composite CN used for runoff volume computations, $i$ is an index of watersheds subdivision of uniform land use and soil type, $CN_i$ is the CN for subdivision $i$, $A_i$ is the drainage area of subdivision $i$.

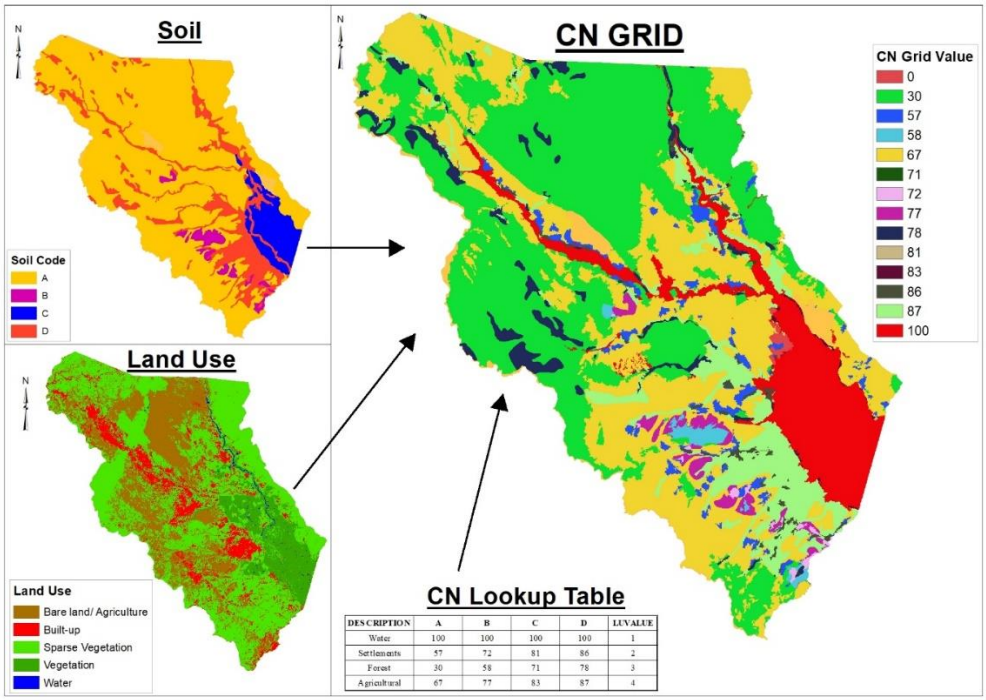


Figure 4-9: Merging soil, land use and CN Lookup table to create CN Grid

*b) Transform*

This simulates the movement of precipitation that has not infiltrated (the impervious surface) and not stored (pervious surfaces) called excess precipitation and the process is called transformation (Fleming & Doan, 2013). Direct-runoff models applied in HEC-HMS are categorized in two: the empirical models which are grouped as the traditional unit hydrograph (UH) models such as User- specific unit hydrograph (UH), Clark's UH, Snyder's UH, and Soil Conservation Services (SCS) Unit Hydrograph (UH); the conceptual models which are kinematic-wave models of overland flow such as ModClark, Kinematic wave transform. The difference between the two categories is that the empirical models have less details of physical mechanics and limited to internal processes that affect the movement of excess precipitation

over a catchment, while the conceptual models take into account all physical mechanisms influencing the flow of excess precipitation (Fleming & Doan, 2013).

The study has applied the empirical model, particularly the SCS UH model, because of the following reasons:

- Data available since it only relies on one parameter, rainfall data, "*which varies as a function of soil type, land use and treatment, surface condition and antecedent moisture condition"* (Fleming & Doan, 2013), unlike the conceptual model that requires all physical mechanics parameters were almost impossible to obtain considering the scope of the research.
- It is *"simple, predictable, and stable method"* (Fleming & Doan, 2013).
- The method is well developed and widely applied globally (Fleming & Doan, 2013).

Lag time $t_P$ is a main parameter for SCS UH representing time in minutes from the center of mass of excess rainfall to UH peak for each subbasin (Fleming & Doan, 2013). The lag time in Table 4-5 was calculated as below:

$$t_P = \frac{L^{0.8}\left(\frac{1000}{CN}-9\right)^{0.7}}{19000y^{0.5}} \qquad Eq\ 6$$

Where: $y$ is average watershed slope (in present-%), $L$ is length to divide (m), as given in Table 4-5.

*c) Routing*

The routing models simulate one-dimensional open channel flow, thus predicting time series of downstream flow, stage, velocity, and upstream hydrographs (Fleming & Doan, 2013). The routing methods are a Kinematic wave, Lag, Modified Puls, Muskingum, Muskingum- Cunge Standard Section, Muskingum- Cunge 8-point Section, Confluence, and Bifurcation. The following guidelines as per Technical Reference Manual for HEC-HMS are used to select routing model.

Table 4-7: Guidelines for selecting routing model (Source: Feldman, 2000: p. 90)

| **If this is true** | **Then consider this model** |
|---|---|
| No observed hydrography data available for calibration | Kinematic wave; Muskingum-Cunge |
| Significant backwater will influence discharge hydrography | Modified puls |
| Flood wave will go out of bank, into flood plain | Modified puls, Muskingum-Cunge with 8-point cross section |
| Channel slopes > 0.002 and $\frac{TS_0u_0}{d_o} \geq 171$<br>T = hydrograph duration, S0 = Slope, U0 = reference mean velocity, d0 = reference flow depth | Any |
| Channel slopes from 0.002 to 0.0004 and $\frac{TS_0u_0}{d_o} \geq 171$ | Modified puls, Muskingum-Cunge, Muskingum |
| Channel slope < 0.0004 and $TS_O\left(\frac{g}{d_o}\right)^{1/2} \geq 30$<br>g = accerelation of gravity | Muskingum-Cunge |
| Channel slope < 0.0004 and $TS_O\left(\frac{g}{d_o}\right)^{1/2} < 30$ | None |

The Muskingum model was used to estimate two parameters: $K$ and $X$, which represent storage-time constant (Song, et al., 2011). Originally, Muskingum routing model for a river reach was derived in the equations without lateral inflow, see below (Song, et al., 2011):

$$\frac{dW}{dt} = I - Q \qquad Eq\ 7$$

$$W = K\,[xI + (1-x)Q] \qquad Eq\ 8$$

Where: $W$ is the water storage, $t$ is time, $I$ is the inflow, $Q$ is the outflow, $K$ is the wave time travel. The wave time travel $K$ in table Table 4-8 was calculated (Song, et al., 2011) by:

$$K = \frac{L}{3600\,V_c} \qquad Eq\ 9$$

Where: $V_c$ is the flood wave celerity which was estimated as 7m/s, $L$ is the reach length in table Table 4-4.

$x$ represents storage- time constant that considers flood peak attenuation and hydrograph shape flattening in motion which can be estimated using the kinematic wave equation by Cunge (Song, et al., 2011):

$$x = \frac{1}{2} - \frac{D}{V_C L} \qquad Eq\ 10$$

$D$ is the diffusion coefficient of a diffusion wave

$x$ ranges from 0 to 0.5, the standard is 0.2

The $K$ and $x$ Muskingum parameters for river reach R10 to R100 are shown in the Table 4-8 below.

Table 4-8: K and x Muskingum parameters

| Channel | Muskingum K (Minutes) | Muskingum X |
|---|---|---|
| R30 | 4 | 0.2 |
| R50 | 8 | 0.1 |
| R70 | 54 | 0.1 |
| R90 | 22 | 0.01 |
| R110 | 16 | 0.01 |
| R130 | 2 | 0 |
| R150 | 40 | 0 |
| R170 | 38 | 0 |
| R190 | 33.2 | 0 |

*d) Baseflow*

The different methods of estimating baseflow in HEC-HMS model are: monthly-varying baseflow, exponential recession and linear reservoir. The exponential recession was used to compute to baseflow considering that the parameters involved could be easily estimated, see Table 4-5 recession parameters for each subbasin.

Typical values of recession constants proposed by Pilgrim and Cordery in 1992 (Feldman, 2000) in Table 4-9, were taken into consideration to come up with values in Table 4-9.

Table 4-9: Typical recession constants (source: Feldman, 2000)

| Flow component | Recession constant, Daily |
|---|---|
| Groundwater | 0.95 |
| Interflow | 0.8 - 9 |
| Surface runoff | 4.3 - 8 |

*e) The meteorological model*

The meteorological model specifies a time series of rainfall at a rainfall gage. HEC- HMS has seven methods of representing rainfall data, namely: (1) Specified Hyetograph, (2) Frequency storm, (3) Gage weights, (4) SCS storm, (5) Gridded precipitation, (6) HMR 52 storm, (7) Inverse distance, and (8) standard project storm. Grid precipitation was identified as the appropriate method for this research because the rainfall estimation was spatially distributed without bias unlike Gage rainfall where the rainfall observation represents only the location of the Gage Station. The rainfall

distribution of the other areas was estimated from the closest Gage Station despite the possibility that areas within the same catchment may experience the different rainfall at a given time.

The average daily rainfall data were entered manually into the Time-Series table from 01 Jan 2012 to 01 April 2015. Sample daily rainfall data are given in Appendix 7.2 for Nchalo and Chikwawa Met stations (see locations of Met stations in Figure 3-1).

*f) The control specifications*

The control specifications were defined to specify time limit of the simulation. The time limit include simulation started on 01 Jan 2012 at 00:00 hrs and ended on 01 April 2015 at 00:00 hrs. The flood event focused in this research was from 01 Jan 2015 to 31 Mar 2015. However, the simulation was run two years before the flood event to understand the discharge trend. The time interval for the rainfall data was 1 day and the units were incremental millimeters. The simulation interval was set as 5 minutes (lower than 0.29 ×Muskingum K) to ensure stability in the routing model.

*g) Computation of discharge volume and flow*

When all the parameters were set, the models computed the discharge volumes and flow of water which were presented as hydrographs or just time series data in tables. The hydrograph can be illustrated as a simple triangle with rainfall duration $D$, time of rise $T_R$ (hr), time of fall $B$, and $Q_P$ in cubic meter per second − cms as shown in Figure 4-10 (Indian Institute of Technology , 2006).

The volume of direct runoff is expressed as below (Indian Institute of Technology , 2006):

$$Vol = \frac{Q_P T_R + Q_P B}{2} \qquad Eq\ 11$$

$B$ is given by:

$$B = 1.67 T_R \qquad Eq\ 12$$

Where: $B$ is time of fall (hr)

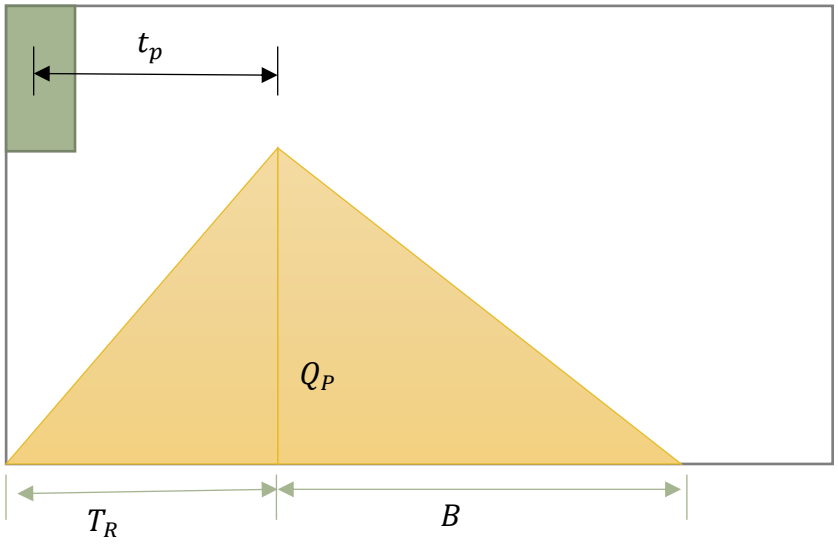


Figure 4-10: Simple triangle representing unit hydrograph (UH) Source: Indian Institute of Technology (2006:7)

By making $Q_P$ the subject of the formula, $Q_P$ peak flow is calculated (Indian Institute of Technology , 2006; Fleming & Doan, 2013):

$$Q_P = \frac{2\ vol}{T_R + B} = \frac{0.75\ vol}{T_R} \qquad Eq\ 13$$

$$Q_P = \frac{0.75\ (640) A (1.008)}{T_R} = \frac{2.08\ A}{T_R} \qquad Eq\ 14$$

Where: 2.08 is conversion constant, $A$ is area of basin (sq m)

### 4.2.4 Model validation and calibration

The calibrated model was validated by assessing the performance of the model against the observed flows (Ouédraogo , et al., 2018). Thus, various calculations were applied to confirm the goodness of fit between the simulated and observed flows, and to measure the predictive power of the HEC HMS model (Romali et. al., 2018).

#### Validation

The validation was done to assess the accuracy of the results to match or closely match the observed flows at 56 GFDS site. The computed results were accepted based on the goodness of fit by calculating whether the computed values were satisfactory or not (Feldman, 2000). According to Feldman (2000) different methods to measure the goodness of fit include: sum of the absolute errors, sum of squared residuals, percent error in peak, peak-weighted root mean square error, and other graphical representations like scatter plot and residual plot. This study used the absolute error index

expressed as Root Mean Square Error (RMSE) to Standard Deviation Ratio (RSR), percent volume bias( PEV) percentage error in peak flow, which were ranked using general performance ratings for recommended statistics to accept the parameters or not (Ouédraogo , et al., 2018) :

Table 4-10: general performance ratings for recommended statistics

| **Performance rating** | **PEPF (%)** | **NSE** | **PEV** |
|---|---|---|---|
| Very good | < 15 | 0.75 to unity | <+/-10 |
| Good | 15 to 30 | 0.65 to 0.75 | +/-10 to +/-15 |
| Satisfactory | 30 to 40 | 0.50 to 0.65 | +/-15 to +/-25 |
| Unsatisfactory | > 40 | <0.50 | >+/-25 |

*"RSR ranges from 0 (optimal value) to 0.5 (very good performance)"* (Ouédraogo , et al., 2018).

a) Root Mean Square Error (RMSE) to Standard Deviation Ratio (RSR) was computed using the following equation:

$$RSR = \frac{\sqrt{\sum_{i=1}^{n}(O_i - S_i)^2}}{\sqrt{\sum_{i=1}^{n}(O_i - \overline{O})^2}} \qquad Eq\ 15$$

Where $O_i$ is the observed flow, $S_i$is the modeled flow, t is time, $\overline{O}$ is observed mean flow

b) The percent bias (PEV) was expressed as (Ouédraogo , et al., 2018):

$$PEV = \left|\frac{Vol_o - Vol_s}{Vol_o}\right| \times 100 \qquad Eq\ 16$$

Where $Vol_o$, $Vol_s$ are the observed and simulated volumes, respectively. Such that:

c) The percentage error in peak flow (PEPF), was solved using the equation (Ouédraogo , et al., 2018) below:

$$PEPF = \left|\frac{Q_{o(peak)} - Q_{s(peak)}}{Q_{o(peak)}}\right| \times 100 \qquad Eq\ 17$$

Where $Q_{o(peak)}$, $Q_{s(peak)}$ are the observed and simulated flows respectively, such that:

d) The NSE was calculated by using the equation below:

$$NSE = \frac{\sum_{t=1}^{T}(o_i^t - \overline{o})^2 - \sum_{t=1}^{T}(o_i^t - s_i^t)^2}{\sum_{t=1}^{T}(o_i^t - \overline{o})^2} \quad Eq\ 18$$

NSE is one of the well-known assessment methods for model efficiency in hydrological studies. The sufficient quality of NSE is suggested to be between more than 0.5 and less than 0.65 (Ouédraogo , et al., 2018). The calculated NSE is ranked based on Table 4-10

### Uncertainty analysis and evaluation of simulated results

The uncertainty analysis and evaluation of simulated results is carried out in HEC-HMS model software to assess the errors in the model calculations given the sample size of 91. The study evaluated the uncertainty of the seven parameters by simulating them individually namely, initial constant-constant Rate; initial and constant - initial loss; initial loss percent impervious, recession - initial discharge; recession - ratio to peak; recession constant; and SCS unit hydrograph - lag time. The uncertainty variables for on each model parameter included the minimum and maximum values in Table 4-9, the lower, upper and mode parameter values as given in the model. The uncertainty simulations were carried out within the same time period of the hydrological model and applied on subbasin W380 as main subbasin, W350 and W370 as additional subbasins linked to subbasin W380.

The uncertainty analyses used simple distribution methods. The triangular distribution was specifically applied to link the uncertainty error between W380, W370 and W350. Accordingly, W370 and W350 were sampled using linear regression with additive error method which measures the amount of error that both subbasins contributed to W380 and outlet point. A simple linear regression was defined for the two additional subbasins with slope (2.7), intercept (0), sigma (.000656168) and Mu (0) to obtain error uncertainty in normally distribution.

### Calibration of HEC HMS model

The calibration was carried out. During calibration the maximum and minimum constraints of various parameters were taken into consideration as listed in Table 4-11.

Table 4-11: Calibration parameter constraints (source: Feldman, 2000)

| Model | Parameter | Minimum | Maximum |
|---|---|---|---|
| Initial and constant rate loss | Initial loss<br>constant rate loss | 0 mm<br>0 mm/hr | 500mm<br>300mm/hr |
| Baseflow | Initial baseflow<br>Recession factor | 0 m3/s<br>0.000011 | 100000 m3/s<br>- |
| Muskingum routing | K<br>X | 0 hr<br>0 | 150 hr<br>0.5 |
| Lag routing | Lag | 0 min | 30000 min |
| SCS loss | Initial abstraction<br>Curve number | 0 mm<br>1 | 500 mm<br>100 |

The calibrations were done in two phases, first the automated optimization simulation, and second by try and error value adjustment. The four models illustrated in Table 4-9 were applied, and the calibration was implemented by adjusting some of the model parameters till the optimized values were obtained. The adjustment of the parameters was constrained to the minimum and maximum values provided in Table 4-9 above. Three optimization simulation (for W350, W370, and W380) were run independently and each one was iterated 100 times. The optimized values are shown in Table 5-2. The optimized model was also validated to be accepted or not.

## 4.3 Develop and simulate the hydraulic model

The main application of hydraulics is to define the behavior of flowing water within a "controlled environment" such as a river (Al-Abed, et al., 2005). Like Cabral, et al. (2015), Gharbi, et al. (2016), Snead (2000), and Al-Abed, et al. (2005), this research adopts Hydrologic Engineering Center's River Analysis System (HEC-RAS) to compute the water surface profiles and to estimate the heights and flows. The simulation input parameters of hydraulic model are primarily river length, lag time, time of concentration and average slope; drainage network, river cross-sections and over banks (Cabral, et al., 2015).

### 4.3.1 Data and Software

#### Software

HEC-HMS software, and ArcGIS 10.5 by ESRI were used to carry out the research. The HEC software processed and simulated the flood model. ArcGIS 10.5 processed, analyzed and visualized maps. The following HEC-HMS software were used:

a) The Geospatial River Analysis System (HEC-GeoRAS), installed as an extension in ArcGIS to create geometric data for hydraulic model.

b) HEC-RAS, a standalone software to simulate the hydraulic model and visualize flood model outputs.

## Data

a) *Digital Terrain Model (DEM)*

DEM is a three-dimensional representation of the land surface elevation with respect to a reference datum (Balasubramanian, 2017). DEM is a key hydraulic and hydrological model input to compute slope, delineate river network and catchment, and water depth by subtracting the terrain elevation from water levels (Abdou, et al., 2018; Feldman, 2000; Els, 2011; Abushandi & Merkel, 2013; Abdou et al., 2018; Cabral et al., 2015;Tong et al., 2017; Devia & Dwarakish, 2015). SRTM DEM digital grid of 30m medium resolution was adopted in this study because of non-availability of high-resolution alternatives covering the case study region and was freely available at United States Geological Survey (USGS) online open data hub. The latest SRTM DEM was acquired on 11 February 2000 and was publicized on 23 September 2014.

*b) River Discharge data*

The Surface Water Division under the Department of Water Resources within the Ministry of Agriculture and Irrigation, Water Resources Monitoring (MoAIWD) in Malawi is responsible for hydrological observations of water level and discharge. This study could not access MoAIWD data because of lack of data due to inadequate up-to-date observation (MoAIWD, 2018). Alternatively, it used satellite river discharge data in Figure 4-5 obtained using Advanced Microwave Scanning Radiometer- Earth Observing System (AMSR-E) by Dartmouth Flood Observation-DFO and the Global Flood Detection System- GFDS (De Groeve, et al., 2015). Each river discharge is an average of the mean annual flows for 5 consecutive years of the record at a time. The satellite gauging site covered the study in Figure 3-1. The annual maximum discharge for 2015 was 14 590 $m^3$/sec at 253 GFDS site.

*c) River channel geometry data*

The river channel geometry in Figure 4-11 including river centerline, cross sections, bank lines and flowpath were digitized from 30m medium resolution Landsat image before January 2015 floods with reference to Google base map in ArcMap 10.5. All datasets were projected to Universal Transverse Mercator (UTM) Arc 1960 coordinate system to make sure that corresponding pixels align geometrically.

*d) Manning n value*

Manning n value represents the Manning roughness coefficient which is the resistance of the river bed and floodplains to the flow of water for open natural flow (Asante, et al., 2008). Using classified land cover features, Manning n values for Chikwawa areas were estimated.

The following in Table 4-12 Manning n roughness values were assigned to the cross sections based on land use classes that the cross section corresponded with (Asante, et al., 2008):

Table 4-12: Manning n roughness values for various land cover classes (Asante, et al., 2008)

| **Anderson code** | **Description land use** | **Manning n roughness** |
|---|---|---|
| 100 | Urban and Built-up land | 0.035 |
| 211 | Dryland, cropland and pasture | 0.03 |
| 212 | Irrigation cropland and pasture | 0.035 |
| 213 | Mixed dryland or irrigated cropland and pasture | 0.033 |
| 280 | Cropland or grassland mosaic | 0.035 |
| 290 | Cropland/ woodland mosaic | 0.05 |
| 430 | Mixed forest | 0.1 |
| 500 | Waterbodies | 0.035 |
| 620 | Herbaceous wetland | 0.005 |
| 770 | Barren or sparsely vegetated | 0.03 |

The land cover themes and their descriptions indicated that Chikwawa is covered by agricultural land, irrigation cropland, waterbodies. built-up, sparsely vegetation. Hence the Manning n values with reference to Table 4-12 were categorized as 0.035 and 0.03. 0.03 represented barren, sparsely vegetation, and dryland. While 0.035 represented built-up, waterbodies, cropland or grassland mosaic.

*e) River Centerline*

When digitizing the river centerline, the image was zoomed in the centre of the river in the direction of flow. Each river was assigned length, river and reach name.

*f) Bank lines*

River bank lines indicated the boundary between the main channel and overbank floodplain areas both at the right and left side of the centerline.

*g) Flowpath*

Flowpath consisted of river centerline, left overbank and right overbanks and provided the distance between the downstream cross sections from the river centerline to the overbank areas.

*h) Cross section cutlines*

Cross section cutlines also called XS cutlines, represent the cross section distance and elevation of the river channel, shown as green lines in Figure 4-11. The elevations are interpolated from the DEM to compute the ground profile of the channel flow.

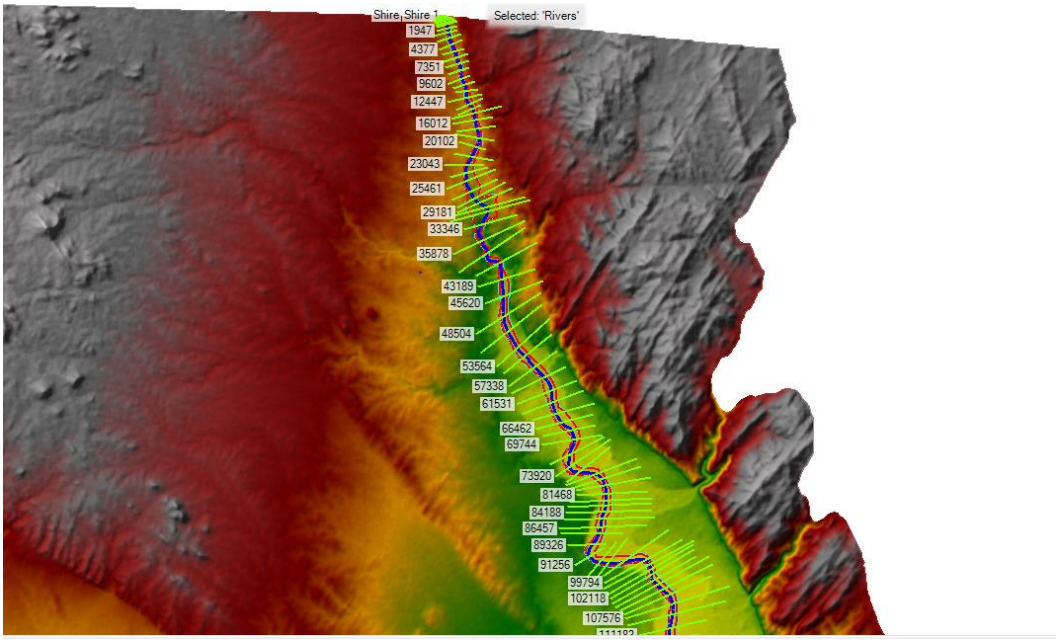


Figure 4-11: Cross sections (green), river centreline (blue), banklines (red) on a DEM

### 4.3.2 Simulation of hydraulic model

The geometry data and the flow data were set up in HEC-RAS to compute velocity, water surfaces profiles, and water surface extents from the river discharge in Figure 4-11. HEC RAS model has three types of computation, namely (1) the steady flow, (2) unsteady flow, (3) the movable boundary flow. The steady flow represents constant flow of water in a river without any changes and is applicable in open channel because the changes in depth and velocity at a point is generally gradual (Dyhouse, et al., 2007; Ponce, 2011; Mehta, 2018). The gradual changes allow satisfactory modeling in simulating steady flow in an open channel (Dyhouse, et al., 2007). The unsteady flow describes the changes in the flow because of changing depth and velocity in the river (Ponce, 2011). The movable boundary calculates the river bed aggradation using sediment continuity and sediment transport equations (*Ibid*). Steady flow was applied because its ability to provide satisfactory solution as per Dyhouse, et al. (2007).

#### Steady flow water surface profiles calculations

The standard step method was applied to compute the water surface profiles using energy equation (Brunner, 2016). Energy equation variables are expressed in Figure 4-12 and equations below. All the input and output variables were set to SI units.

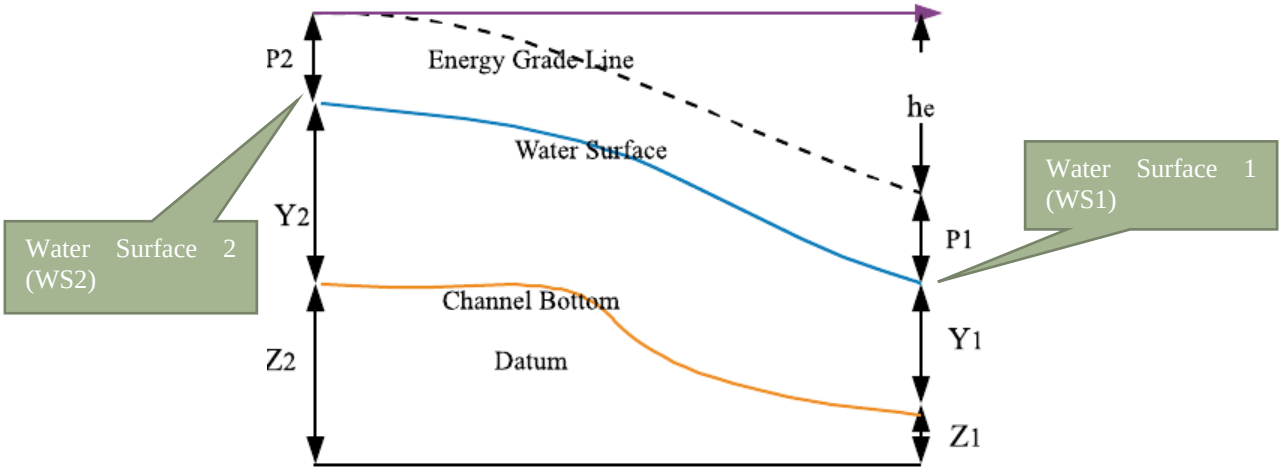


Figure 4-12: Representation of terms in energy equation (Brunner, 2016 p.2-3)

Based on Figure 4-12 energy grade line is the imaginary elevation of total energy head, water depth $Y_1$ and $Y_2$ are vertical distances of water from the channel bottom to water surface (Dyhouse, et al., 2007). The altitude $Z_1$ and $Z_2$ are the vertical distances of the ground from Mean Sea Level to channel botttom. Energy losses $P_1$ and $P_2$ are the differences in water surface and energy grade line. Using energy equation Water Surface 1 (WS1) and Water Surface 2 (WS2) were computed in equations 19 and 20 respectively.

$$WS1 = Z_2 + Y_2 + P_2 \qquad Eq\ 19$$

$$WS2 = Z_1 + Y_1 + P_1 + h_e \qquad Eq\ 20$$

Where: $h_e$ = energy head loss

The equations 19 and 20 were iterated 20 times. The WS1 and WS2 required first computing mean kinematic energy ($P_1$ and $P_2$) using equation 21 and energy loss ($h_e$) using equation 22, Such that:

$$P_1 = \frac{a_1 V_1^2}{2g}, \quad P_2 = \frac{a_2 V_2^2}{2g} \qquad Eq\ 21$$

Where:

$V_1$, $V_2$ = average velocity (total discharge/total flow area), $a_1$, $a_2$ = velocity weighting coefficients, g = gravitation acceleration

The energy loss $h_e$ in equation 21 was computed as below:

$$h_e = L\bar{S}_f + C\left|\frac{a_2 V_2^2}{2g} - \frac{a_1 V_1^2}{2g}\right| \qquad \textit{Eq 22}$$

Where: $\bar{S}_f$= representative friction slope between two sections, C = expansion or contraction loss coefficient, and discharge weighted reach length, L:

$$L = \frac{L_{lob}\bar{Q}_{lob} + L_{ch}\bar{Q}_{ch} + L_{rob}\bar{Q}_{rob}}{\bar{Q}_{lob} + \bar{Q}_{ch} + \bar{Q}_{rob}} \qquad \text{Eq 23}$$

Where: $L_{lob}, L_{ch}, L_{rob}$ = cross section reach specific for flow in the left overbank, channel, and right overbank respectively, $\bar{Q}_{lob}, \bar{Q}_{ch}, \bar{Q}_{rob}$= arithmetic average of the flows between sections for the left overbank, channel, and right overbank respectively.

The representative friction slope $\bar{S}_f$ also expressed as velocity of energy grade line of the river reach was computed as input for the energy loss $h_e$ as follows:

$$\bar{S}_f = \left(\frac{Q}{K}\right)^2 \qquad \text{Eq 24}$$

Where: K = conveyance of subdivision, $Q$= flow subdivided in the overbank areas where Manning n value changes on a cross section; $n$ = Manning roughness coefficient for subdivision.

Conveyance $K$ in the representative friction slope $\bar{S}_f$ equation was solved from flow area $A$ for subdivision and hydraulic radius $R$ for the channel area or perimeter, see equation 25 (Dyhouse, et al., 2007).

$$K = \frac{1.488}{n} AR^{2/3} \qquad \textit{Eq 25}$$

Lastly, WS1 and WS2 were compared using equation 26 to agree to within 0.03m and tolerance of 0.015m (Brunner, 2016; Dyhouse, et al., 2007).

$$WSI = WS2 \qquad \textit{Eq 26}$$

The HEC RAS software has a built-in functionality for data checking, errors, warnings, and computational log output file. The error and warning messages assisted in identifying parameters to adjust and improve the output. Thus, model was recalculated and checked more than 10 times until the model output were acceptable. This checking of output was part of initial model calibration which was further done in section below.

## 4.4 Conclusion

Two models, namely, HEC-HMS was processed and run to provide river flow and hydrographs, and HEC RAS was set-up and simulated to develop the flood extents, depth and velocity for flood mapping. The results of these models are given, analyzed and discussed in the next chapter.

# 5 Results and Analysis

## 5.1 Introduction

The results and analysis chapter provide the output of the developed and analyzed hydrological and hydraulic models. The results obtained were validated to assess their quality. The validation was conducted based on the observed discharge measurements and from site validation observation.

## 5.2 Developed and analyzed the hydrological model

### 5.2.1 Model output

The hydrological model was simulated in HEC-HMS model and provided the following outputs: the peak discharge ($m^3/s$); total flow ($m^3/s$); and Volume ($m^3$) per given drainage area ($km^2$) for all the subbasins, reaches, and junctions. The comparison between the observed and simulated flows at the outlet from 01 Jan 2012 to 01 Apr 2015 were represented as a hydrograph in Figure 5-1.

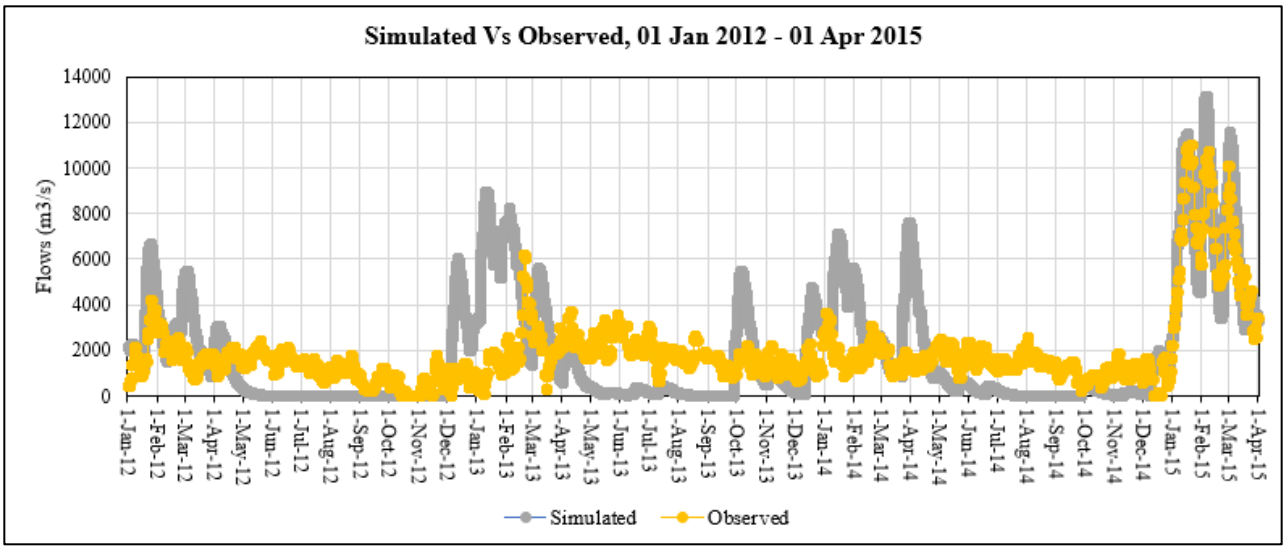


Figure 5-1: Graph of channel flow at the outlet from 01 Jan 2012 to 01 Apr 2015

Table 5-1: Flows and volumes at each subbasin, junction and channel, and outlet. shows peak volumes and flows of subbasins, reaches, junctions and the outlet on specific dates.

Table 5-1: Flows and volumes at each subbasin, junction and channel, and outlet.

| Basin elements | Area(km2) | Date | Flow (m3/s) | Volume (mm) |
|---|---|---|---|---|
| W380 | 13.6 | 24Feb2015, 09:15 | 1058.43 | 165338.252 |
| W370 | 13.6 | 31Jan2015, 03:45 | 964.34 | 160692.084 |
| W360 | 36.4 | 24Feb2015, 04:45 | 2835.43 | 164754.052 |
| W350 | 51.0 | 24Feb2015, 03:25 | 4097.49 | 183726.582 |
| W340 | 23.3 | 24Feb2015, 06:45 | 1865.39 | 183795.67 |
| W330 | 21.5 | 24Feb2015, 09:50 | 1518.50 | 123506.992 |
| W320 | 30.0 | 24Feb2015, 03:35 | 2123.94 | 123656.852 |
| W310 | 18.8 | 24Feb2015, 06:35 | 1504.37 | 184062.878 |
| W300 | 8.3 | 24Feb2015, 03:20 | 670.25 | 186337.448 |
| W290 | 22.0 | 24Feb2015, 05:05 | 1764.40 | 184088.786 |
| W280 | 20.5 | 24Feb2015, 02:20 | 1643.73 | 184551.066 |
| W270 | 49.2 | 24Feb2015, 02:10 | 3483.82 | 123346.21 |
| W260 | 64.5 | 24Feb2015, 03:55 | 4563.77 | 123027.694 |
| W250 | 19.6 | 24Feb2015, 04:10 | 1387.73 | 124191.776 |
| W240 | 12.0 | 24Feb2015, 03:15 | 850.58 | 125369.574 |
| W230 | 0.0002 | 01Jan2012, 00:00 | 113.27 | 159859.218 |
| W220 | 18.2 | 24Feb2015, 02:35 | 1290.29 | 124480.574 |
| W210 | 33.4 | 24Feb2015, 00:40 | 2366.69 | 123772.422 |
| W200 | 37.6 | 24Feb2015, 00:35 | 3018.41 | 183758.078 |
| Outlet1 | 494.6 | 05Feb2015, 23:50 | 13134.27 | 150774.654 |
| J44 | 480.9 | 04Feb2015, 00:00 | 14601.15 | 150492.968 |
| J47 | 416.3 | 04Feb2015, 00:05 | 13809.32 | 146175.476 |
| J54 | 356.6 | 02Feb2015, 00:20 | 12680.15 | 141889.48 |
| J57 | 316.4 | 04Feb2015, 00:00 | 10997.26 | 140640.308 |
| J64 | 278.0 | 25Feb2015, 00:00 | 10268.28 | 141129.258 |
| J69 | 235.5 | 25Feb2015, 00:00 | 10519.65 | 133373.368 |
| J74 | 121.8 | 25Feb2015, 00:10 | 8577.26 | 142897.352 |
| J79 | 90.1 | 24Feb2015, 21:50 | 6700.16 | 149293.834 |
| J82 | 55.8 | 24Feb2015, 02:35 | 4306.62 | 164387.784 |
| R30 | 55.8 | 25Feb2015, 00:10 | 4712.34 | 164413.438 |
| R50 | 90.1 | 25Feb2015, 00:10 | 6375.55 | 149306.026 |
| R70 | 121.8 | 04Feb2015, 05:10 | 4297.42 | 142907.258 |
| R90 | 235.5 | 04Feb2015, 00:30 | 7953.54 | 133345.174 |
| R110 | 278.0 | 04Feb2015, 00:35 | 9590.67 | 141102.334 |
| R130 | 316.4 | 04Feb2015, 00:15 | 10969.67 | 140638.022 |
| R150 | 356.6 | 04Feb2015, 02:55 | 11308.65 | 141824.71 |
| R170 | 416.3 | 04Feb2015, 20:20 | 12050.47 | 146085.052 |
| R190 | 480.9 | 06Feb2015, 01:15 | 12923.24 | 150362.92 |

The larger the area size of subbasin, channel or junction was, the high likelihood of volume and flow to be large also for that basin element. The peak discharge at the outlet was 14601 $m^3/s$ on 04

Feb 2015, with the volume of 150492mm covering the area of 480.9 $km^2$ on 4th Feb 2015 at Junction J47, while the peak flow of the observed was 10 962.99 $m^3/s$.

Based on the graph in Figure 5-1, the model had exaggerated the flows where compared against the observed flow values. The differences in the flows between the simulated and observed flows were minimized through calibration of the model by refining the model parameters.

### 5.2.2 Model calibration and validation

This study is interested in a flood event between 01 Jan 2015 to 31 March 2015 as shown in the hydrograph in Figure 5-2, hence this period of flood event was validated, and simulated during model optimization and calibration.

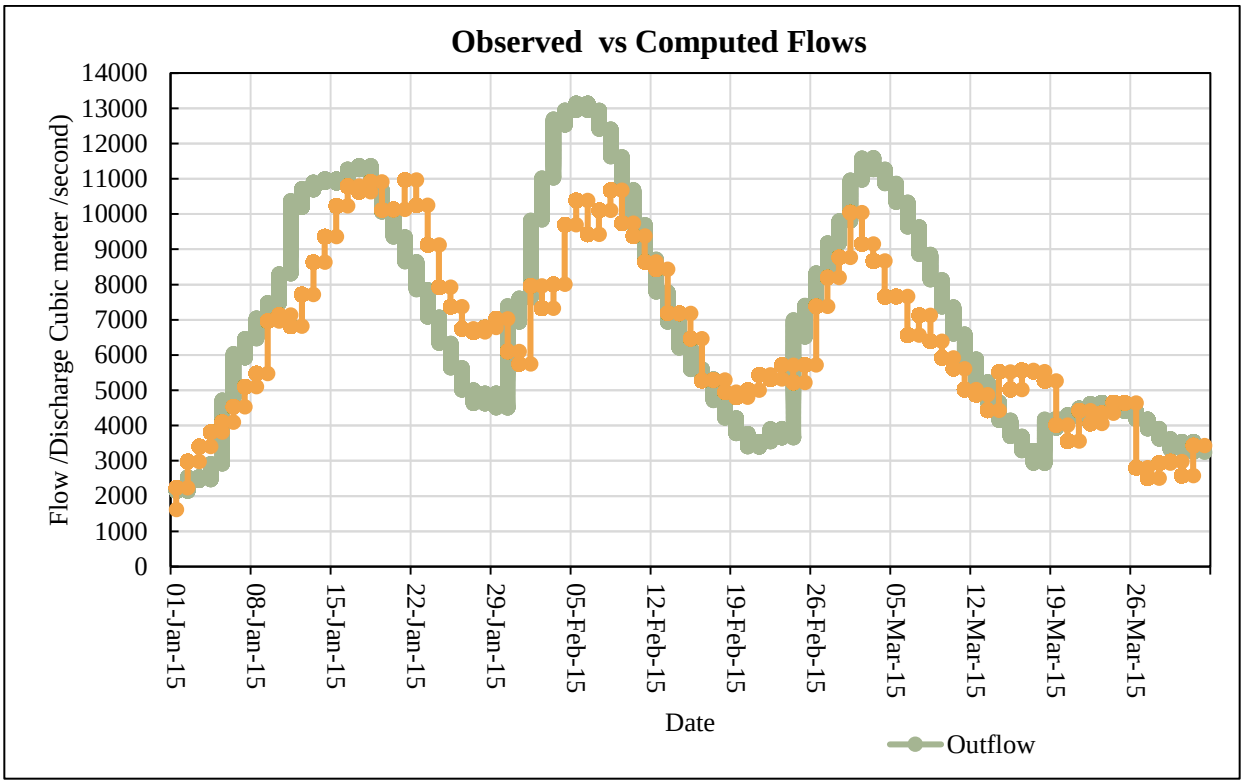


Figure 5-2: Hydrograph between 01 Jan 2015 to 31 March 2015

#### Model validation

The model validation was carried out to evaluate whether the model was acceptable or not. The model's performance and goodness of fit results are expressed below:

a) Root Mean Square Error (RMSE) to Standard Deviation Ratio (RSR) of flood event between 01 Jan 2015 to 31 March 2015:

$$RSR = \frac{\sqrt{222640050.6\ m^3/s}}{\sqrt{499436018.9\ m^3/s}}$$

$$RSR = \frac{14921.13}{22348.06}$$

$$RSR = 0.67$$

RSR was more than 0.5, meaning the model needed to be improved.

b) The PEV was expressed as (Ouédraogo , et al., 2018):

$$PEV = \left|\frac{402.19\ m - 428.53\ m}{402.19\ m}\right| \times 100$$

$$Bias = 6.54\%$$

The PEV was less than 10% and it was rated as very good according general performance rating in Table 4-10.

c) The percentage error in peak flow (PEPF), was calculated as below:

$$PEPF = \left|\frac{10962.99\ m^3/s - 13131\ m^3/s}{10962.99\ m^3/s}\right| \times 100$$

$$PEPF = 19.8\%$$

The PEPF is within 15 to 35%, thus rated as good.

The NSE was calculated as below:

$$NSE = \frac{499436018.9\ m^3/s - 222640050.6\ m^3/s}{499436018.9\ m^3/s}$$

$$NSE = 0.55$$

The NSE was rated satisfactory because its value was with 0.50 to 0.65

Based on the results above the RSR, PEFP, the accuracy and acceptability could be accepted, however there was room for improvement especially for the PEV, RSR and NSE. Thus, the model was tested for error uncertainty, and guided by the uncertainty results the model was calibrated, and the results are provided in the next section.

### Uncertainty analysis outcome

The outcome of the uncertainty analysis was the outflow minimum, outflow, maximum, outflow mean plus standard deviation, outflow mean minus standard deviation, and mean outflow visualized in graphs for easy interpretation. Among the seven parameters recession-ratio to peak parameter had the highest uncertainty, followed by initial constant-constant rate, then recession constant. The other parameters caused insignificant uncertainty to the model.

The graph in Figure 5-3 illustrated indicated the recession-ratio to peak parameter with outflow minimum, outflow maximum, outflow mean plus standard deviation, outflow mean minus standard deviation, deviate from the outflow mean (continuous blue line).

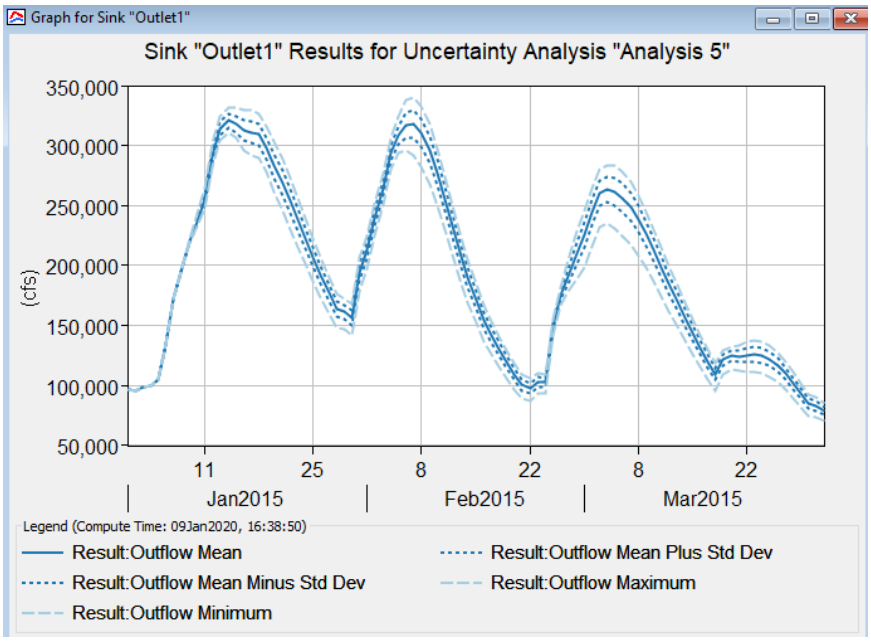


Figure 5-3: Uncertainty outcome for recession- ratio to peak parameter

The graphs for in initial loss, recession initial discharge, percent impervious rate, and lag time (see Figure 5-4) showed only one line, meaning that there was no deviation of outflow minimum, outflow maximum, outflow mean plus standard deviation, outflow mean minus standard deviation, from the outflow mean.

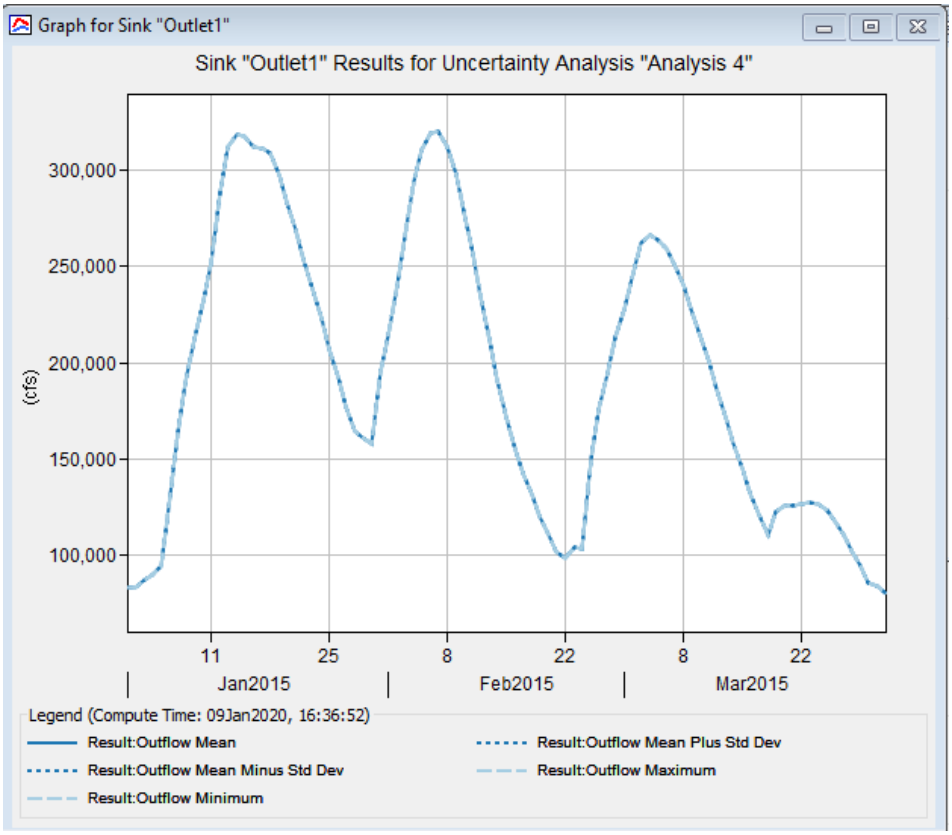


Figure 5-4: Lag time uncertainty outcome

## Model calibration

Taking into consideration the uncertainty analysis outcome, the automated optimization and at least 30 try and error adjustments of the model parameter values, the optimized values in Table 5-2 were obtained.

Table 5-2: Optimized values for W350, W380, and W370 subbasin parameters

| | **W380** | | **W350** | | **W370** | |
|---|---|---|---|---|---|---|
| Parameter | Initial Value | Optimized value | Initial Value | Optimized value | Initial Value | Optimized value |
| Initial and Constant - Constant Rate (mm/hr) | 6.35 | 13.87 | 6.35 | 13.87 | 6.35 | 13.87 |
| Initial and Constant - Initial Loss (mm) | 0.50 | 85.07 | 0.50 | 85.07 | 0.50 | 85.07 |
| Recession - Initial Discharge (m3/s) | 113.27 | 147.2 | 113.27 | 147.2 | 113.27 | 147.2 |
| Recession - Ratio to Peak | 0.35 | 0.35 | 0.35 | 0.35 | 0.35 | 0.35 |
| Recession - Recession Constant | 0.92 | 0.919 | 0.92 | 0.919 | 0.92 | 0.919 |
| SCS Unit Hydrograph - Lag Time (Minutes) | 900.00 | 1000 | 900.00 | 1000 | 900.00 | 1000 |

Using the optimized values, the hydrograph of the observed and simulated flows at the outlet were as in Figure 5-5 below. Visually, the graph shows improvements in the flows and correlation. For instance,

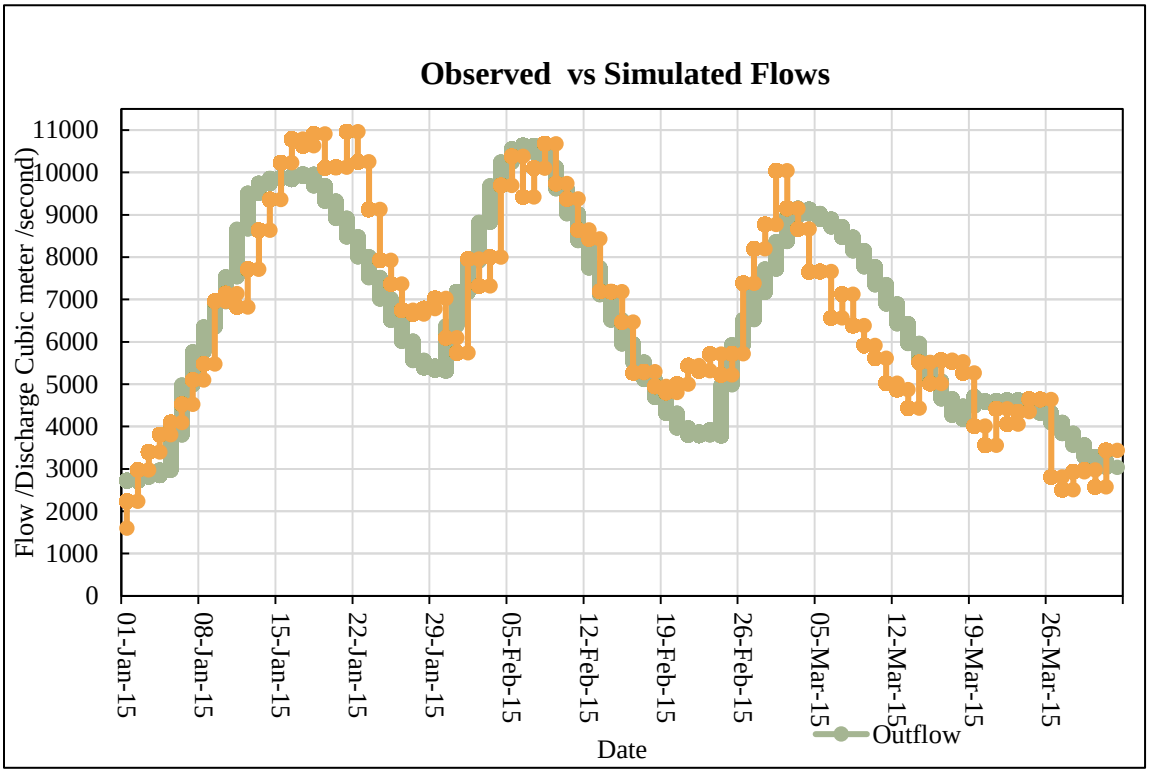


Figure 5-5: Graph of observed and result outflow

The second peak seem to almost match as compared to the previous graph. The improvements in the optimized model were verified by validating the model using RSR, PEFP, PEV, and NSE as follows:

a) RSR:

$$RSR = \frac{\sqrt{98805561.4\ m^3/s}}{\sqrt{469529589.5\ m^3/s}}$$

$$RSR = \frac{9940.098}{21668.63}$$

$$RSR = 0.458$$

b) The percent bias:

$$Bias = \left|\frac{402.19\,m - 402.61\,m}{402.19\,m}\right| \times 100$$

$$Bias = 0.10\%$$

c) The percentage error in peak flow (PEPF), after calibration of parameters:

$$PEPF = \left|\frac{10962.99\,m^3/s - 10645.58\,m^3/s}{10962.99\,m^3/s}\right| \times 100$$

$$PEPF = 2.89\%$$

d) The NSE:

$$NSE = \frac{469529589.5\,m^3/s - 98805561.4\,m^3/s}{469529589.5\,m^3/s}$$

$$NSE = 0.79$$

The validation results of the optimized model improved the RSR, PEV, PEPF, and RSR. When RSR, PEV, PEPF, and NSE were ranked based on the general performance ratings in Table 4-10, RSR was deemed very good performance, PEV was very good, PEPF was very good, and NSE was very good. These ratings confirmed the goodness of fit between the optimized model and observed flows and indicated a good the predictive power of the optimized model. Hence the model was accepted.

### 5.2.3 Discussion

Analysis of the riverine flood is dependent on a flood model that represents the flood scenario. Among different models, this study developed the hydrological model using HEC HMS model and integrated GIS. The model was developed in a poor data environment where only medium resolution data like 30m resolution SRTM DEM was accessible.

Developing the model required a wide range of consideration including data collection, model selection criteria, and determining suitable parameters to run the model. Sinclair & Pegram (2004) demonstrated that there is no ideal flood model because of data limitations and complexities in the models. Ideal model would mean data with highest quality and resolution. Most developing countries like Malawi have resorted to low to medium resolution data. Thus, this study being implemented in a poor data environment faced similar data challenges.

The simulation of the hydrological model required specific model parameters to compute water flow and volume for each subbassin, river channel and at the outlet point within specified flood event period. The four parameters implemented in the model were transform, routing, baseflow, and loss. These parameters have been recommended by Flemming (2000). Some parameters were easy to determine especially those computed using river and basin characteristics like Muskingum K which represented the travel time of flood wave, which was channel length divided by channel velocity. Contrary, some parameters like recession constant rate were determined based on basin soil group and the value was extracted from a range corresponding to the soil group. Similarly estimation of Muskingum X has a range of 0 to 0.5, based on channel slope and overbank flow, such that channels with large storage volume areas were assigned 0 value and steeper channels with smaller storage were assigned the maximum value (Dyhouse, et al., 2007). Using Dyhouse meant no definite figure but rather assignment of X value based on one's judgement as long as the value meets the criteria. This study also considered Valle Junior, et al. (2019) in their study of estimating initial abstraction ratio and CN using rainfall and runoff data for a tropical suggested the use of 0.05 as the initial abstraction ratio and when applied to this study despite being different environment, it was a success.

One advantage of using HEC HMS model was the availability of automated optimization to refine parameters and uncertainty analysis to identify errors in parameters. According to the uncertainty analysis carried in the model in the order of highest to lowest peak to ratio, constant rate and initial discharge contributed to errors in the model, apart from the optimized output, during try and error parameter adjustment it was observed that there was significant difference when the initial discharge (a baseflow parameter) was increased or reduced. For instance, using initial discharge of 2193 $m^3/s$ exaggerated the flow, while 147 $m^3/s$, made the flow stable.

The model was accepted through evaluation of the model accuracy and predictive power using NSE, PEFP, PEV, and RMSE RSR (Ouédraogo , et al., 2018; Fleming & Doan, 2013; Alaghmand, et al., 2012; Gharbi, et al., 2016). Based on the performance rating which was also applied by Ouédraogo , et al(2018), NSE (0.79), PEFP (2.89%), PEV (0.10), and RSR (0.485%). The NSE was above 0.75 the model performed = very good, and the 0.10% PEV showed that there was insignificant error bias for the peak volumes.

Despite the success in developing the model using medium resolution data, this study could not fully calibrate peak flow error of 2.89% between the simulated peak flow and the observed peak

flow though the rating was good and acceptable. To sum up, it could be recommendable to carryout out further field observations to validate each model parameter and optimize the parameter values.

## 5.3 Developed and simulated hydraulic model results

### 5.3.1 Model Output

The water discharge at each cross section was simulated from 1 January to 30 March 2015 and created 91 water profiles. The model results were obtained in form of tables, profiles and visual graphics. The profile table shown in Figure 5-6 contains values for 13 January 2015 representing the river stations, the flow, minimum channel elevation, critical water surface, energy slope, channel velocity, flow area, top width, and froude number. Top width is the horizontal width across water surface of a channel (Dyhouse, et al., 2007). The froude number is greater than 1 for supercritical flows meaning that the velocity was high, and depth was low specifically where the slope was steep. The froude number was less than 1 for subcritical flows where the velocity was low and the depth was high (*Ibid*).

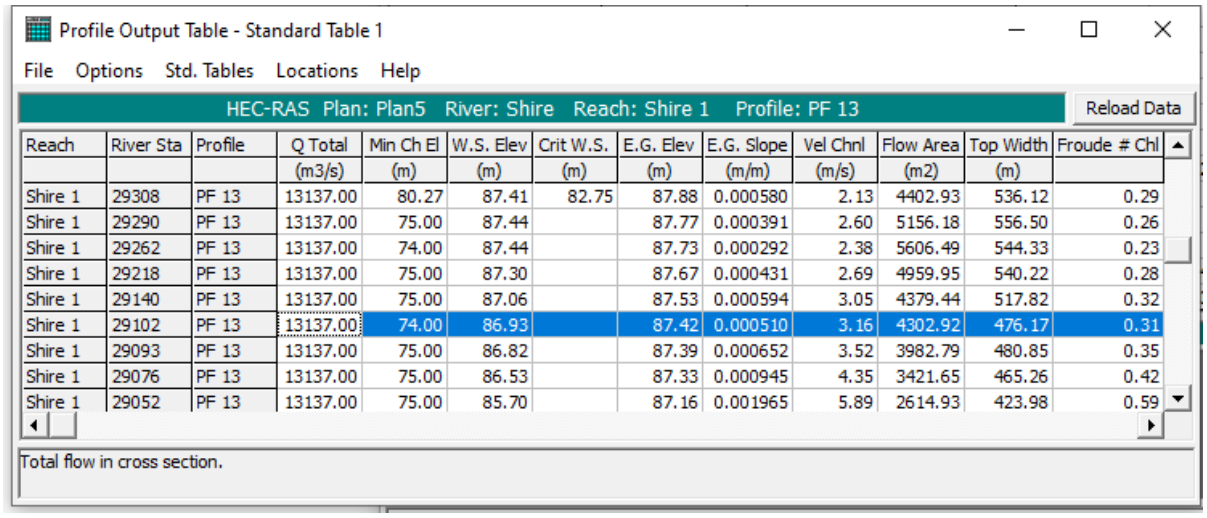


| Reach | River Sta | Profile | Q Total | Min Ch El | W.S. Elev | Crit W.S. | E.G. Elev | E.G. Slope | Vel Chnl | Flow Area | Top Width | Froude # Chl |
|---|---|---|---|---|---|---|---|---|---|---|---|---|
| | | | (m3/s) | (m) | (m) | (m) | (m) | (m/m) | (m/s) | (m2) | (m) | |
| Shire 1 | 29308 | PF 13 | 13137.00 | 80.27 | 87.41 | 82.75 | 87.88 | 0.000580 | 2.13 | 4402.93 | 536.12 | 0.29 |
| Shire 1 | 29290 | PF 13 | 13137.00 | 75.00 | 87.44 | | 87.77 | 0.000391 | 2.60 | 5156.18 | 556.50 | 0.26 |
| Shire 1 | 29262 | PF 13 | 13137.00 | 74.00 | 87.44 | | 87.73 | 0.000292 | 2.38 | 5606.49 | 544.33 | 0.23 |
| Shire 1 | 29218 | PF 13 | 13137.00 | 75.00 | 87.30 | | 87.67 | 0.000431 | 2.69 | 4959.95 | 540.22 | 0.28 |
| Shire 1 | 29140 | PF 13 | 13137.00 | 75.00 | 87.06 | | 87.53 | 0.000594 | 3.05 | 4379.44 | 517.82 | 0.32 |
| Shire 1 | 29102 | PF 13 | 13137.00 | 74.00 | 86.93 | | 87.42 | 0.000510 | 3.16 | 4302.92 | 476.17 | 0.31 |
| Shire 1 | 29093 | PF 13 | 13137.00 | 75.00 | 86.82 | | 87.39 | 0.000652 | 3.52 | 3982.79 | 480.85 | 0.35 |
| Shire 1 | 29076 | PF 13 | 13137.00 | 75.00 | 86.53 | | 87.33 | 0.000945 | 4.35 | 3421.65 | 465.26 | 0.42 |
| Shire 1 | 29052 | PF 13 | 13137.00 | 75.00 | 85.70 | | 87.16 | 0.001965 | 5.89 | 2614.93 | 423.98 | 0.59 |

Figure 5-6: profile table

The water depth of every point within the modeled flow was calculated by the difference between the top water surface elevation and ground water surface elevation, see Figure 5-7.

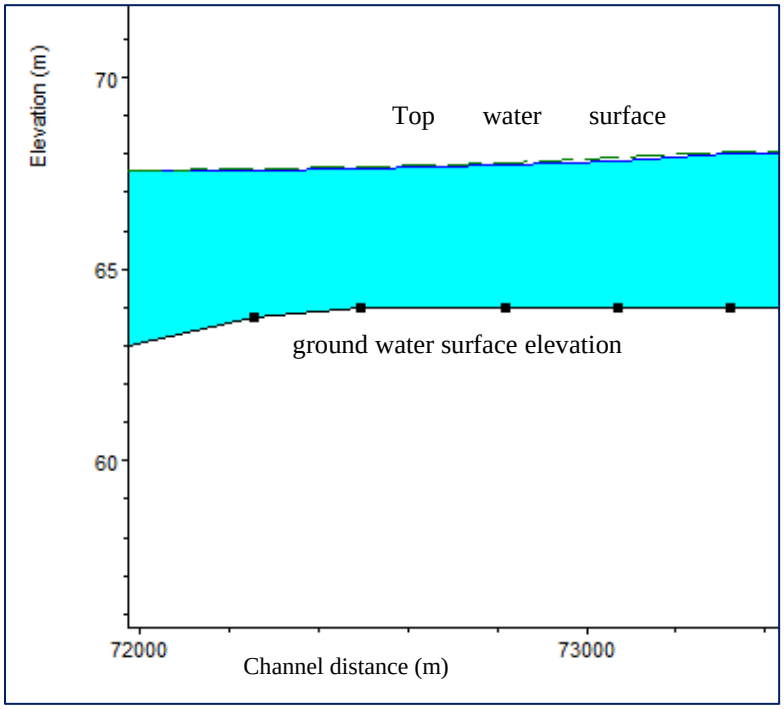


Figure 5-7:Top and ground water surface elevation

The computed water depth is shown as a map layer in Figure 5-8 with minimum depth of 0m and maximum depth of 15m. The modeled water depth provided water boundary in terms of water extent on the ground.

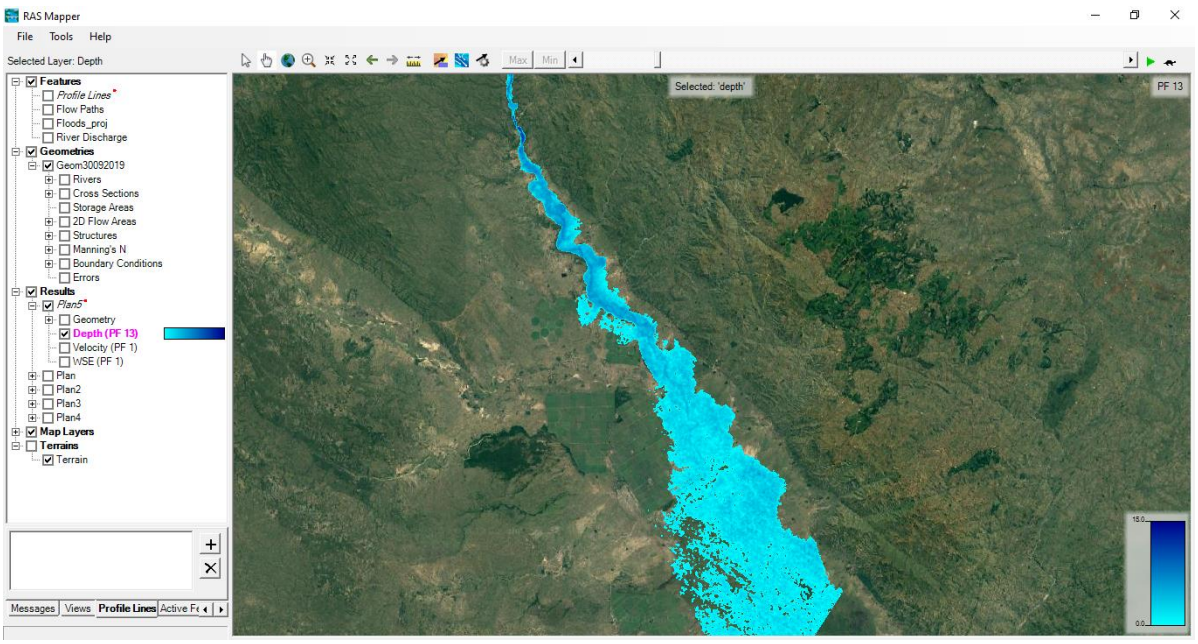


Figure 5-8: Computed discharge profile translated into water depth that is distributed over the river channel on 13 January 2015

The detailed output for each cross section included energy gradeline elevation (E.G. Elev), velocity head (Vel Head), water surface elevation (W.S. Elev), critical water surface (Crit W.S), energy slope (E.G Slope), total discharge (Q total), Top Width, total velocity (Vel Total), maximum channel depth (Max Chl Dpth), total conveyance (Conv. Total), minimum channel depth (Min Chl Dpth), alpha, friction loss (Friction Loss), critical and energy loss (C&E Loss), and the computed water surface elevation and average velocities (see below Figure 5-9).

Model calibration and validation

shows cross section 29102 segmented into the left overbank, channel and right overbank. Applying the values in Figure 5-9, discharge computations were carried out as follows:

*Left over bank flow area = left overbank Length × Water/hydro depth* *Eq 27*

$=29.60\text{m} \times 3.31\text{m}$

$= 167.58\text{m}^2$

Left overbank discharge = Left overbank average velocity × Left overbank flow area Eq 28

$= 1.60\text{m/s} \times 167.58\text{m}^2$

$=267.32\text{m}^3/\text{s}$

Similarly, equations 27 and 28 calculations were applied to the channel and right overbank segments, such that the total discharge for cross section 29102 was:

*= Left overbank discharge + Right overbank discharge + Channel discharge* *Eq 29*

$= 167.58\text{m}^3/\text{s} + 6251\text{m}^3/\text{s} + 6618.45\text{m}^3/\text{s}$

$= 13137.03\ \text{m}^3/\text{s}$

Total discharge (Q Total) 131317 $\text{m}^3/\text{s}$ on the left of Figure 5-9 represented WS1 in equation 26, and total discharge 13137.03 $\text{m}^3/\text{s}$ in equation 29 represented WS2 in equation 26. At this stage, equation 26 was applied to test if WS1 and WS2 were within 0.03:

131317 $\text{m}^3/\text{s}$ = 13137.03 $\text{m}^3/\text{s}$

$0 = 0.03$

Thus, WS1 and WS2 were within 0.03 indicating that there was an agreement between the input discharge and the modeled discharge. This means that the results were reasonable.

Despite that the results of the model were reviewed for reasonableness, consistency and completeness, calibration against independent data was carried out for the results to be accepted

(Brunner, 2016; Dyhouse, et al., 2007). The flood extent shapefile created by the Malawi Department of Survey where they extracted water from Radasat 2 image of the day of flood (13 January 2015).

The flood extent shapefiles (in Orchid colour) was overlaid with the modeled Water Surface depth (in blue) on 13 January 2015 as illustrated in Figure 5-10.

Cross Section Output

File Type Options Help

River: Shire Profile: PF 13

Reach Shire 1 RS: 29102 Plan: Plan5

Plan: Plan5 Shire Shire 1 RS: 29102 Profile: PF 13

| | | Element | Left OB | Channel | Right OB |
|---|---|---|---|---|---|
| E.G. Elev (m) | 87.42 | | | | |
| Vel Head (m) | 0.49 | Wt. n-Val. | 0.035 | 0.035 | 0.035 |
| W.S. Elev (m) | 86.93 | Reach Len. (m) | 29.60 | 30.70 | 34.70 |
| Crit W.S. (m) | | Flow Area (m2) | 167.58 | 1979.64 | 2155.70 |
| E.G. Slope (m/m) | 0.000510 | Area (m2) | 167.58 | 1979.64 | 2155.70 |
| Q Total (m3/s) | 13137.00 | Flow (m3/s) | 267.32 | 6251.23 | 6618.45 |
| Top Width (m) | 476.17 | Top Width (m) | 50.65 | 182.50 | 243.02 |
| Vel Total (m/s) | 3.05 | Avg. Vel. (m/s) | 1.60 | 3.16 | 3.07 |
| Max Chl Dpth (m) | 12.93 | Hydr. Depth (m) | 3.31 | 10.85 | 8.87 |
| Conv. Total (m3/s) | 581970.8 | Conv. (m3/s) | 11842.3 | 276930.2 | 293198.3 |
| Length Wtd. (m) | 32.67 | Wetted Per. (m) | 51.03 | 182.73 | 243.64 |
| Min Ch El (m) | 74.00 | Shear (N/m2) | 16.41 | 54.14 | 44.21 |
| Alpha | 1.02 | Stream Power (N/m s) | 26.18 | 170.95 | 135.74 |
| Frctn Loss (m) | 0.02 | Cum Volume (1000 m3) | 184901.40 | 845505.80 | 195158.30 |
| C & E Loss (m) | 0.01 | Cum SA (1000 m2) | 66822.94 | 439135.50 | 89854.10 |

Figure 5-9: Detailed cross section output

The water boundary of both layers aligned spartially especially at upstream. Some extent differences between the flood (red circles in Figure 5-10) and modeled layer (yellow circles in Figure 5-10) were observed downstream where the terrain was relatively flat, and in tributaries where the simulations was not ran. Future work may require to carry out hydrological and hydraulic observations of those tributaries which later could be added to the hydraulic simulation.

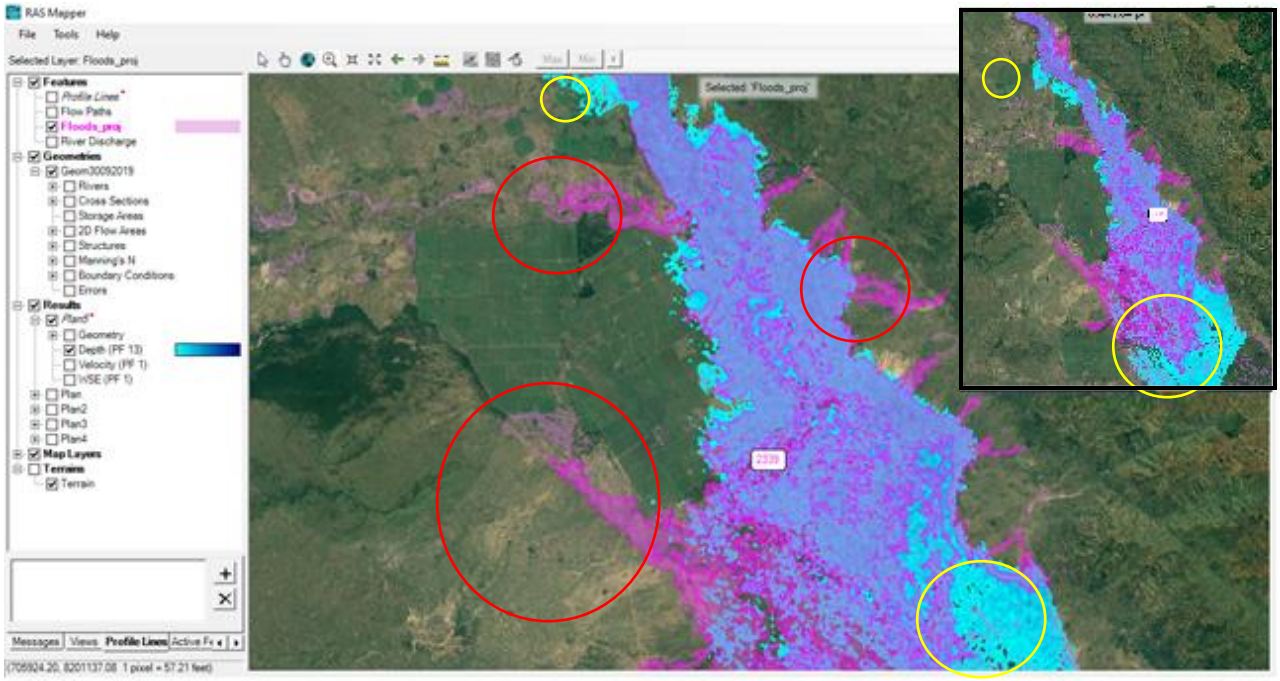


Figure 5-10: Modeled water depth overlaid with flood layer extracted from Radarsat 2 image on 13 January 2015

### 5.3.2 Discussion

The hydraulic model was developed using HEC RAS model to meet the second objective of this study. Obtaining the acceptable HEC RAS solutions required clearing all errors and taking into considerations the warning messages like: 1) checking minimum and maximum range of variables, 2) alpha and numeric data checks to ensure that correct data were entered in every field, 3) consistency checks on bank stations to correspond to cross section stations and elevation data, 4) ensure completeness of the data, and 5) increasing order of station for cross sections. Hence, more cross sections were added by digitizing to improve the gradual varied flow that could influence the conveyance ratio to be less or greater than standard values of 0.7m or 1.4m respectively (Dyhouse, et al., 2007). According to Dyhouse (2007), the Manning n values should range from 0.003 to 0.05. Thus, the Manning n values for each cross section was adjusted within that range. However, changing manning values did not cause any noticeable improvement in the model. The model improved when the flow classification was changed from subcritical flow to supercritical flow and got much better when mixed flow was applied. The mixed flow computations used both subcritical and supercritical flows. For instance, in Figure 5-11 the profile plot for the simulated river channel shows the critical flow in green borders and supercritical flow in red borders or red dotted profile. Where seem applicable adjustments were made to improve consistency or identify any outliers that would have affect the model, for instance, the Froude numbers being large (more than one for

subcritical station), or drastic change in the energy slope and energy elevation between consecutive stations.

Some of the challenges of simulating the open natural channel using HEC RAS were to do with the variation and complexity of the natural open channel, for example the surface of the channed is not smooth, it changes could changed in a very short distance in terms of roughness, slope, geometric properties such as topwidth, perimeter and cross sections (Dyhouse, et al., 2007). Therefore, the short distance changes may easily be generalized when medium or small scale data are used as inputs. The could be resolved by detailed data observations to capture the variations in flow depth. Unfortunately the detailed observations requirements were too high for Malawi, a developing country where resources and skills are limited or not well utilized.

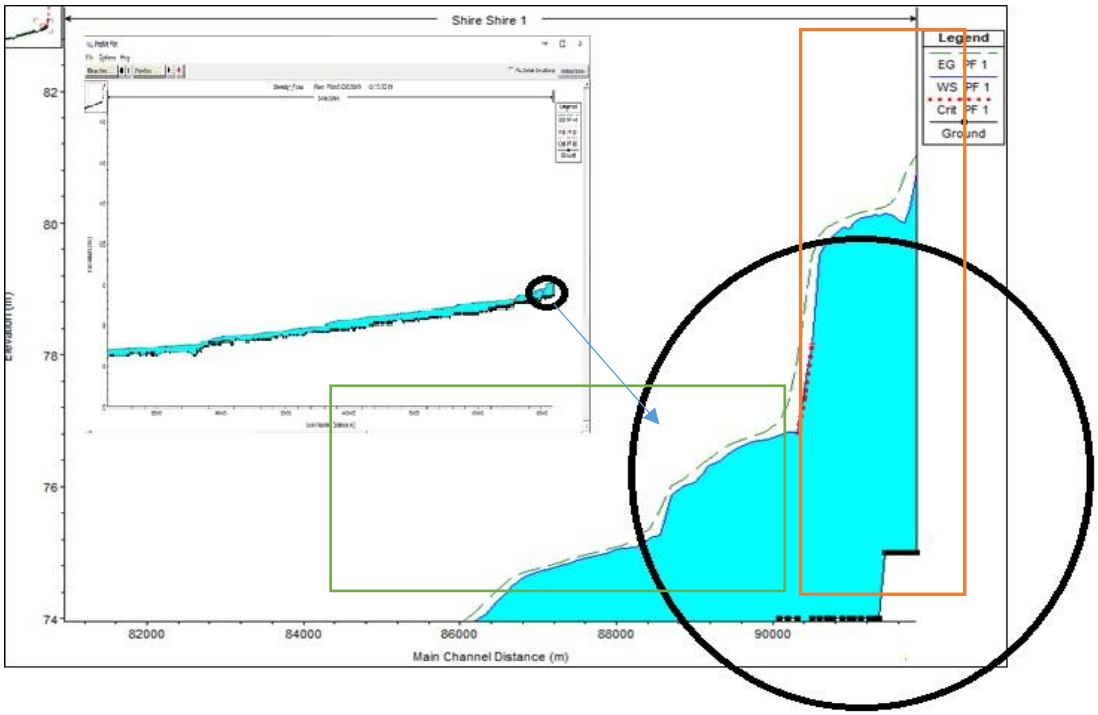


## 5.4 Flood analysis

Flood analysis on land use is carried out to visualize the extent of flood impact on land use and other public facilities in Chikwawa district. The map below (Figure 5-12) indicates that some Built-up (shown in red color) circled in yellow are inundated. The inundated buildings are exposed to

Figure 5-11: Zoomed in profile showing mixed flow plot

damage and needs to be protected from floods. With respect to the terrain elevation, the inundated buildings are on relatively flat terrain. The flat terrain increases duration of inundated water.

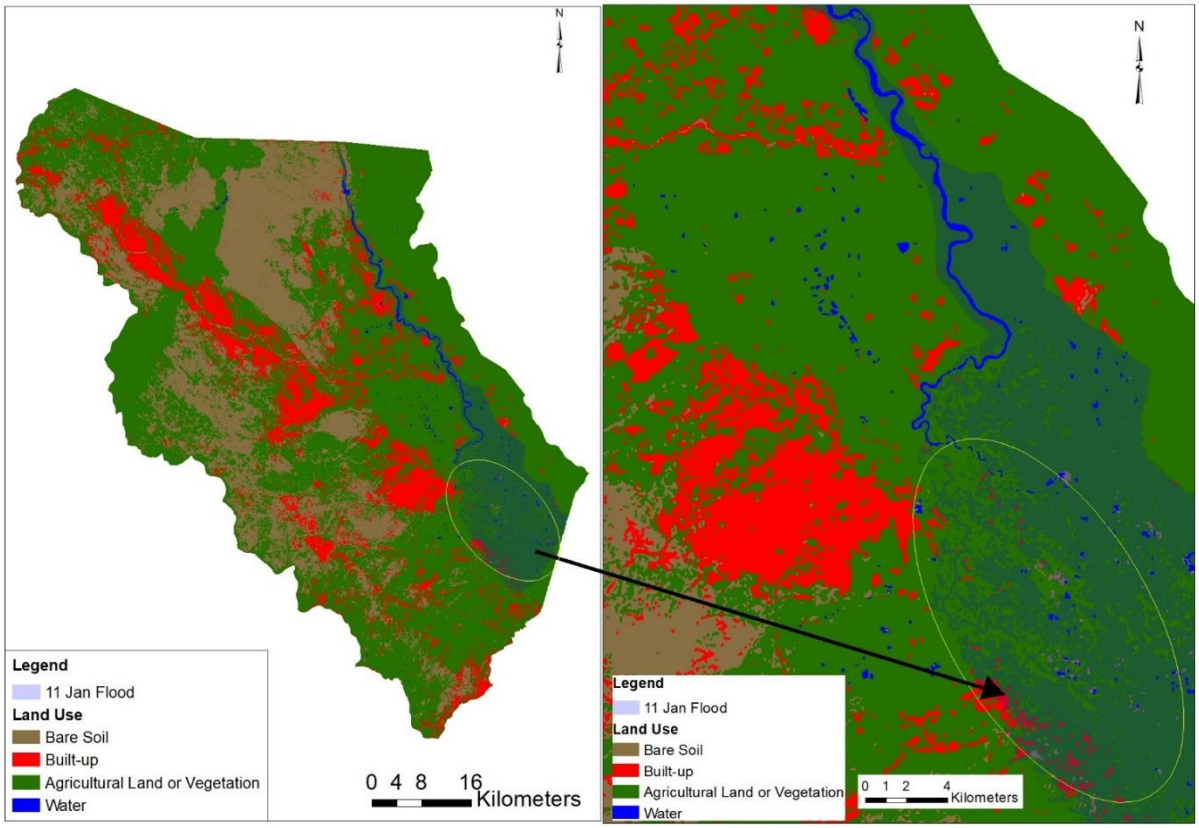


Figure 5-12: Floods analysis on land use

The protection of the agricultural land and building may require flood risk management strategies such as construction of levee to block the water, or big canals to channel water, among others.

The flooded water also has impacted on social services. Based on the information available for the Malawi Surveys Department, point data for school facilities are analyzed with respect to floods. Out of 189 schools in the district, 21 are within 1km proximity to flood water. This means that students going to those school are mostly likely affected my flood.

# 6 Conclusion

Through the hydrological modeling using HEC HMS model, and hydraulic modeling using HEC RAS model and integrating GIS and remote sensing, this study met its overall objective of analysing riverine floods in a poor data environment, where only low to medium resolution data were accessible. Both models performed above average and were accepted. However, optimal results were not achieved because of limited access to observed data and time to calibrate all the data.

The hydrological model was developed using 30 SRTM DEM of the area of interest to delineate basin elements (sub basins, river channels, junctions, and outlet). The DEM and the basin elements were used to compute the basin parameters which included: river length, slope, upstream and downstream elevation, hydraulic length, basin area, average slope, and centroid. Based on the basin parameters four model parameters necessary to simulate the hydrological model were determined. The model parameters included the base flow that defined the underground or interflow; loss defining the infiltrated or lost runoff due to evapotranspiration or other factors; transform which defined the flow that transformed from surface runoff into channel flow at a specific period.

The simulation of the hydrological model produced hydrographs, tables of flows and discharge volumes for each sub basin, reach, outlet and junction at given time and date between the 01 Jan 2015 and 01 April 2015. Among other factors, the amount of the flow and volume was affected by size, steepness and soil group of sub basin, reach, outlet and junction. For instance, large sub basins and reaches with steep slopes had large discharge volume and flows, vice versa.

The accuracy of the simulated flows and volumes was evaluated using statistical methods for measuring model's goodness of fit, predictive power and error deviation between the simulated and observed satellite flow observations from Dartmouth Flood Observation data portal. The Percent Error of Peak Flows (PEPF) computed the error of 2.89% between the observed and simulated flows. The Random Mean Square Error (RMSE) RSR was calculated as 0.485 standard deviation of the simulated flows from observed flows. The Percent Error of Volume (PEV) indicated 0.01% error bias between the observed and simulated flows. The NSE was 0.79, which according the performance rating of standard statistics was rated as very good in terms of performance and model predictive power. In general, all the statistical analysis above translated that the model could be accepted and was a good fit.

Regardless of the positive statistical analysis results of the simulated flows and values, the uncertainties in the model could not be ignored. The uncertainties were errors in the model due to significant differences between the estimated model parameters and true values. As per the automated uncertainty analysis conducted on all the model parameters in this study, significant uncertainties were identified in recession peak to ratio, initial loss- constant rate, and recession initial discharge. The recession peak to ratio uncertainties were reflected in the 2.89% of the PEPF. IF an optimal ratio to peak value was determined, the PEPF would be minimized to even 0%. However, because of various limitation including data resolution, limited ground truthing of model parameter values, repetitiveness of try and error adjustment of parameters to improve the model and model complexities, the model could not be 100 % optimized to achieve 0% parameter errors.

The hydraulic model was the second model developed and simulated in this study using HEC RAS. Similarly, the hydraulic model used 30m DEM, land use data derived from classification of 30m Landsat image, and geometric data. The geometric data included digitized river centreline from upstream to downstream; left and right banks defining river boundary, flow path representing overbank boundary and direction of flow; and river cross section cutlines representing the cross section of river channel.

The outcome of the HEC RAS simulation included the flood depth computed as water profiles at specific date at every cross-section point; and the water extents. The simulated water extents were validated by overlaying it with a flood extent layer created from extracted from RADARSAT satellite image captured on 13 Jan 2015. The overlay validation showed that at least 80% of the simulated water extents corresponded with the RADARSAT flood extent. The non-corresponding areas were mostly downstream area where the terrain was relatively flat and the channel connected with small tributaries that might contributed to channel flow. The flat terrain might have been smoothened by the 30m DEM by generalizing the small depth within 30m by 30m area into a single point.

Therefore, this research has concluded that application of flood modeling in poor data environments requires intensive data enhancements and adjustments; multiple utilization of open sources data; carrying out multiple model computation iterations and calibration; multiple field observation which may be constrained with time and resources to get reasonable output. Thus, this paper recommends as future work to carrying series of field observations for the tributaries

contributing to channel flow, and verification of the model parameters to be added to refine future model simulation.

## 6.1 Research Challenges

### 6.1.1 Technical

Learning how to operate the models (HEC-GeoHMS, HEC-GeoRAS, HEC-HMS, HEC-RAS) that are used in this research demanded a lot of effort in terms of understanding the theory behind hydrology and hydraulics, the algorithms, the data formats and conversions, the attribute data needed to do necessary calculations, and also the efficiency of the computer processing speed. The computer available sometimes could not handle big images and data thus the processing is slower and time consuming.

### 6.1.2 Data and software accessibility

As already explained in the research, high resolution data are costly and almost impossible unavailable in Malawi due to lack of resources to invest in such; and regarding software, the research only had access to software available in the Geomatics Computer Laboratory and free trustworthy online software. The research has capitalized to make the best of the readily data and software available in order to answer the questions and achieve the objectives of this research. Using high resolution data and wide choice of software could possibly improve the quality of the research

# 7 Appendix

## 7.1 Major satellite related precipitation products currently available (Source: Sun et al., 2017)

| Data set | Adjusted | Res. | Freq. | Coverage | Period | Data source |
|---|---|---|---|---|---|---|
| GPCP | GPCC, GHCN | 2.5° | Monthly | Global | 1979–present | GPI, OPI, SSM/I scattering, SSM/I emission, TOVS |
| GPCP 1dd | GPCC, GHCN | 1.0° | Daily | Global | 1996–present | SSM/I-TMPI, TOVS |
| GPCP_PEN_v2.2 | GPCC, GHCN | 2.5° | 5-daily | Global | 1979–2014 | OPI, SSM/I, GPI, MSU |
| CMAP | GPCC, GHCN | 2.5° | Monthly | Global | 1979–present | GPI, OPI, SSM/I scattering, SSM/I emission, MSU, NCEP–NCAR |
| CPC-Global | GTS, COOP, NMAs | 0.5° | Daily | Global land | 2006–present | GTS, COOP, NMAs |
| TRMM 3B43 | GPCC | 0.25° | Monthly | 50°S–50°N | 1998–present | TMI, TRMM Combined Instrument, SSM/I, SSMIS, AMSR-E, AMSU-B, MHS, and GEO IR |
| TRMM 3B42 | X | 0.25° | 3 h/Daily | 50°S–50°N | 1998–present | TMI, TRMM Combined Instrument, SSM/I, SSMIS, AMSR-E, AMSU-B, MHS, and GEO IR |
| GSMaP | X | 0.1° | 1 h/Daily | 60°S–60°N | 2002–2012 | TMI, AMSR-E, AMSR-E, SSM/I, multifunctional transport satellites (MTSAT), Meteosat-7/8, GOES 11/12 |
| PERSIANN-CCS | X | 0.04° | 30 min/3, 6 h | 60°S–60°N | 2003–present | Meteosat, GOES, GMS, SSM/I, polar/near the polar precipitation radar, TMI, AMSR |
| PERSIANN-CDR | GPCP | 0.25° | 3, 6 h/Daily | 60°S–60°N | 1983–present | GOES 8, GOES 10, GMS-5, Metsat-6, and Metsat-7, TRMM, NOAA 15, 16, 17, DMSP F13, F14, F15. |
| CMORPH | X | 0.25°/8 km | 30 min/3 h/Daily | 60°S–60°N | 2002–present | TMI, SSM/I, AMSR-E,AMSU-B, Meteosat, GOES, MTSAT |
| GPM | | 0.1° | 30 min/3 h/daily | 60°S–60°N | 2015–present | GMI, AMSR-2, SSMIS, Madaras, MHS, Advanced Technology Microwave Sounder |
| MSWEP | CPC, GPCC | 0.1°/0.5° | 3 h/daily | Global | 1979–present | CPC, GPCC, CMORPH, GSMaP-MVK, TMPA, ERA-Interim, JRA-55 |

## 7.2 Daily rainfall observation in millimeters for Chikwawa from 1 Jan to 1 Apr 2015 (Source Malawi Meteological Surveys)

| Date | Chikwawa (mm) | Nchalo (mm) | Date | Chikwawa (mm) | Nchalo (mm) |
|---|---|---|---|---|---|
| 1-Jan | 19.8 | 21.7 | 16-Feb | 2.4 | 21.9 |
| 2-Jan | 9.3 | 2.2 | 17-Feb | 0 | 12.8 |
| 3-Jan | 19.4 | 25.8 | 18-Feb | 0 | 0 |
| 4-Jan | 1.7 | 1 | 19-Feb | 0 | 0 |
| 5-Jan | 11.4 | 53 | 20-Feb | 3.1 | 0 |
| 6-Jan | 10.9 | 60 | 21-Feb | 0 | 0 |
| 7-Jan | 12.3 | 40.4 | 22-Feb | 24.9 | 0 |
| 8-Jan | 33.2 | 30 | 23-Feb | 34.6 | 59.9 |
| 9-Jan | 1.1 | 3 | 24-Feb | 52.8 | 10.1 |
| 10-Jan | 0 | 0 | 25-Feb | 0 | 100 |
| 11-Jan | 38.6 | 27 | 26-Feb | 0 | 0 |
| 12-Jan | 62.8 | 100 | 27-Feb | 0 | 0 |
| 13-Jan | 22.3 | 29 | 28-Feb | 0 | 0 |
| 14-Jan | 1.6 | 23 | 29-Feb | | |
| 15-Jan | 12.2 | 11.4 | 1-Mar | 0 | 0 |
| 16-Jan | 0 | 0 | 2-Mar | 14.7 | 2 |
| 17-Jan | 17.2 | 26.2 | 3-Mar | 15.7 | 23.5 |
| 18-Jan | 8.4 | 1 | 4-Mar | 0 | 0 |
| 19-Jan | 0 | 0 | 5-Mar | 0 | 0 |
| 20-Jan | 0 | 0 | 6-Mar | 3.6 | 2.9 |
| 21-Jan | 0 | 0 | 7-Mar | 0.8 | 8.4 |
| 22-Jan | 0 | 0 | 8-Mar | 0 | 0 |
| 23-Jan | 0 | 0 | 9-Mar | 0 | 2.2 |
| 24-Jan | 0.8 | 0 | 10-Mar | 0 | 0 |
| 25-Jan | 17.9 | 0.8 | 11-Mar | 0 | 0 |
| 26-Jan | 3 | 0 | 12-Mar | 0 | 0 |
| 27-Jan | 0 | 0 | 13-Mar | 0 | 0 |
| 28-Jan | 0 | 46.1 | 14-Mar | 0 | 0 |
| 29-Jan | 10.6 | 15.6 | 15-Mar | 0 | 0 |
| 30-Jan | 12.8 | 0 | 16-Mar | 0 | 0 |
| 31-Jan | 24.5 | 55.4 | 17-Mar | 0 | 0 |
| 1-Feb | 0 | 0 | 18-Mar | 0 | 0 |
| 2-Feb | 8.1 | 1.4 | 19-Mar | 0 | 3.3 |
| 3-Feb | 20.1 | 6.3 | 20-Mar | 0 | 0 |
| 4-Feb | 37.7 | 52 | 21-Mar | 0 | 0 |
| 5-Feb | 1.6 | 0 | 22-Mar | 0 | 0 |
| 6-Feb | 2.4 | 2.9 | 23-Mar | 0 | 0 |
| 7-Feb | 0 | 0 | 24-Mar | 0 | 0 |
| 8-Feb | 0 | 0 | 25-Mar | 0 | 0 |
| 9-Feb | 0 | 0 | 26-Mar | 1.6 | 3 |
| 10-Feb | 0 | 0 | 27-Mar | 0.6 | 0 |
| 11-Feb | 21.8 | 0 | 28-Mar | 0 | 24.3 |
| 12-Feb | 0 | 0 | 29-Mar | 11.4 | 11.3 |
| 13-Feb | 0 | 0 | 30-Mar | 0 | 0 |
| 14-Feb | 26.2 | 0 | 31-Mar | 11.1 | 0 |
| 15-Feb | 14.5 | 24.7 | 1-Apr | 0 | 0 |

# 8 Bibliography

Abdou, B., Mohammed, G., Battay, A. E. & Mohamed, N. H., 2018. Comparison of SRTM-V4.1 and ASTER-V2.1 for Accurate Topographic Attributes and Hydrologic Indices Extraction in Flooded Areas. *Journal of Earth Science and Engineering,* Volume 8, pp. 8-30.

Abushandi, E. & Merkel, B., 2013. Modelling Rainfall-Runoff Relations Using HEC-HMS and IHACRES for a single Rain Event in an Arid Region of Jordan. Jordan: Springer Science+Business Media Dordrecht.

Adeloye, A. J., Mwale, F. D. & Dulanya, Z., 2015. A metric-based assessment of flood risk. PIAHS, Volume 370, pp. 139-145.

Al-Abed, N., Abdulla, F. & Khyarah, A. A., 2005. GIS-hydrological models for managing water resources in the Zarqa River basin. Environmental Geology [Environ. Geol.], 47(3), pp. 405-411.

Alaghmand, S., Abdullah, R. B., Behdokht, V. & Abustan, I., 2010. GIS-based River Flood Hazard Mapping in Urban Area (A Case Study in Kayu Ara River Basin, Malaysia). International Journal of Engineering and Technology, pp. 488-500.

Alaghmand, S., Abdullah, R., Abustan, I. & Md Said, M. A., 2012. Gis-based river basin flood modelling using HEC-HMS and MIKE11 - Kayu Ara river basin, Malaysia. Journal of Environmental Hydrology, Volume 20, pp. 1-16.

Al-doski, J., Mansor, S. B. & Shafri, H. Z. M., 2013. Image Classification in Remote Sensing. Journal of Environment and Earth Science, 3(10), pp. 141 - 147.

Alexander, M., 2012. Decision-Making using the Analytic Hierarchy Process (AHP) and SAS/IML. [Online] Available at: https://analytics.ncsu.edu/sesug/2012/SD-04.pdf [Accessed 25 6 2018].

Alexander, W. J. R., 2000. Flood risk reduction measures. Pretoria: South Africa: s.n..

Ameta, D., 2015. Integration of Remote Sensing data with Geographic Information System (GIS): Application and changes detection techniques. International Journal of Managing Public Sector Information and Communication Technologies (IJMPICT), 6(4), pp. 1-10.

Asante, K. O., Artan A. G, Pervez, S, Bandaragoda, Verdin, J. P., C 2008. Technical Manual for the Geospatial Stream Flow Model (GeoSFM). U.S. Geological Survey, Open-File Report 2007(1441), pp. 1-65.

Balasubramanian, A., 2017. *Digital Elevation Model (DEM) in GIS*, Mysore: University of Mysore.

Baumbach, T. J., Burckhard, S. R. & Kant, J. M., 2015. Watershed Modeling Using Arc Hydro Tools. Geo HMS, and HEC-HMS. *Civil and Environmental Engineering Faculty Publications*, pp. 1-35.

Brakenridge, G. R., Kettner A. J., De Groeve T., Paris S., Cohen S., Nghiem S.V.,2019. Dartmouth Flood Observatory. [Online] Available at: http://floodobservatory.colorado.edu/SiteDisplays/255.htm [Accessed 12 July 2017].

Brunner, G. W., 2016. HER-RAS Hydraulic River Analysis Reference Manual, version 5, s.l.: US Army Corps of Engineers Hydrologic Engineering Center (HEC).

Bryant, E., 2005. Natural Hazard. 2nd ed. Newyork: Cambridge University Press.

Bueche, T., Vetter, M. & Weinberger, S., 2015. Estimation of flood area and depth using ArcHydro Toolbox. *ResearchGate.*

Cabral, S. L., Nilson, J. B., Silveira, C. d. S. & Teixeira, F. A. d. A., 2015. Hydrological and Hydraulic Modelling Integrated with GIS: A Study of the Acarau RiverBasin-CE. *Journal of Urban and Environmental*, 8(2), pp. 167-174.

Campell, J. B., 2002. Introduction to Remote Sensing. 3 ed. Taylor & Francis: The Guilford Press.

Chan, E. Y. Y., 2017. Public Health Humanitarian Responses to Natural Disasters. In: Hydrological Hazards. New York: Routlegde, pp. 97 - 101.

Chatterjee, R. S., Lakhera, R. C. & Dadhwal, V. K., 2010. InSAR coherence and phase information for mapping environmental indicators of opencast coal mining: A case study in Jharia Coalfield, Jharkhand, India. Canadian journal of remote sensing, 36(4), p. 361–373.

Chiwambo, C., 2017. Application of UNFC in Malawi: lessons learned, experiences and proposals. Cairo, African Mineral Development Centre.

Chu, X. & Steinman, A., 2009. Event and continuous modeling with HEC_HMS. *Journal of Irrigation and Drainage Engineering,* pp. 119 - 123.

Cunderlik, J. M., 2003. *Hydrological model selection for CFCAS project: Assessment of Water Resources Risk and Vulnerability to Changing Climatic Conditions,* s.l.: Western.

Danumah, J. H., Odai S. N., Saely, B. M., Thiel, S. M. T., Kouame, F. K., Akpa, Y. A., 2016. Flood risk assessment and mapping in Abidjan district using multi-criteria analysis (AHP) model and geoinformation techniques, (cote d'ivoire). In: Geoenvironmental Disasters. s.l.:Springer International Publishing, pp. 1-13.

DCCMS, 2006. Ministry of Natural Resources, Energy and Mining: Department of Climate Change and Meteorological Services. [Online] Available at: https://www.metmalawi.com/about.php [Accessed 3 Jan 2019].

Demir, V. & Kisi, O., 2016. Flood Hazard Mapping by Using Geographic Information System and Hydraulic Model: Mert River, Samsun, Turkey. Advances in Meteorology, 10(1155), pp. 1-9.

Department of Disaster Management Affairs, 2015. Malawi Hazard and Vulnerability Atlas. pp. 1-67.

Devia, G. K. & Dwarakish, G. G., 2015. A Review on Hydrological Models. *ScienceDirect,* pp. 1001 - 1007.

Díez-Herrero, A., Laín-Huerta, L. & Llorente-Isidro, M., 2009. A Handbook on Flood Hazard Mapping Methodologies. Madrid: Geological Survey of Spain.

Dijkshoom, J. A., Leenaars, J. G. B., Kempen, B. & Hutting, J., 2016. Soil and Terrain Database of the Republic of Malawi, s.l.: ISRIC Report.

Dimet, F.-X. L., Mazauric, C. & Castaings, W., 2000. *Models and data for flood modelling,* Cedex: s.n.

Disaster Management, 2015. *Youtube Video.* [Online] Available at: https://www.youtube.com/watch?v=itf0GTVYe8g [Accessed 2 November 2017].

Djokic, D., 2015. *Hydrological and Hydraulic Modeling with ArcGIS,* Redlands: Esri.

Dongchen, E., Chunxia, Z. & Mingsheng, L., 2004. Application of SAR Interferometry on DEM Generation of the Grove Mountains. Photogrammetric Engineering & Remote Sensing, 70(10), pp. 1145-1149.

Doocy, S., Daniels, A., Murray, S. & Kirsch, T. D., 2013. The Human Impact of Floods: A Historical Review of Events 1980-2009 and Systematic Literature Review, Baltimore: 2013.

Dooge, J. C., 1973. Linear Theory of Hydrologic System. Dublin: U.S Government Printing Office.

Doswell III, C. A., 2003. Flooding, OK, USA: Elsevier Science Ltd.

Durand, P., Robson, A. & Neal, C., 1992. Modelling the Hydrology of Submediterranean Montane Catchments (Mont-Lozère, France) Using TOPMODEL: Initial Results. Journal of Hydrology, pp. 1-300.

Dye, P. J. & Croke, B. F. W., 2003. Evaluation of streamflow predictions by the IHACRES rainfall-runoff model in two South African catchments. ScienceDirect: Environmental Modelling & Software, 18(8-9), pp. 705-712.

Dyhouse, G. R., Hatchett, J., Benn, J., 2007. Floodplain Modeling using HEC-RAS. Pennsylvania: Bentley Institute Press.

Els, Z., 2011. *Data Availability and Requirements for Flood Hazard Mapping in South Africa,* Cape Town: University of Stellenbosch.

Emerton, R. E., Stephens, E. M., Pappernberger, F., Pagano, T. C., Weerts, A. H., Wood, A. W., Salamon, P., Brown, J. D., 2016. Continental and global scale flood forecasting systems. WIRESa Water, 3(10.1002/wat2.1137), pp. 319-418.

Escobar, F., Hunter, G., Bishop, I. & Zerger, A., 2008. Introduction to GIS, Melbourne: Department of Geomatics, The University of Melbourne.

Esri, 2012. *What is GIS,* New York: s.n. https://www.esri.com/en-us/what-is-gis/overview

EXCIMAP, 2007. Handbook on good practices for flood mapping in Europe. s.l.: s.n.

Farooq, M. & Rabbani, A. H., 2018. Geospatial Technologies for Flood Hazard Assessment in Pakistan. Vienna, UNOOSA.

Al-Abed, N., Fayez, A., & Khyarah, A. A., 2005. GIS-hydrological models for managing water resources in the Zarqa River basin. ResearchGate, February.pp. 405 - 411.

Fekete, B. M. & Vörösmarty, C. J., 2007. *The current status of global river discharge monitoring and potential new technologies complementing traditional discharge measurements.* Brasilia, IAHS.

Feldman, A. D., 2000. Hydrologic Modelling System HEC-HMS, Technical Reference Manual. pp. 1-148.

Fleming, M. J. & Doan, J. H., 2013. User's Manual: HEC-GeoHMS Geospatial Hydrological Modeling Extension Version 10.1, Davis, CA: US Army Corps of Engineers.

Gao, X., Liu, Y., Li, T. & Wu, D., 2017. High Precision DEM Generation Algorithm Based on InSAR Multi-Looking Iteration. remote sensing, Volume 9, pp. 1-19.

Gharbi, M., Soualmia, A., Dartus, D. & Masbernat, L., 2016. Comparing 1D and 2d Hydraulic Models for flood Simulation on Medjerda River, Tunisia. J. Mater. Environ. Sci., 7(8), pp. 3017-3026.

GISGeography, 2018. The Remarkable History of GIS. [Online] Available at: https://gisgeography.com/history-of-gis/ [Accessed 08 09 2019].

Government of Malawi, 2015. Malawi 2015 Floods Post Disaster Needs Assessment Report.

Government of Malawi, UN Resident Coordinator for Malawi, 2019. *Malawi: Floods - Situation Report No. 4 (as of 27th April 2019).* https://reliefweb.int/report/malawi/malawi-floods-situation-report-no-4-27th-april-2019

Guha-Sapir, D., Hoyois, P., Wallemacq, P. & Below, R., 2016. Annual Disaster Statistical Review 2016: The Numbers and Trends, Brussels: CRED: Université catholique de Louvain.

Haack, B., Mahabir, R. & Kerkering, J., 2015. Remote sensing-derived national land cover land use maps: a comparison for Malawi. *Geocarto International,* 30(3), pp. 270-292.

Hamburg University of Technology, 2010. *Flood Manager: E-learning.* [Online] Available at: http://daad.wb.tu-harburg.de/knowledge-base/entry-points-of-the-knowledge-base-from-a-to-z/flood-modelling/ [Accessed 28 December 2018].

Icaga, Y., Tas, E. & Kilit, M., 2016. Flood Inundation Mapping by GIS and a Hydraulic Model (HEC RAS): A Case Study of Akarcay Bolvadin Subbasin, in Turkey. Acta Geobalcanica, 2(2), pp. 111-118.

Indian Institute of Technology, 2006. Module 3, Lecture 6: Synthetic Unit Hydrograph, s.l.: National Programme on Technology Enhanced Learning (NPTEL).

Jones, R., 2017. Uncertainty in Climate Change Impacts on Southern Alps River Flow: The Role of Hydrological Model Complexity, Dunedin: s.n.

Jonkman, S. N. & Kelman , I., 2005. An analysis of the causes and circumstanes of flood disaster deaths. *Disasters,* 29(1), pp. 75-97.

Kamaruddin, M., Hamid, J. R., Hamid, P. M. & Balzter, H., 2003. Digital Elevation Model (DEM) Generation from SAR Interferometry (ESA SP-529). Frascati, Italy, CDROM., id.37.1.

Khosrow-Pour, M., 2018. Encyclopedia of Information Science and Technology, Fourth Edition. 4th ed. Hershey PA: IGI Global.

Kopp, S. M., 1996. Linking GIS and hydrological models: where we have been, where we are going? In: K. Karel & H. P. Nachtnebel, eds. Application of Geographic Information Systems in Hydrology and Water Resources Management. Vienna: International Association of Hydrological Sciences, pp. 133-139.

Kourgialas, N. N. & Karatzas, G. P., 2011. Flood management and a GIS modelling method to

Langhammer, J., 2008. Geographic Approaches to Flood Risk Modelling. In: P. Dostál, ed. Evolution of Geographical Systems and Risk Processes in the Global Context. s.l.: P3K, pp. 82-99.

Leedy, P. D. & Ormrod, J. E., 2011. Practical Research: Panning and Design. 9th ed. New Jersey: Pearson International Education.

Llantwit School, 2010. (hazard mitigation) Modify human vulnerability Modify the loss, Wales: s.n.

Lunetta, R. S., Congalton, R. G., Fenstermaker, L. K., Jensen, R. J., McGwire, C. K., Tinney, Larry., 1991. Remote Sensing and Geographic Information System Data Integration: Error Sources and Research Issues. Photogrammetric Engineering & Remote Sensing, 57(6), pp. 677-687.

Makineci, H. B. & Karabörk, H., 2016. Evaluation Digital Elevetation Model Generated by Synthetic Aperture Radar Data. The International Archives of the Photogrammetry, Remote Sensing and Spatial Information Sciences, Volume XLI-B1, pp. 57-62.

Matori, A. N. B. & Lawal, D. U., 2014. Flood Disaster Forecasting: A GIS-Based Group Analytic Hierarchy Process Approach. Applied Mechanics and Materials, Volume 567, pp. 717-723.

McHarg, I. & American Museum of Natural History, 1971. Pbk ed. New York: Published for the American Museum of Natural History; Garden City, N.Y: Doubleday/Natural History Press.

Mehta, M., 2018. A Study of Steady Flow Energy Equation. [Online] Available at: https://www.toppr.com/bytes/steady-flow-energy-equation/ [Accessed 12 January 2019].

Mekni, M., 2010. Automated Generation of Geometrically-Precise and Semantically-Informed Virtual Geographic Environments Populated with Spartially-Reasoning Agents. Florida: Dissertation.com.

Merwade, V. & Rajib, A., 2018. Setting up a SWAT Model with ArcSWAT, s.l.: Lyles School of Civil Engineering, Purdue University.

Merwade, V., 2012. Hydrologic Modeling using HEC-HMS, s.l.: U.S, Army Corps of Engineers.

Ministry of Agriculture, Irrigation and Water Development, 2015. *Modernising Hydrological and Meteorological Monitoring Systems in the Shire River Basin* , s.l.: WS Atkins International Ltd.

MoAIWD, 2014. Project for National Water Resources Master Plan in the Republic of Malawi: Final Report: Part I Existing Condition, s.l.: s.n.

Musa, Z. N., Popescu, I. I. & Mynett, A., 2016. Approach on modeling complex deltas in data scarce areas: a case study of the lower Niger delta. Procedia Engineering, Volume 154, p. 656 – 664.

National Academy of Sciences (U.S.), 1973. Report of the National Academy of Sciences; Annual Report Friscal Year 1969-70, Washington, D.C.: National Research Council.

National Spatial Data Center, 2019. MASDAP. [Online] Available at: http://www.masdap.mw/layers/?limit=20&offset=0&type__in=vector [Accessed 29 May 2017].

National Statistics Office, , 2018, Malawi.

Nelson, A., Reuter, H. I. & Gessler, P., 2009. Chapter 3 DEM Production Methods and Sources. *ScienceDirect*, Volume 33, pp. 65-85.

Niekerk, D. V. & Nemakonde, L. D., 2017. Natural Hazards and Their Governance in Sub-Saharan Africa. Natural Hazard Science, pp. 1-30.

Ouédraogo, W. A. A., Raude , J. M. & Gathenya, J. M., 2018. Continuous Modeling of the Mkurumudzi River Catchment in Kenya Using the HEC-HMS Conceptual Model: Calibration, Validation, Model Performance Evaluation and Sensitivity Analysis. MDPI:Hydrology, 5(3), pp. 1-18.

Ponce, V. M., 2011. (When to use) Unsteady flow with HEC-RAS. [Online] Available at: http://ponce.sdsu.edu/unsteady_flow_with_hec_ras.html [Accessed 12 January 2019].

Pretorius, H., 2011. *Flood modelling using data available on the Internet*, Cape Town: MSc. Thesis, University of Cape Town.

Prinos, P., 2008. Review on Flood Hazard Mapping, Wallingford: FLOODsite Consortium.

Prosdocimi, I., Stewart, L., Faulkner, D. & Mitchell, C., 2016. FEH Local: Improving flood estimates using historical data. s.l., EDP Sciences, pp. 1-16.

Raghuwanshi, N. S., 2014. Soil & Water Conservation Structures 3(2+1). [Online] Available at: http://ecoursesonline.iasri.res.in/mod/page/view.php?id=2172 [Accessed 31 December 2018].

Romali, N. S., Yusop, Z. & Ismail, A. Z., 2018. Hydrological Modelling using HEC-HMS for Flood Risk Assessment of Segamat Town, Malaysia. s.l., IOPScience, pp. 1-6.

Sabatini, G., 2014. UN-Spider Knowledge Portal, Step by Step: Flood Hazard Mapping | UN-SPIDER Knowledge Portal. [Online] Available at: http://www.un-spider.org/advisory-support/recommended-practices/recommended-practice-flood-hazard-mapping/step-by-step#C.%20Hydraulic%20Modeling%20Workflow [Accessed 20 June 2017].

Schramm, D. & Dries, R., 1986. Natural Hazards: cause and effects, study Guide od Disaster Management, Madison Wisconsin: The University of Wisconsin- Madison.

ShahiriParsa, A., Noori, M., Heydari, M. & Rashidi, M., 2016. Floodplain Zoning Simulation by Using HEC-RAS and CCHE2D Models in the Sungai Maka River. Air, Soil and Water Research, 10(4137), pp. 55-66.

Simonov, Y., 2017. Latest tools and methodologies for flood modeling, s.l.: Hydrometcentre of Russia. [Accessed 20 June 2017].

Sinclair, S. & Pegram, G., 2004. A Flood Nowcasting System for The Ethekwini Metro Volume 1: Umgeni Nowcasting Using Radar, Pretoria: An integrated Pilot Study, report number 1217/1/04, Water Research Commission.

Snead, D., 2000. Development and Application of Unsteady Flood Models Using Geographic Information Systems, Texas: University of Texas at Austin, Master Thesis.

Song, X.-m., Kong, F.-z. & Zhu, Z.-x., 2011. Application of Muskingum routing method with variable parameters in ungauged basin. Water, Science and Engineering, 4(2), pp. 1-12.

Sui, D. Z. & Maggio, R. C., 1991. Integration GIS with hydrological modeling: practices, problems, and prospects. Computer, Envirnment and Urban Systems, 23(1), pp. 33-51.

Sun, Q., Miao, C, Duan, Q., Ashouri, H., Sorooshian, S., Hsu, K., 2017. A Review of Global Precipitation Data Sets: Data Sources, Estimation, and Intercomparisons. Review of Geophysics, 56(1), pp. 79-107.

Tarboton, D. G., 2003. Chapter 6 Simulation of Runoff Generation in Hydrologic Models. In: Rainfall-Runoff Processes. Utah: University of Utah, pp. 1-17.

Thakur, J. K., Singh, S. K. & Ekanthalu, V. S., 2017. Integrating remote sensing, geographic information systems and global positioning system techniques with hydrological modeling. *Applied Water Science*, 7(4), pp. 1595-1608.

Tomlinson, R., 2012. Origins of the Canada Geographic Information System, s.l.: ArcNews.

Tong, X. et al., 2017. An approach for flood monitoring by the combined use of Landsat 8 optical imagery and COSMO-SkyMed radar imagery. *ISPRS Journal of Photogrammetry and Remote Sensing*, pp. 144 - 153.

U.S. Geological Survey, 2019. USGS Science for a changing World, EarthExplorer. [Online] Available at: https://earthexplorer.usgs.gov/ [Accessed 3 June 2017].

USGS, 2018. The USGS Water Science School. [Online] Available at: Recurrence intervals and probabilities of occurrences [Accessed 22 December 2018].

Verdin, J, Verdin, K., Mathis, M. L., Magadzire, T., Kabuchanga, E., Woodbury, M., Gadain, H., 2016. A Software Tool for Rapid Flood Inundation Mapping, Virginia: USGS Science for a changing World.

Vincent, K., Dougill, D., Cull, T., Stringer, L. C., Chanika, D., 2014. Analysis of Existing Weather and Climate Information for Malawi, s.l.: s.n.

Vos, F., Rodriguez, J., Below, R. & Guha-Sapir, D., 2010. Annual Disasater Stastical Review 2009: The Numbers and Trends. Brussels: CRED.

Waters, N., 2010. GIS: History. [Online] Available at: https://www.researchgate.net/publication/315385359_GIS_History [Accessed 08 September 2019].

Westen, C. V., 2015. Multi-Hazard and Risk Assessment: Why is it so Difficult? Kuala Lumpur, University of Twente, Faculty of Geo-Information Science and Earth Observation (ITC).

Wicks, J., 2016. Introduction to Flood Modelling. [Online] Available at: https://www.youtube.com/watch?v=E-B7o-81Yt0 [Accessed 19 7 2018].

Wilson, J. P. & Gallant, C. J., 2000. Digital Terrain Analysis. In: J. C. Gallant & J. Wilson, eds. *Terrain Analysis: Principles and Applications.* s.l.:John Wiley & Sons, pp. 1-28.

Winsemius, H., Ward, P., Veldkamp, T., Jongman, B., Hallegatte, S., Bangalore, M., Global 2018, Exposure Analysis on Floods/Drought and Poverty, pp. 1-25. https://www.worldbank.org/content/dam/Worldbank/document/Climate/Climate%20and%20Poverty%20Conference/D1S3_WINSEMIUS_slide_deck_poverty_WB.pdf

Yang, D., Herath, S. & Musiake, K., 2000. Comparison of different distributed hydrological models for characterization of catchment spatial variability. Hydrological Processes, 14(3), pp. 403-416.